Project 7: Microgrid Impact Study

Final Report

Donald and Tarnagulla Microgrid Feasibility Study

The University of Melbourne

May 2022

Title:	**Project 7: Microgrid Impact Study**
Date:	May 2022
Prepared For:	Centre for New Energy Technologies (C4NET), Powercor
Lead Researcher:	Dr Maria Vrakopoulou
Research Team:	Dr Guanchi Liu Dr Julian de Hoog Salah Hajtaleb Nathan Wong Hongji Hu Prof Pierluigi Mancarella Dr Arash Vahidnia A/Prof Lasantha Meegahapola Dr. Reza Razzaghi
Contact:	Dr Maria Vrakopoulou maria.vrakopoulou@unimelb.edu.au
Organization:	The University of Melbourne
Partners:	RMIT University, Monash University
Acknowledgements:	Powercor provided network map and data and continuous feedback RMIT provided steady-state DIgSILENT models

Executive Summary

The Donald and Tarnagulla Microgrid Feasibility Study was launched under a Grant Agreement between the Centre for New Energy Technologies Limited (**C4NET**) and the Commonwealth of Australia, represented by the Department of Industry, Science, Energy and Resources (**DISER**).

The study includes 12 interdisciplinary projects where among them Project 7, “Microgrid Impact Study”, analyses the impact of disturbances on the reliability and security of the two towns, i.e. Donald and Tarnagulla, under grid-connected and off-grid microgrid operation. Project 7 was a 6-month project that run from October 2021 until March 2022.

Specifically, Project 7 aims to develop steady-state and dynamic power system operation models, statistical models for disturbances and also provide an assessment of the options, risks and benefits of specific control strategies for microgrid operation. Special consideration is given to bushfires risks regarding outages and unavailability of fuel.

This final report includes both the theoretical setup and numerical results for both towns supporting the microgrid feasibility analysis in line with the aforementioned goals.

Table of Contents

Abbreviations and Acronyms

FFDI	Forest Fire Danger Index
MAE	Mean Absolute Error
MSE	Mean Squared Error
NMI	National Metering Identifier
RMSE	Root Mean Squared Error
Sym	Symmetrical Fault
Asym	Asymmetrical Fault

1 Background

Project 7, “Microgrid Impact Study”, analyses the impact of disturbances on the reliability and security of the two towns, i.e. Donald and Tarnagulla, under grid-connected and off-grid microgrid operation. Specifically, Project 7 aims to develop steady-state and dynamic power system operation models, statistical models for disturbances and also provide an assessment of the options, risks and benefits of specific control strategies for microgrid operation. Special consideration is given to bushfires risks regarding outages and unavailability of fuel.

The objectives of this project can be summarized:

- O1: Develop steady-state and dynamic operation simulation tools in Julia/JuMP, Matlab and DIgSILENT Powerfactory, that could be integrated into a Monte Carlo simulation engine for techno-economic and reliability probabilistic assessment of microgrids;
- O2: Model the economic, reliability, and resilience impact of the Donald and Tarnagulla microgrids and broader networks, in grid-connected and off-grid modes and under different operating conditions;
- O3: Provide an assessment of the options, risks, and benefits of specific control strategies for the microgrid to provide resilience against bushfires, including risk-based control strategies to mitigate the probability of unsafe operation and decrease the associated costs.

These objectives are addressed within four tasks:

Task 1: Network Modelling (O1)
This task deals with the development of a steady-state (for cost and capacity adequacy assessment) and dynamic (for operational security assessment) model using Julia/JuMP, Matlab, and Powerfactory DIgSILENT. The size and location of the resources are informed by Project 4 and Project 5. A model of the under-study towns of the broader network is considered.

Task 2: Identification and statistical modelling of disturbances (O1)
This task analyses the statistical properties, and develops relevant probabilistic models, of potential disturbances internal and external to the towns, divided into continuous (e.g., PV generation, loads, bushfire risk) and discrete events (e.g., component loss), and specifically including the characteristics of potential bushfires in the areas based on available data and ongoing projects.

Task 3: Techno-economic impact analysis of microgrids and broader networks (O2)
This task will assess the impact of the disturbances of Task 2 on the economic, reliability, and resilience performance of the microgrid and broader network by implementing a Monte Carlo engine that uses the models developed in Task 1 along with the islanding configurations proposed in Project 5. Microgrid operation will be assessed under grid-connected and involuntary and controlled islanding (total or partial). Specific risk metrics for economic, reliability, and resilience performance assessment will be calculated based on probabilistic Monte Carlo simulations with high temporal resolutions, for which advanced sampling techniques will be used to improve computational performance.

Task 4: Risk and resilience-driven control strategies (O3)
This task identifies specific microgrid control algorithms to mitigate the risk of unreliable operation and high resulting costs, and to improve resilient operation before, during, and recovering from extreme events such as bushfires, and test them in the two microgrids.

The report is organised as follows:

In Chapter 2, the data analysis that is used for setting up the data in the network of the Donald and Tarnagulla area is introduced at first. Then, the internal distribution network modelling for dynamic security analysis accompanied with the modelling assumption of the broader network is introduced. An equivalent simplified network topology that represents the connection between Donald and Tarnagulla area and upstream network is also provided. Chapter 2 addresses Task 1.

In Chapter 3, the modelling and statistical analysis for disturbances are introduced, which include the extreme demand/generation ramping events, the failure probability of network components, and the impact modelling of bushfire risk on the supply availability from the upstream grid. Forecasting techniques are compared for both generation and demand signals. Chapter 3 addresses Task 2.

In Chapter 4, the capacity adequacy assessment framework is developed to evaluate the impact of disturbances on the reliability of the two towns in quasi-steady-state operation. Expected energy not supplied (EENS) is selected as the capacity adequacy metric. Different control strategies are considered concerning storage dispatch and emergency dispatch deviations for grid-connected and off-grid cases of the microgrid. Chapter 4 addresses the objectives of Task 3 and Task 4.

In Chapter 5, an impact analyses of a wide range of disturbances on the dynamic performance of the towns and the broader MV feeder is carried out. The performance is assessed against identified metrics; then the strengths and shortcomings are identified, and high-level mitigation solutions are proposed. Chapter 5 addresses objectives of Task 3 and Task 4.

2 Network modelling

In this chapter, the network modelling and necessary input data analysis is provided.

2.1 Smart meter and network data

2.1.1 Time series data

A smart meter time series dataset was made available by project partners in the form of two .csv files, and a descriptive .doc file that is partially reproduced below.

The .csv files are:

- *PCOR_donaldtarnagulla_30min_consumption_and_generation_data.csv*:
  Half-hourly intervals of consumption and solar generation for feeders – Donald (CTN006) and Tarnagulla (MRO007), characterized by postcode and customer type, for non-contestable customers for the year 2020
- *PCOR_donaldtarnagulla_15min_consumption_and_generation_data.csv*:
  15 mins intervals of consumption and solar generation for feeders – Donald (CTN006) and Tarnagulla (MRO007), characterized by postcode and customer type, for contestable customers for the year 2020

The two files consist of:

- 48 half-hourly / 96 fifteen mins intervals of consumption (in kWh)
- Date of consumption
- National Meter Identifier, NMI (de-identified)
- broken down by postcode
- broken down by customer type
- broken down by feeder

There are two types of customers. Non-contestable customers are mostly residential customers; and contestable customers are large use customers who can choose their own electricity provider. Most commercial and industrial customers are eligible to become contestable.

Some de-identification was conducted to meet data privacy requirements: there were a few cases where the number of unique customers/NMIs in the data specific to a postcode and customer type were less than four. The postcodes for such NMIs were masked to adhere to data privacy policies of distribution business. In addition:

- For contestable customers (30 mins interval data), postcodes for 1.3% of customers were de-identified (replaced by Null Value).
- For non-contestable customers (15-mins data), postcodes for 11 out of 48 customers were de-identified (replaced by Null Value). Since the number of such customers is really low, it was necessary to mask such percentage of customers for data privacy.

For all time series in the dataset, the “customer type” was also provided. The following customer types appear in the dataset: 1) A, Farm, 2) C, Commercial, 3) DF, Domestic Farm, 4) I, Industrial, 5) R, Domestic / Residential.

2.1.2 Basic dataset statistics

The full dataset (across both feeders, contestable and uncontestable) consists of 3,733 individual time series.

Contestable vs uncontestable: Of the total set of time series, 47 (1.26%) are contestable, and 3,686 (98.74%) are uncontestable. For the Donald feeder alone, 35 are contestable, 1,876 are uncontestable. For the Tarnagulla feeder alone, 12 are contestable, 1,810 are uncontestable.

Distribution across postcodes: Each feeder includes time series associated with 12 different postcodes, as shown in Figure 2. For the postcode specific to the town of Donald (3480) there are 1049 demand time series, and 207 generation time series. For the postcode specific to the town of Tarnagulla (3551), there are 147 demand time series, and 35 generation time series.

Numbers of customers for each customer type: The number of customer types for each town (postcodes 3480 and 3551, respectively) are shown in Figure 1. The majority of customers in both towns are residential.

Contribution to total load: The aggregate contribution of each customer type to total load, across the whole year (2020) is shown in Figure . Although the contribution of non-residential customers to total load rises, the bulk of total load is still consumed by residential customers.

Contribution to total export: The aggregate contribution of each customer type to total export (i.e., solar PV generation that does not offset load locally), across the whole year (2020) is shown in Figure .

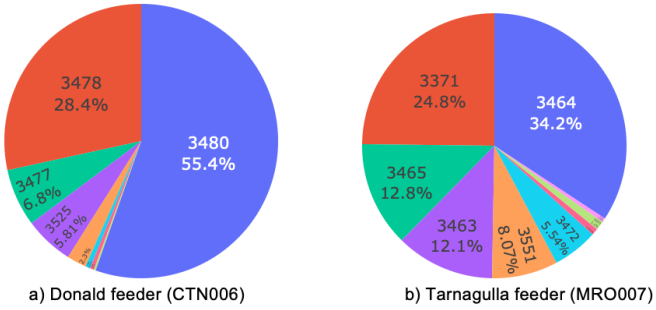

a) Donald feeder (CTN006) b) Tarnagulla feeder (MRO007)

Figure 1. Postcodes represented in the smart meter data

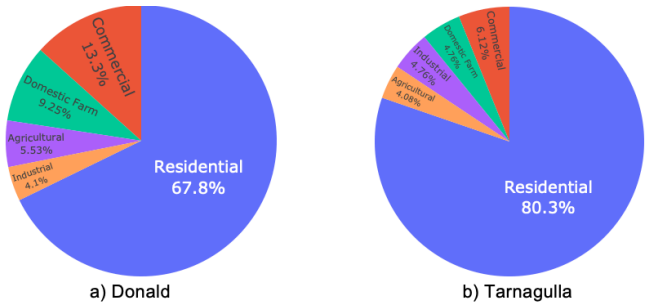

a) Donald b) Tarnagulla

Figure 2. Postcodes represented in the smart meter data

The bulk of total export is generated by residential customers. However, industrial customers also provide a significant amount of remaining export.

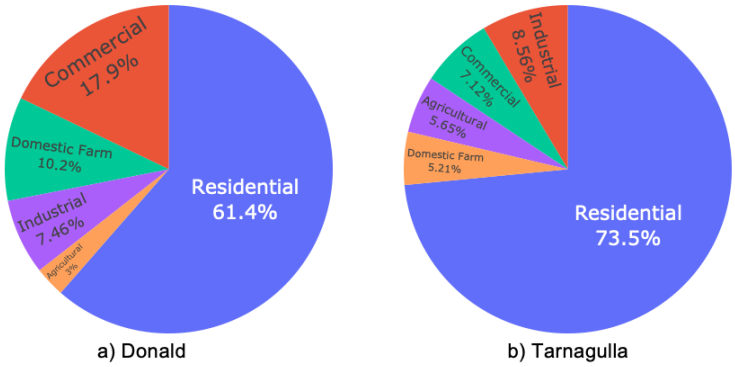

Figure 3. Contribution to total load (sum of all import) by customer types

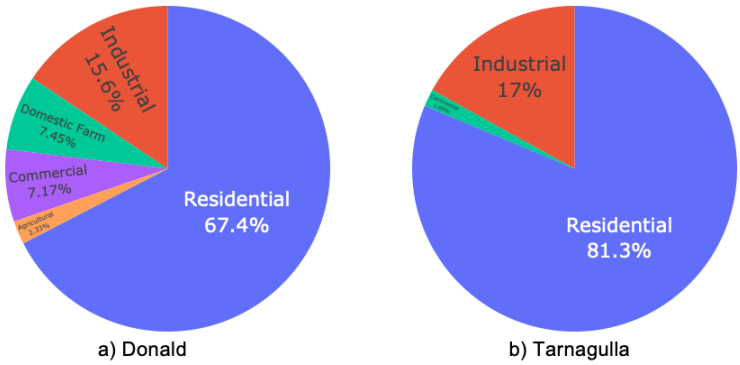

Figure 4. Contribution to total export (from solar PV) by customer types

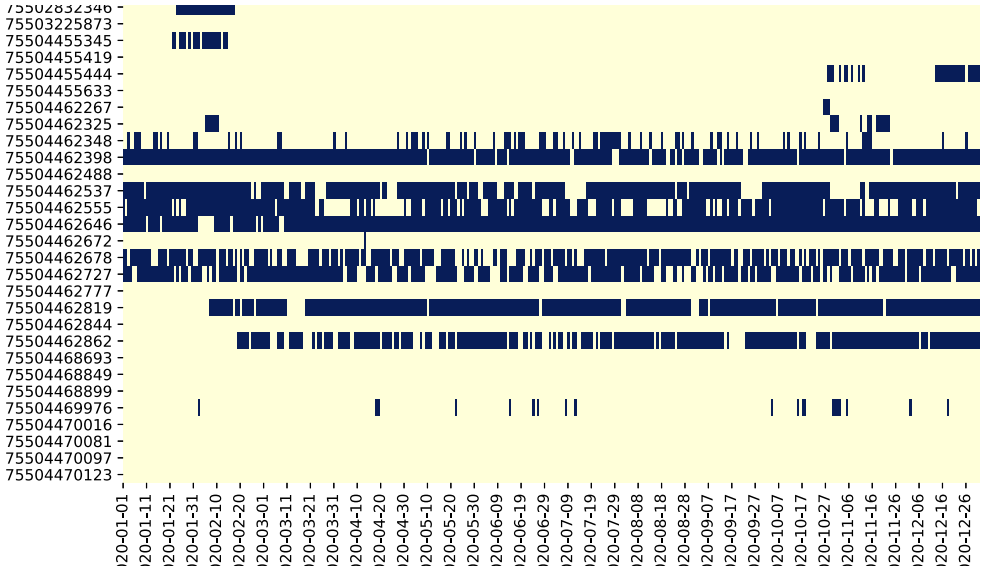

Figure 3. Examples of gaps in the dataset. Each row represents one year's worth of data for one NMI, and dark areas indicate missing data

2.1.3 Data quality

There are a significant number of gaps in the dataset, which is not unusual for smart meter data. Examples of this are presented in Figure 3. This figure shows 30 import time series in the Donald postcode. Each row represents the data for one time series over the course of the full year. Dark sections indicate gaps in the data (in other words, no value available). As can be seen, in many cases there are significant amounts of data missing. As a result, it was decided that a detailed analysis of gaps in the data should be undertaken in order to ensure that subsequent analyses would properly accommodate true conditions in the actual networks for Donald and Tarnagulla.

A number of individual time series known to have many gaps were manually inspected. Some examples of these are shown in Figure 4. For many of these, the total contribution to load (where data was available) was found to be very small.

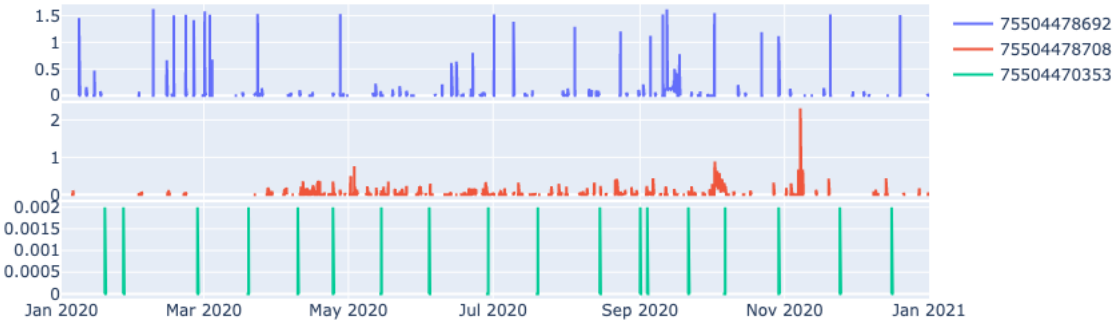

Figure 4. Examples of gaps for individual time series

However, to conduct a more thorough analysis, the total contribution of time series with gaps to import and export was further explored. Time series were grouped according to how much data was available throughout the full time period (2020), using the following grouping:

- Time series for which all data was available
- Time series for which 90-100% of data was available (up to 10% of the data consisted of gaps)
- Time series for which 80-90% of data was available
- Time series for which less than 80% of data was available

The numbers of time series falling into each of these categories for both Donald and Tarnagulla, for both import and export, are shown in Table 2-1.

Table 2-1. Numbers of time series having gaps

	Donald - import	Donald - export	Tarnagulla - import	Tarnagulla - export
Total	1049	207	147	35
100%	909	110	116	19
90-100%	42	43	4	8
80-90%	16	8	0	1
< 80%	82	46	27	7

Some examples of the total contributions of each of these time series to total import and total export are shown in Figure . It can be seen that:

- Donald - import: total contribution of time series with gaps is small
- Donald - export: time series with gaps do make a significant contribution to total export

- Tarnagulla - import: in general, total contribution of time series with gaps is small, but occasionally it can be significant (see March 1)
- Tarnagulla - export: time series with gaps do make a significant contribution to total export

Since time series with gaps do generally have an important impact for both Donald and Tarnagulla, the next step was to consider whether the gaps should be filled – particularly for individual time series having a significant contribution to aggregate import / export. Figure shows some examples of individual time series for different levels of gaps for Donald - import. It can be observed that:

- For time series having 90-100% of data available, the gaps appear to often result from periods having zeros, or from periods in which there is a step change in load before / after the gap. This suggests that these gaps may be due to meter disconnections, perhaps while a home is vacant.
- For time series having 80-90% of data available, the gaps often occur at the start or end of the time series – again likely due to a meter being connected or disconnected.
- For time series having < 80% of data available, there are often significant gaps.

In all of the above cases, gap filling may be either incorrect (e.g., when due to meter disconnection) or very difficult (e.g., during very long gaps). It was decided therefore that gaps should not be filled artificially, in order to avoid introducing incorrect data into subsequent analyses.

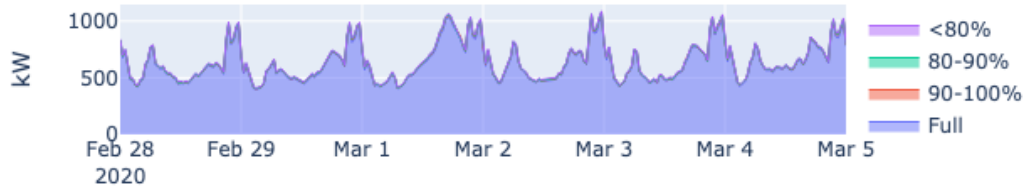

a) Donald - import

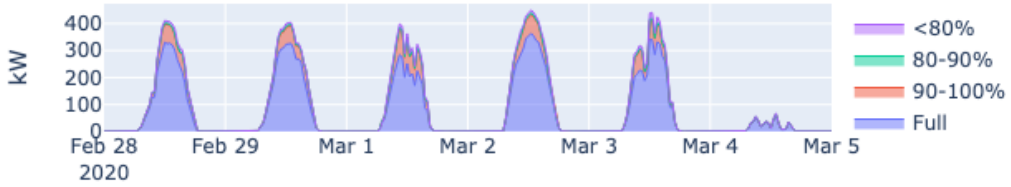

b) Donald - export

c) Tarnagulla - import

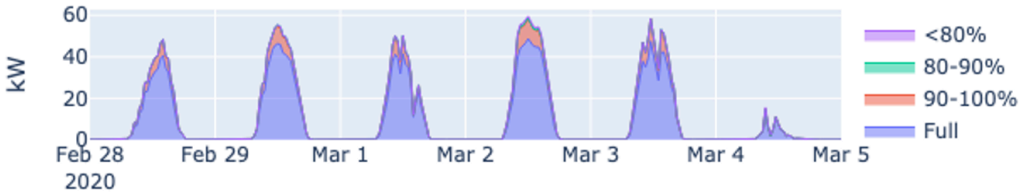

d) Tarnagulla – export

Figure 7. Examples of individual time series for different levels of data gaps

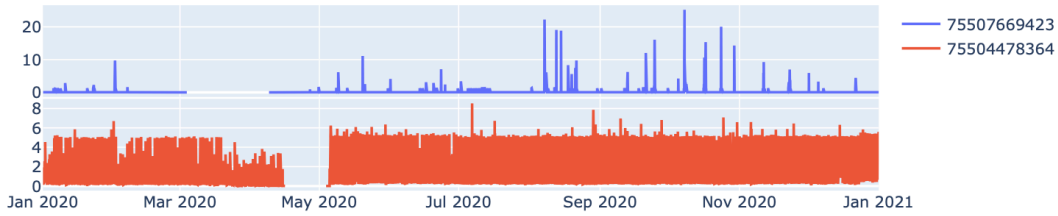

a) Two examples of time series having 90-100% of data available

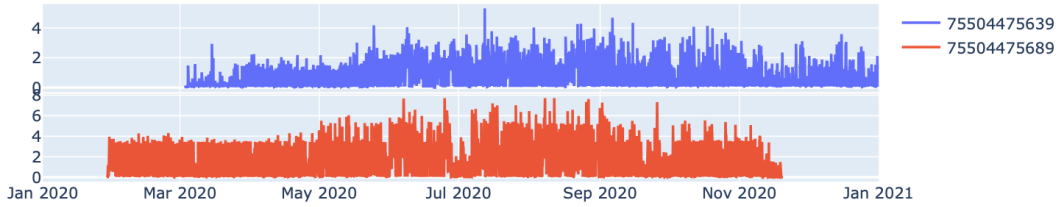

b) Two examples of time series having 80-90% of data available

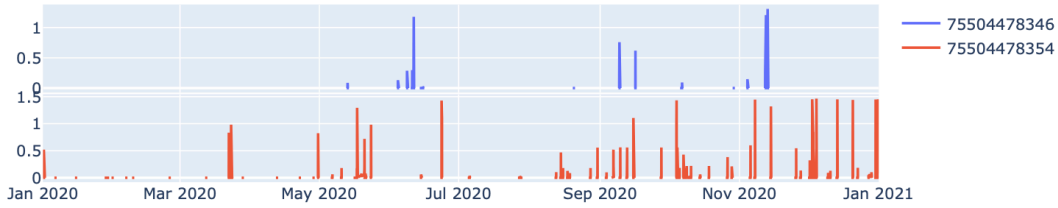

c) Two examples of time series having < 80% of data available

Figure 8. Contribution to total import / export of time series based on the percentage of data having gaps

Although there are many gaps in the data, the vast majority of these are unlikely to affect subsequent analyses of potential disturbances in these two towns. Many gaps are assumed to be the result of meter

(dis-) connection and should therefore not be filled. It is therefore considered acceptable to treat all existing gaps as zero values.

However, to ensure a conservative analysis and to ensure that worst-case scenarios are also considered, in subsequent analyses the following steps should be taken:

1. For Donald - import time series, all imports should be scaled up by 9%. In general, the time series having gaps contribute similarly to total import in Donald throughout the year, reaching a maximum contribution of 8.76%. Scaling up by 9%, therefore, ensures that the maximum possible import for Donald in 2020 is appropriately considered.

2. For Tarnagulla - import, when considering aggregate import, an addition of 40kW of load should be considered. In Tarnagulla there are three time series that have a significant contribution to aggregate import, but only sporadically (see March 1 in Figure above for an example). 40kW represents the maximum contribution that all three may make at any given time, and therefore represents a worst-case scenario of missing data at any time.

3. For export of both Donald and Tarnagulla, the weeks at the end of the year (December 2020) should be given priority in the analysis, since more solar PV systems will have been installed by the end of the year than the beginning of the year.

In addition, further scenarios beyond the above should be considered to take into account future growth of solar PV and demand. This is further discussed in future works.

2.1.4 Mapping of smart meter data to transformers

In addition to the time series smart meter data described in the previous sections, the project partners also made available a mapping of smart meter NMIs and solar PV capacities to transformers. This was requested so that an appropriate mapping of aggregate load to each transformer in the network models would be possible.

This dataset contains, for a large number of NMIs on both the Donald and Tarnagulla feeders, the name of the transformer that the NMI is connected to, as well as the nominal capacity of the solar PV system (if any) at that NMI. It further contains the ratings of a large number of transformers on each of these feeders.

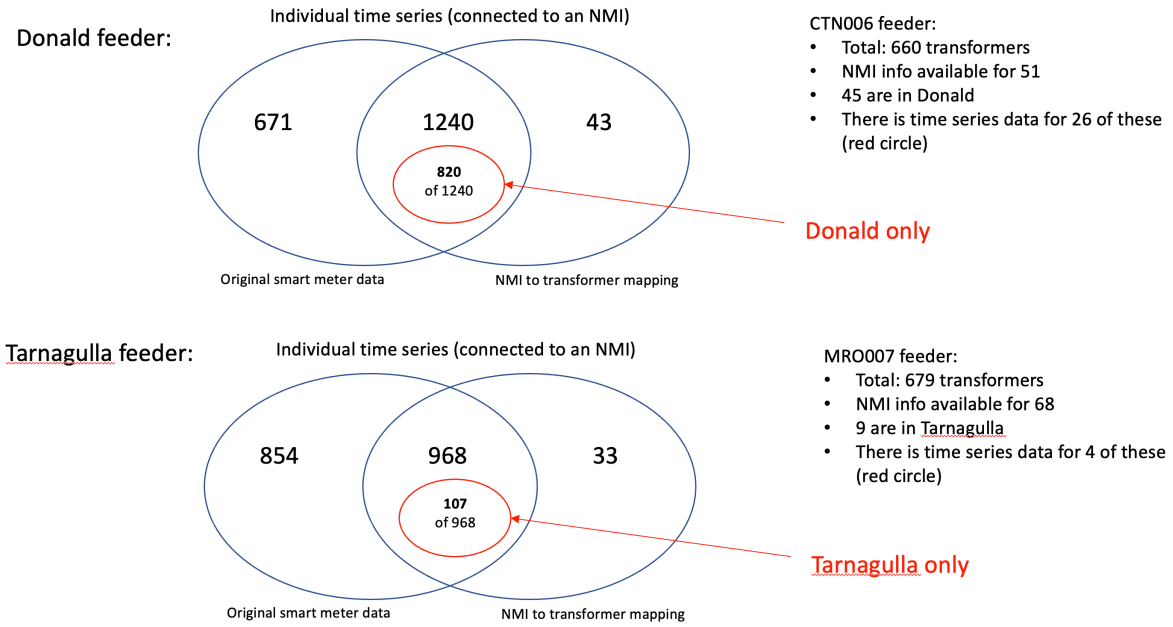

Figure 5. A summary of the available data and the overlap between the two datasets provided

This dataset was highly valuable towards accurately representing the load at individual transformers throughout the network. There were some differences between the meter identifiers provided in the first smart meter dataset (described in Section 2.1.1) and this new dataset. For example, there are some NMIs for which there is time series data in the first dataset, but which do not appear in the second dataset (no mapping to transformer). Conversely, there are some NMIs that appear in the second dataset (mapping to transformer), but for which there is no time series data in the first dataset. Figure 5 represents the available data, and where the two datasets overlap. There may be many reasons for these differences, such as the need to ensure data confidentiality for certain customers.

The mapping of NMIs to transformers nevertheless made it possible to assign individual smart meter time series to specific transformers, and subsequently, analyse the total demand and generation on a transformer-by-transformer basis. This is further described in Section 2.3.

2.2 Weather data

In order to better model demand and generation (Section 2.3) and for forecasting purposes (Section 3.2), it was necessary to obtain weather and solar irradiation data.

Weather data was obtained for Donald and Tarnagulla from OpenWeather[1]. This dataset consists of:

- Hourly values, for the full period (2020) of the following variables: temperature, pressure, humidity, wind speed, wind direction, and cloud cover (sky cloudiness as a percentage)
- Historical weather forecasts, for the full period, where individual forecasts are made 3 hours apart, for the next 16 days, at hourly resolution, for the same variables.

[1] https://openweathermap.org/

Additional variables exist (such as dew point, “feels like”, etc.) but were not included in subsequent analyses since they were either not relevant, or duplicated existing variables, or were not available for significant parts of the year.

Solar irradiation data was obtained from the authors of the previous Project 4: Area Hosting Capacity Assessment. This dataset was originally collected from NASA surface metrology and consists of solar irradiance values (kWh/m2) at an hourly resolution. Figure 6 presents the full weather dataset.

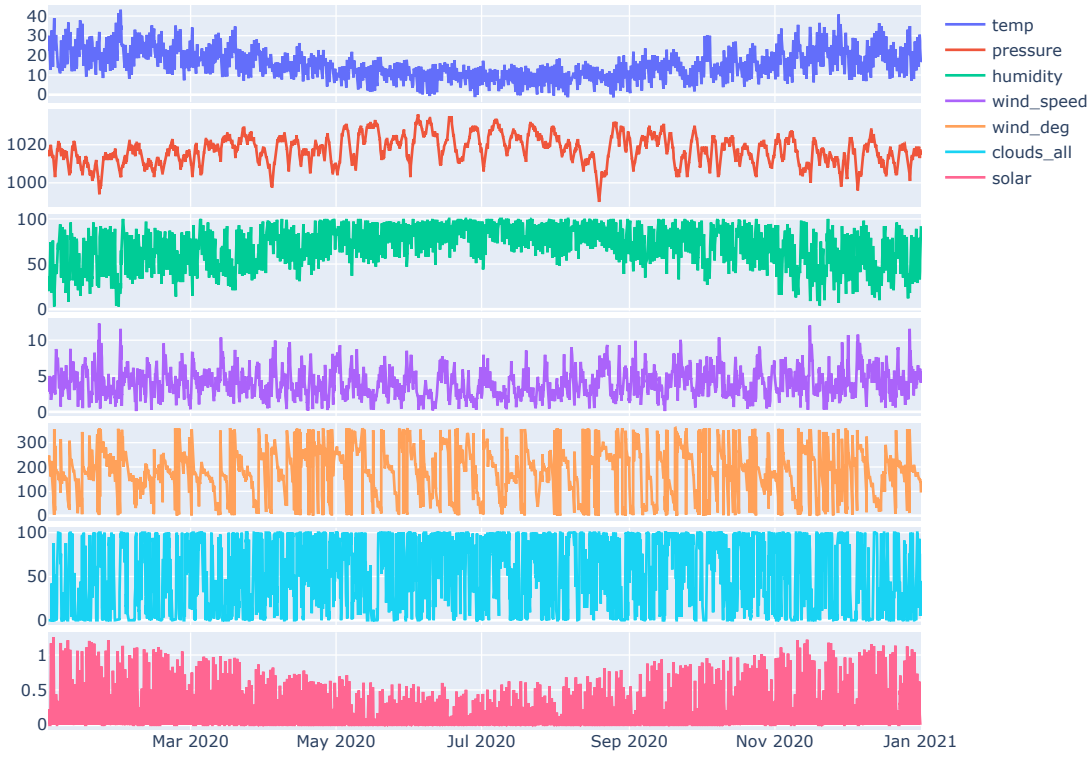

Figure 6. Weather and solar irradiation data used in this study

2.3 Conversion to Demand and Generation

The smart meter time series data provided by the project partners consists of import and export data for every available NMI, at a half-hourly resolution. Such data does not accurately represent demand and generation, however. For any customer that has solar PV, locally generated energy offsets local demand first, and is only exported when solar generation exceeds local energy demand. The import and export time series therefore “mask”, so to say, the actual demand and generation that occurs at each NMI.

Having more accurate time series of demand and generation is however in some cases more valuable than having time series of import and export. By more accurately knowing total solar generation at each NMI, it is possible to:

- Better understand the impact of solar PV
- Generate more accurate forecasts – of either demand or generation (or even net demand)
- More accurately understand and model the dispatch of energy storage
- More accurately model potential future scenarios of load growth and/or solar PV growth

As a result, it was decided that a conversion of import / export time series to demand / generation time series should be conducted. This conversion process consists of five steps, each described in more detail below.

It should be emphasised that this process of conversion provides an estimate only of demand and generation, and without separately metered data it is not possible to validate the approach. However, empirically the results appear valuable, and the validity of this approach can be evaluated as part of the forecasting process (in other words, does this conversion lead to more accurate forecasts).

It should also be noted that for any NMI, the sum of import and export will always equal the sum of demand and generation – in other words, there is no impact on net demand for any time series in the dataset. Note that the described entities are considered positive when the power could be withdrawn from the grid (e.g., demand, import) and negative when power could be sent back to the grid (e.g., generation, export).

The individual steps are now described in more detail.

Step 1: Model solar generation as a function of weather data

As described in Section 3, a number of weather variables were obtained for Donald and Tarnagulla for the time period under consideration (2020). There are also a number of time series in the original dataset for which there is only export (import is zero, or close to zero, at all times). In other words, we have a small number of time series that represent a pure solar PV generation profile, with no "noise" introduced by demand that is offset locally.

It is therefore possible to model solar PV generation as a function of weather. This can be thought of as a standard machine learning problem in which an output variable (solar generation) is expressed as a function of a number of input variables (temperature, humidity, pressure, wind speed, solar irradiation, as well as hour of day and month of year).

Three different machine learning models were applied (multiple linear regression, support vector regression, and random forest regression), and the results are shown in Table 2-2. The error metrics used are mean absolute error (MAE), mean squared error (MSE), and root mean squared error (RMSE). For all metrics, random forest regression provided the best results, and this was subsequently chosen as the preferred model.

Table 2-2. Machine learning models used to model solar generation as a function of weather variables

	MAE	MSE	RMSE
Multiple linear regression	0.20	0.08	0.29
Support vector regression	0.31	0.19	0.43
Random forest regression	0.13	0.05	0.23

Step 2: Estimate the maximum possible solar generation of any export time series

Recent research in the energy informatics community has shown how the maximum solar profile of either an export (or even a net) time series may be determined, just from a small amount of recent

data[23]. The full details are available in the provided citations, but in short, for any interval, the maximum generation for that same interval across the recent past (such as the past two weeks) may be determined. When done for every interval across a whole day, this provides a fairly accurate representation of what that particular system would have generated on a perfectly sunny day at that time of year. This is sometimes referred to as that system's "characteristic profile".

Determining the characteristic profile for any solar PV system is a straightforward and simple exercise that requires only that system's time series data. An example for one of the time series in our dataset is provided in Figure 7.

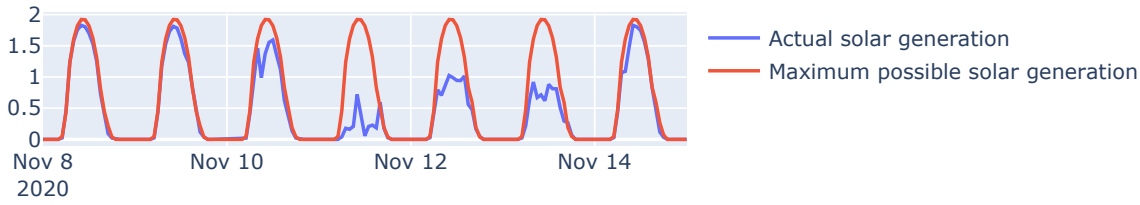

Figure 7. Example of the characteristic profile (maximum possible solar generation) for one solar export time series

Step 3: Generate an interval-wise multiplier that takes into account that interval's weather

The solar generation model developed in Step 1 can subsequently be applied to the export time series for which there is no associated import (the clean solar generation time series that exist in the dataset). At every interval, the output of the solar generation model may be compared with what that system would have generated under optimal conditions. As a result, for every interval a multiplier can be determined, which indicates how much solar generation was reduced due to weather conditions.

This approach only makes sense if all the time series are generated within close proximity to one another (and are therefore similarly affected by weather). For each of Donald and Tarnagulla, this was considered a reasonable assumption. For similar studies covering a wider geographic area, this assumption may not hold and individual multipliers would need to be generated for each region of interest.

Step 4: Use this multiplier to convert export time series into generation time series

The multiplier generated in Step 3 can subsequently be applied to all time series in the whole dataset, interval by interval. For every time series, therefore, an estimate of the true total generation can be obtained. An example (for one of the clean solar generation time series not impacted by local demand) showing the actual solar generation and the solar generation estimated through this approach is

[2] Chen, D., Breda, J., and Irwin, D. Staring at the sun: A physical black-box solar performance model. In Proceedings of the 5th Conference on Systems for Built Environments (New York, NY, USA, 2018), BuildSys '18, Association for Computing Machinery, p. 53–62.

[3] De Hoog, J., Perera, M., Ilfrich, P., and Halgamuge, S. Characteristic profile: Improved solar power forecasting using seasonality models. SIGENERGY Energy Inform. Rev. 1, 1 (Dec 2021), 95–106.

shown in Figure 8:

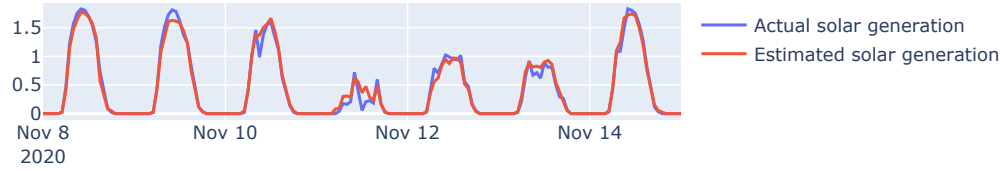

Figure 8. Example of the estimated solar generation using the model and multiplier described above

Step 5: Determine the corrected demand time series, using the new generation time series

For every NMI, the net demand is known (sum of import and export). The corrected demand can therefore be calculated in a straightforward way: it is the difference between the known net demand, and the corrected solar generation calculated in Step 4 above. This can be applied to every NMI in the entire dataset.

Some examples showing the conversion of import and export time series into demand and generation time series are shown in Figure 9. As can be seen, spikes in the original export time series (which most likely represent spikes in demand) are smoothed in the corrected generation time series, and instead show up more accurately as demand spikes.

Figure 9. Examples of conversion of import/export to demand/generation for two different NMIs

2.4 Dynamic model development

This section aims to develop dynamic models of the Donald and Tarnagulla microgrid networks that will enable simulating and assessing the impacts of various dynamic and transient events across both networks in grid-connected and off-grid modes. The developed models will also be examined by their dynamic response capability and performance under a wide range of operational scenarios.

The primary objective in distribution network operation is to maintain voltage levels within regulatory limits and maintain loading of network assets within their thermal ratings in both steady-state operation and following a network disturbance [1]. In DER-rich networks, maintaining these limits becomes more challenging due to the unpredictable, decentralized and uncoordinated nature of DER. Increasing PV

penetration may result in network congestion, voltage rise or voltage fluctuations issues [2],[3]. In particular, stability of generating units, i.e., inverters, which has a direct impact on supply continuity, has been of particular concern.
The output of this task will feed into the disturbance impact assessment of the two towns, and play a crucial role in determining the viability of forming the microgrids.

In order to develop a model that will mitigate the aforementioned challenges, three key metrics have been established:

Table 2-3. Key metrics

Metric	**Acceptable if**
Voltage magnitude*	MV voltages are within 0.90 pu – 1.10 pu** LV voltages are within 0.90 pu – 1.13 pu
Thermal limits	Transformer loadings are within 0 – 100%
Inverter stability and supply continuity	Inverter remains stable and connected

**As per Electricity Distribution Code of Practice, March 2022 v14, Essential Service Commission – Clause 4.2.2 Table 1*

***The load and generation for each town network have been aggregated on transformer level. Therefore, in order to satisfy the acceptable voltage magnitude interval on both LV and MV sides of the transformers, the 0.9 pu – 1.1 pu range has been selected as the minimum condition to be met for both voltage levels.*

The network models will be tested against the above metrics under a range of disturbances and operating modes.

This task is informed by the inputs provided by Powercor, Project 4, and demand and generation modelling developed within Project 7 as shown in Table 2-4.

Table 2-4. Dynamic modelling inputs

Input	**Informed by**
• Network configuration and MV feeder model • Size, type, and location of network and customer assets, e.g. transformers, loads, PV and battery storage	Powercor Project 4 – Area Hosting Capacity Assessment Project 5 – Islanding Design and Cost Analysis
• Customer smart meter data (de-identified) and mapping to the distribution transformers	Powercor
• Decoupled load and generation profiles	Project 7 – Network modelling

• Extreme and typical events, e.g., ramping events, max/min import and export, net feeder flows	Project 7 – Disturbance modelling

2.4.1 Battery and PV dynamic models

The microgrid models developed in Project 4 have been taken as reference networks. While these networks are suitable for dynamic simulation, they only contain static control models for generation and storage systems connected across the LV network. To enable analysis of the dynamic capability and behaviour of PV and battery systems at each network node, the models from Project 4 have been augmented with dynamic inverter and controller models. The back-up diesel generators have also been augmented with dynamic AVR (automatic voltage regulator) and governor models that will be enabled in off-grid operation. These models have been developed in DIgSILENT Powerfactory to maintain modelling consistency with the previous projects. The nominal (kW) ratings of the battery, PV and backup generators are informed by the P5 – Islanding Design and Cost Analysis.

Since one of the performance objectives is to regulate terminal voltage levels, Volt-Var Control has been adopted as the default voltage control method for PV and battery inverters. Volt-Var control is regarded as an innovative voltage regulation method both in the literature and in industry standards [2]-[5]. This method has also been proposed in Project 4 as a potential effective way to improve hosting capacity.

Volt-Var control utilizes the strong coupling between voltage magnitude and reactive power level in a network. Therefore, deviations in local voltage levels can be compensated by a proportionate amount of change in reactive power output that can be injected or absorbed by PV and/or battery inverters. A simple illustration of the relationship between the voltage and the reactive power using this method is shown in below.

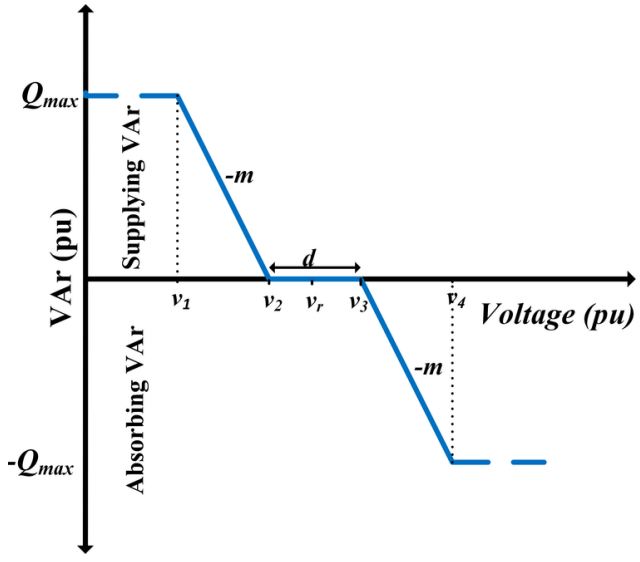

Figure 10. Volt-Var Control [6]

The m coefficient represents the droop setting that determines the change in reactive power with respect to the change in voltage magnitude. It should be noted that an optional dead-band d can be set to allow for acceptable voltage fluctuations.

Typical grid connected power electronic inverters can operate in four different modes, as illustrated in Figure 11. It should be noted that the active and reactive power output of an inverter is bound by its apparent power rating via the following relationship:

$$S^2 = P^2 + Q^2$$

where,

- S represents the apparent power (kVA),
- P represents the active power (kW),
- Q represents the reactive power (kVAr) of the inverter.

Therefore, because the reactive power output will be prioritised by the Volt-Var control, the active power output may decrease following a disturbance if the inverter has been operating close to its kVA capacity.

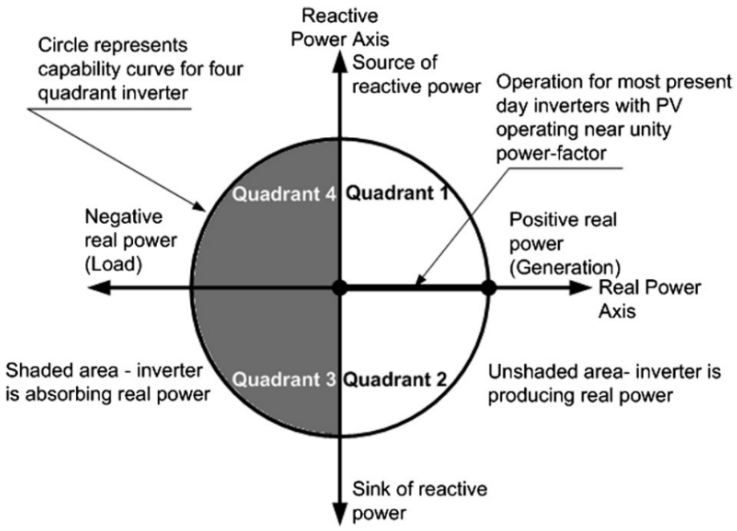

Figure 11. Four quadrant inverter operation [7]

While a battery inverter can utilize all four quadrants to absorb and inject both active and reactive power, a PV inverter can only utilize quadrant 1 and 2 since it cannot absorb any active power. A comparison of PV and battery inverter functions are summarised below.

	Active Power (P)	**Reactive Power (Q)**
PV Inverter	Inject only	Inject / Absorb
Battery Inverter	Inject / Absorb	Inject / Absorb

Furthermore, PV inverters are embedded with a Maximum Power Point Tracking (MPPT) algorithm which maintains the maximum possible active power output the PV system can generate. This places further limitation on the reactive power that a PV system can provide without compromising its active power output. Therefore, battery inverters are deemed more flexible and can play a more crucial role in achieving satisfactory dynamic performance across the network.

High-level block diagrams of the developed dynamic PV and battery system models are illustrated below.

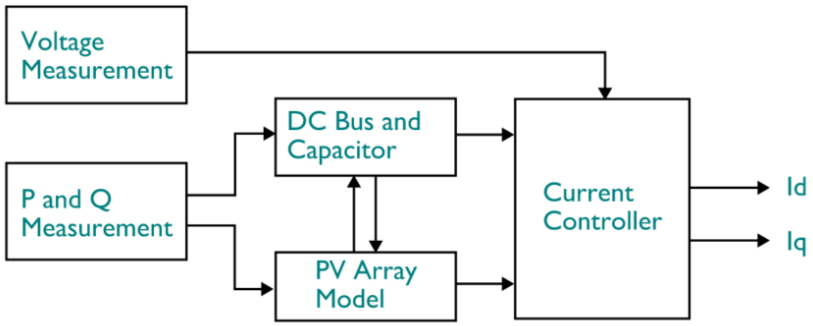

Figure 12. Block diagram of PV system dynamic model

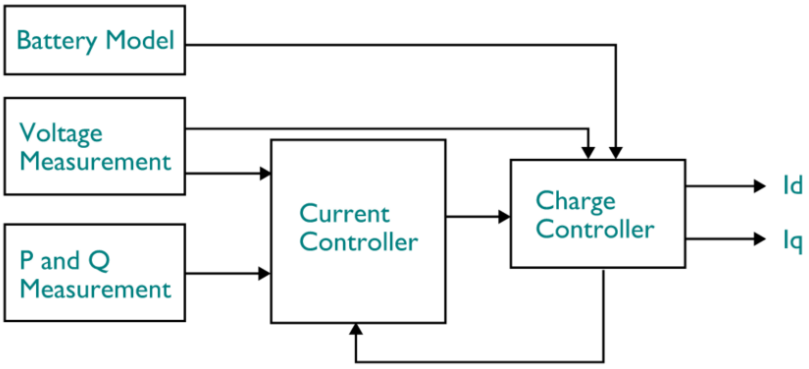

Figure 13. Block diagram of battery system dynamic model

Both PV and battery systems maintain their power output according to their predefined dispatch commands. When a voltage deviation is measured at the inverter terminal, the inverter immediately adjusts its reactive power output (overriding its dispatch command) according to its Volt-Var droop setting in order to curb the voltage deviation. If the voltage deviation is positive, the inverter absorbs reactive power from the network, and if the deviation is negative, the inverter injects reactive power into the network.

The amount of reactive power response is determined by the droop setting (reactive power gain). These droop setting values for all inverters have been set according to the Volt-Var response in AS/NZS 4777.2-2020.

All inverters in both Tarnagulla and Donald networks have been augmented with these dynamic models to enable investigation into both microgrids' capability to respond to a range of network disturbances. The network diagrams for both microgrids are shown in Figure 14 and

Figure 15.

The existing network model also contains nominal capacities of connected loads at each LV node. To enable analysis across a wide range of demand profiles, a transformer-smart meter data mapping has been obtained from Powercor. However, due privacy concerns, this mapping was provided for only about half the transformers in both towns. The unmapped transformers have been assumed to have a similar power flow pattern as the mapped ones, therefore, the load and generation profiles have been approximated from the known mapping to the unmapped transformers by scaling them according to their kVA ratings.

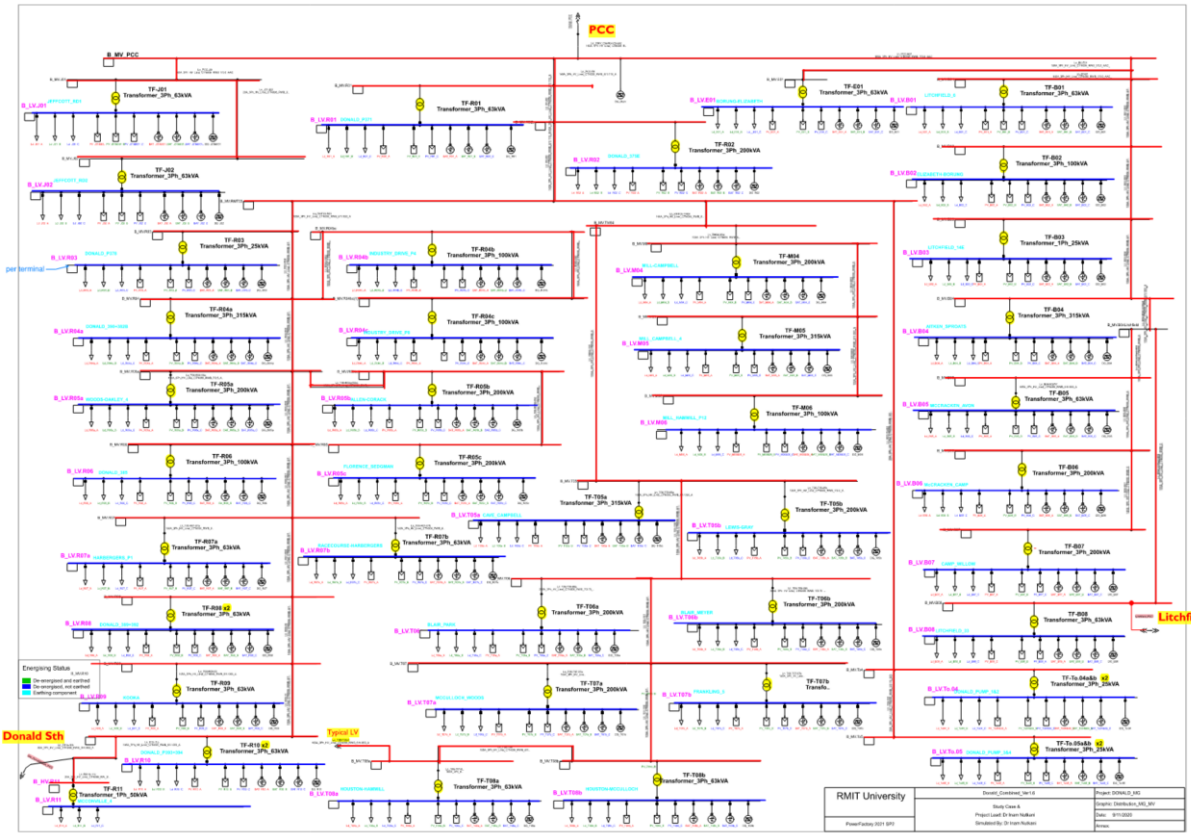

Figure 14. Donald Microgrid

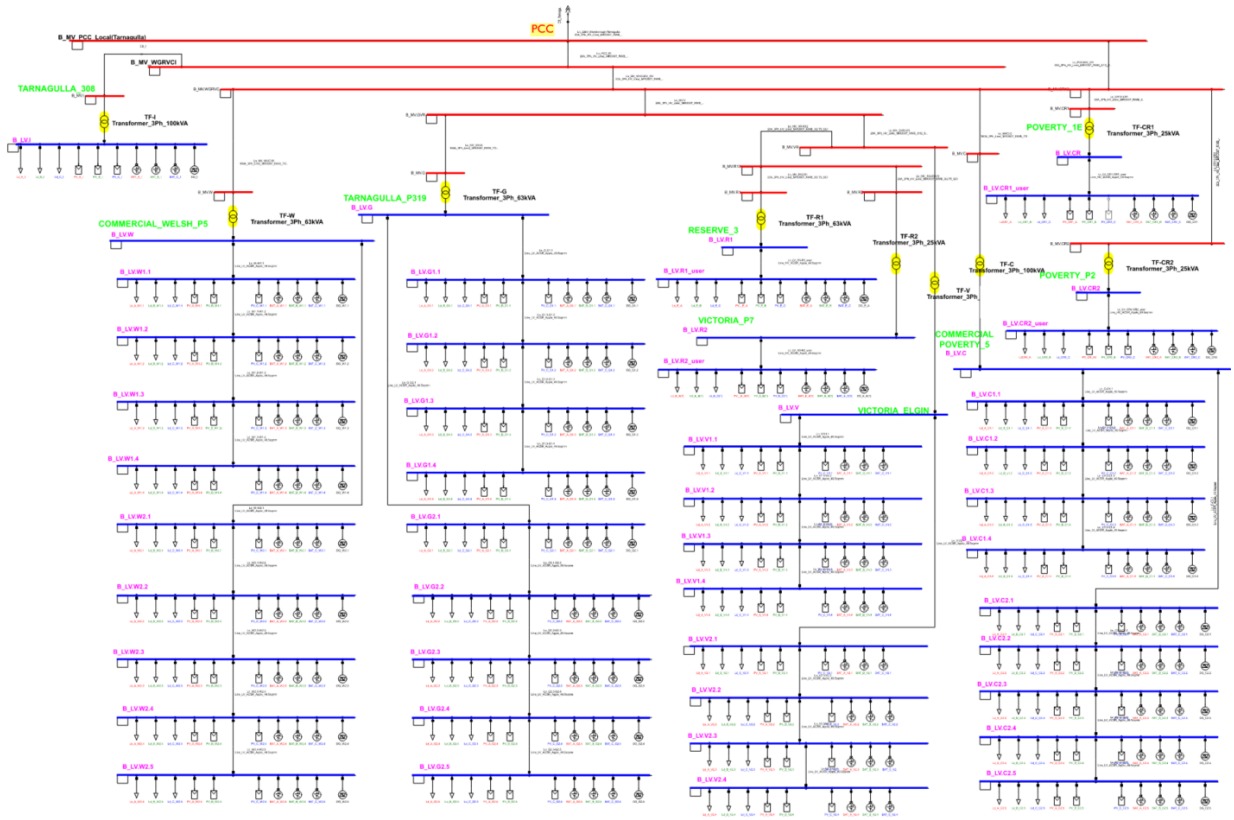

Figure 15. Tarnagulla Microgrid

2.4.2 Assessing the inverter's dynamic capability

The next step after developing the dynamic network models is to demonstrate their performance and capability as well as how they compare with the static models. It should be noted that the "static model" refers to the network Project 4 without any dynamic control capability, while "dynamic model" refers to the network augmented with dynamic inverter and control models that enable dynamic response to disturbances. For this demonstration, a range of probable network disturbances have been applied on a small section of Tarnagulla network:

First, a series of load and generation disturbances have been simulated to represent credible changes in load and generation:

- A combined 40 kW load connection across LV.W1 and LV.W2
- A combined 40 kW load disconnection across LV.W1 and LV.W2
- A combined 48 kW generation disconnection across LV.W1 and LV.W2
- A combined 24 kW generation reconnection across LV.W1
- A combined 24 kW generation reconnection across LV.W2

The above kW values have been derived from the smart meter data analysis that identified the largest load and generation ramping events. These values have been scaled up to account for the unmapped transformers, continuing growth in PV installations and load, and other unknowns. Further details can be found in the Disturbance Modelling section.

Similarly, the following fault events have been applied at an LV node (LV.W2.2)

- 20 ms 1Ph-G fault (Asym)
- 20 ms 2Ph fault (Asym)
- 20 ms 3Ph-N fault (Sym)
- 20 ms 3Ph-N-G fault (Sym)

The above events have been applied across two radial LV feeders connected to a 100 kVA transformer. Time-domain simulations have been performed with the static and dynamic network models using DIgSILENT Powerfactory, and the simulation results have been presented in the following section.

A performance comparison has been completed with the analysis of key similarities and differences. Figure 16 shows where the identified disturbances have been simulated and the corresponding measurements with respect to the network.

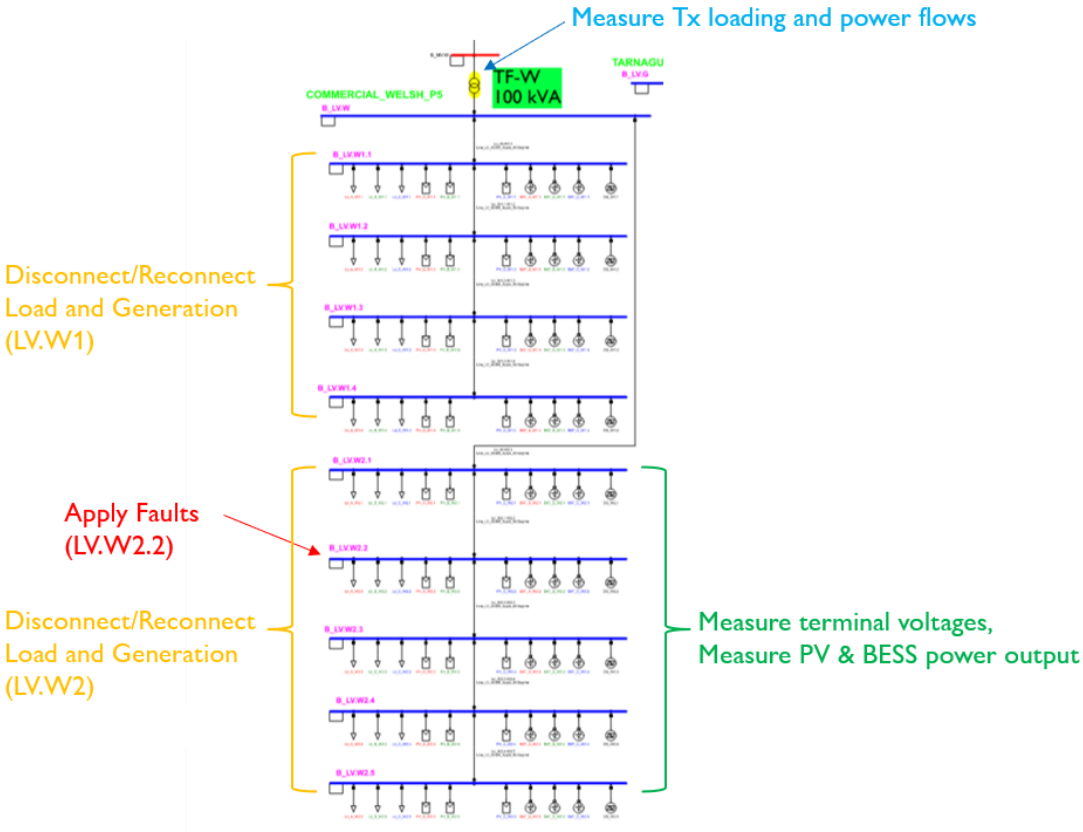

Figure 16. Network disturbance

2.4.3 Comparison of model performance

A. Load and generation events

The switching of a combined 40 kW load increases the overall loading across the LV feeders and causes a noticeable drop in voltage levels.

In the static model, the battery and PV inverters can be seen to maintain a constant power output following the voltage drop, however, a proportionate reactive power response can be observed in the dynamic model. This dynamic response aids in voltage recovery and results in a smaller net change in the voltage magnitude. A similar response is also observed following the load disconnection where the battery and PV reactive power output have returned to their initial values.

The loss and reconnection of PV generation resulted in noticeable oscillations in the static PV system output, yet these oscillations are not present with the dynamic model. The absence of oscillatory behaviour indicates stronger stability.

Since the reactive power to mitigate voltage changes is provided locally by the dynamic model, the power draw from the upstream network has reduced, which in turn reduces the loading on the transformer. An approximate 10% less loading can be observed in the dynamic model. In higher utilizations this also reduces the risk of overloading.

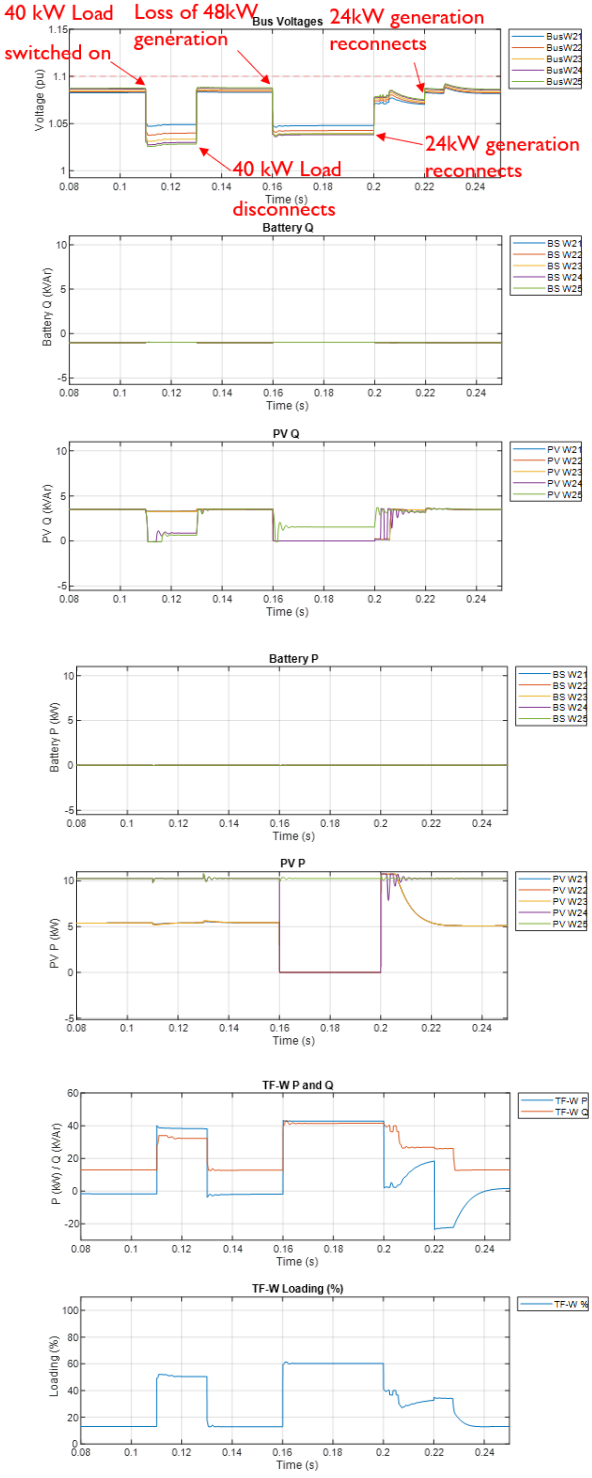

Figure 17. Dynamic Model

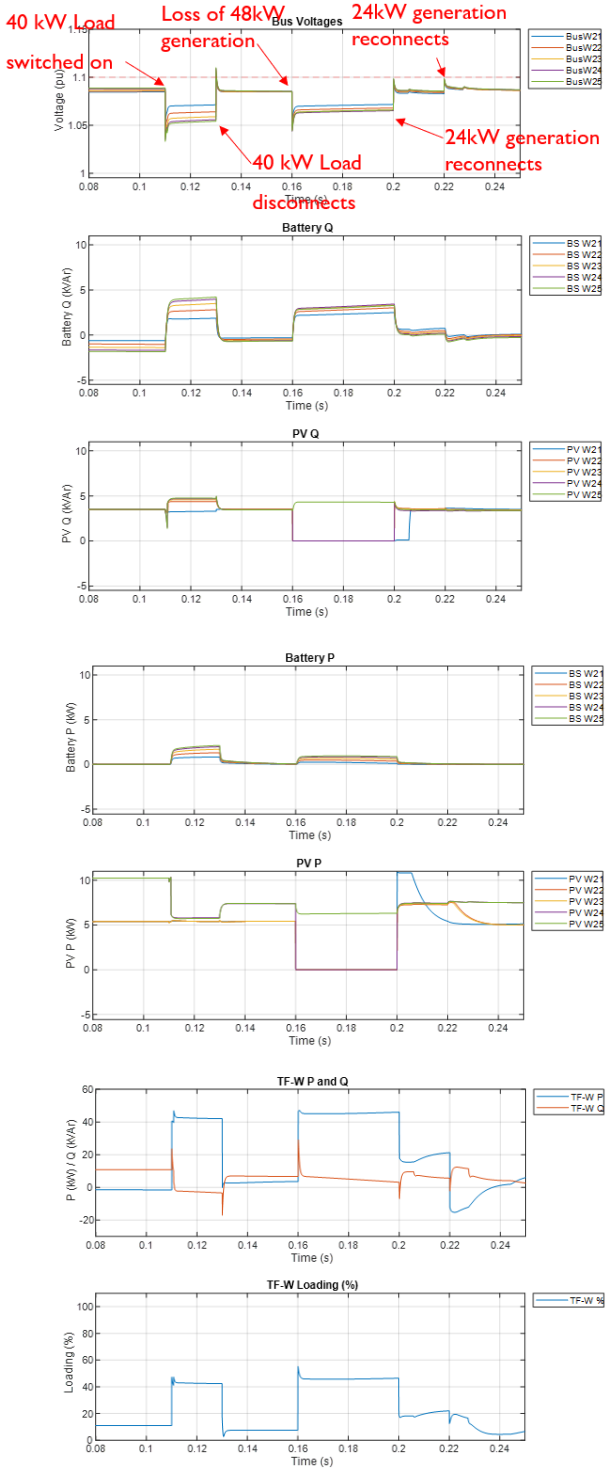

Figure 18. Static Model

B. Fault events

In the static model, severe oscillations are observed following each fault clearance. These oscillations, if appeared on a larger scale, can jeopardize the overall network stability and disrupt supply continuity. On the other hand, the dynamic model exhibits little to no oscillations and maintains stable behaviour following each fault. This is one of the key differences between the static and dynamic models in achieving post-fault stability.

It can also be observed that the dynamic inverter models feed the faults with short-circuit power within their maximum rating. This reduces the amount of fault current draw from the upstream network, resulting in lower loading of lines and network assets.

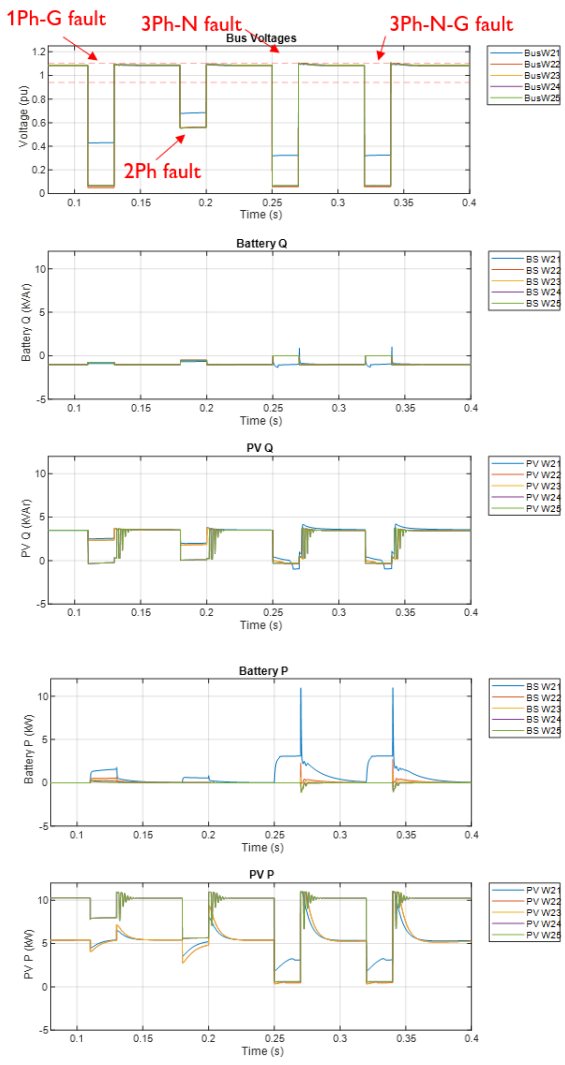

Figure 19. Static Model

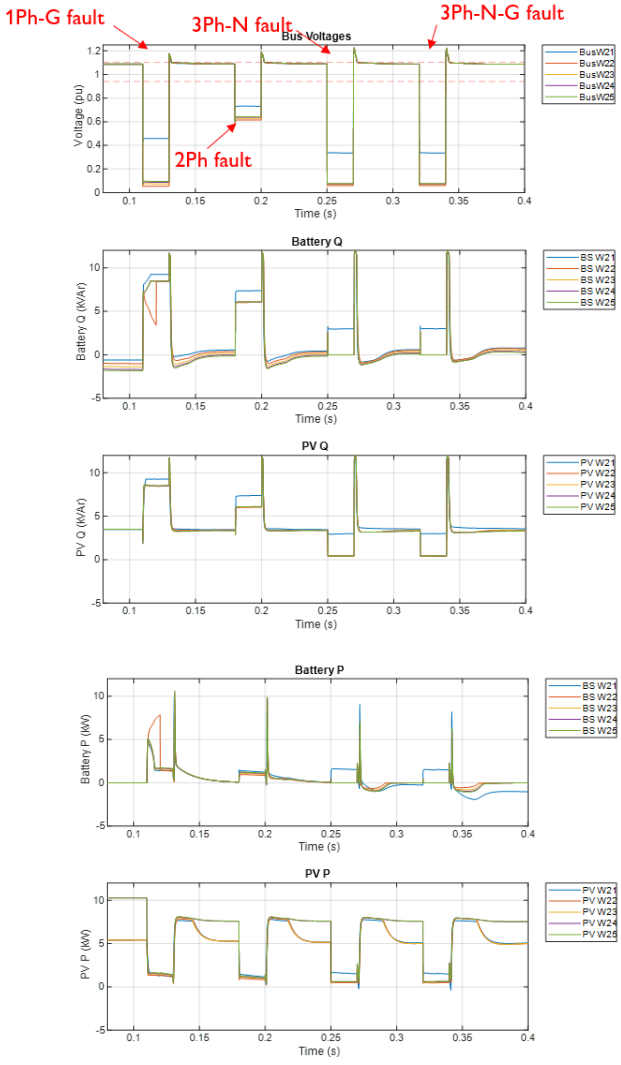

Figure 20. Dynamic Model

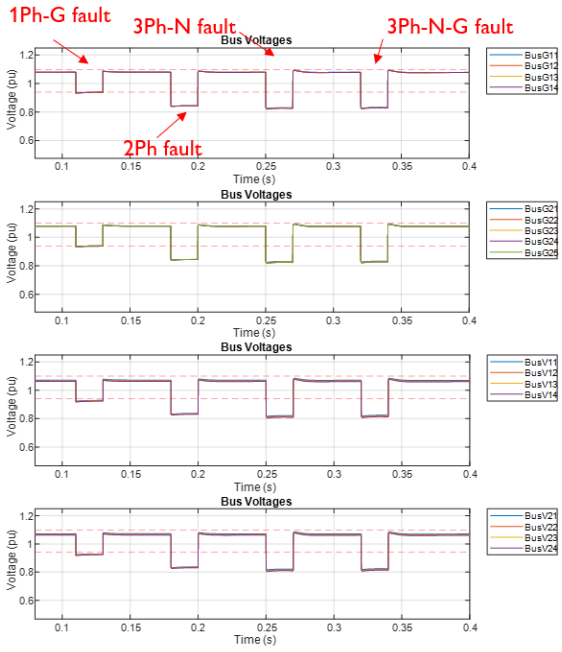

Figure 21. Static Model

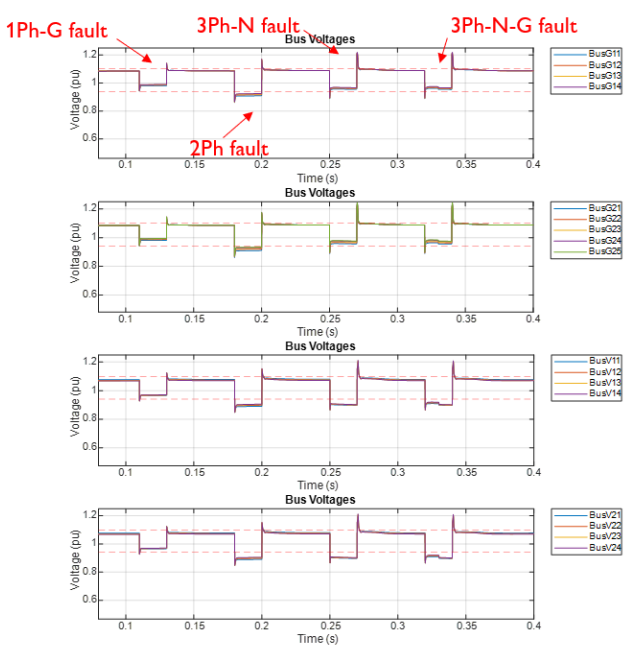

Figure 22. Dynamic Model

The above figures show the voltage levels in remote LV nodes that are connected to different transformers across the network. In the dynamic model, the voltage levels are observed to remain within the operating band or slightly below the lower limit, whereas in the static model, most node voltages have fallen significantly below the lower limit.

The developed dynamic models are shown to be capable of adequately responding to a range of disturbances.

In summary:

- Voltage deviations can be reduced by local dynamic reactive power support. This can reduce the risk of violating the voltage operating interval.
- Transformer loading can be reduced by local response to disturbances. This can reduce the risk of network asset failure by avoiding operation above the nominal thermal rating.
- Inverters can maintain stable operation during and following a disturbance, which is critical in post-fault voltage recovery, and therefore, the overall supply reliability.

2.4.4 Protection device considerations

As a part of the Bushfire Safety Program, Charlton and Maryborough zone substations have been equipped with Rapid Earth Fault Current Limiters (REFCL) that are capable of detecting single-phase-to-ground faults across the feeder. These zone substations supply the feeders to which Donald and Tarnagula are connected, respectively. Therefore, to be able to simulate the correct operation of REFCLs and their impact on both microgrids, the single-phase-to-ground fault detection, clearance and associated time delays have been modelled in line with the REFCL operation and Electricity Safety Regulations[1]. According to these regulations, in the event of a single-phase-to-ground fault on a polyphase line, the system must:

a. *reduce the voltage on the faulted conductor in relation to the station earth when measured at the corresponding zone substation for high impedance faults to 250 volts within 2 seconds; and*

b. reduce the voltage on the faulted conductor in relation to the station earth when measured at the corresponding zone substation for low impedance faults to
i. 1,900 volts within 85 milliseconds; and
ii. 750 volts within 500 milliseconds; and
iii. 250 volts within 2 seconds

In this project low impedance single-phase-to-ground faults and low impedance symmetrical faults are examined. For single-phase-to-ground faults, the REFCL protection was not explicitly modelled, but its response was imitated by adding an impedance to reduce the voltage as per the requirement (b.i) of the Electricity Safety Regulations[1]. The fault is considered to be temporary and self-cleared after 10 ms. For symmetrical faults, a low impedance self-clearing fault is implemented for 150 ms without any protection tripping device in place.

2.5 Equivalent network topology for capacity adequacy assessment

This work also aims to evaluate how the supply availability from the upstream grid may impact the overall capacity adequacy of Donald and Tarnagulla area community, with consideration of the potential impact of bushfire on the transmission feeder online status that connecting the upstream grid and the two rural area communities. Capacity adequacy refers to the existence of sufficient generation and transmission facility within the community to cover the system demand [8].

In this section, the connection topology of Donald and Tarnagulla community with upstream grid and the equivalent network model topology that will be used for capacity adequacy assessment for these two areas are introduced.

2.5.1 Donald community connection with upstream grid

According to the operation diagram provided by Powercor, Donald area network is connected to the zone substation “CTN” via the 22kV distribution feeder CTN006.

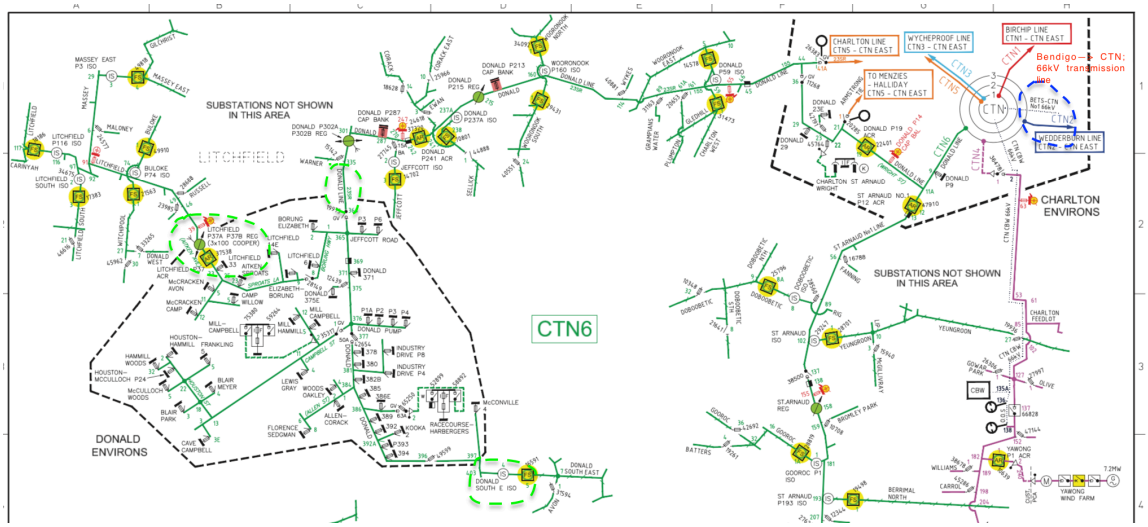

Figure 23. Operation diagram of Donald area network [9]

[1]*Electricity Safety (Bushfire Mitigation) Regulations 2013, S.R. No. 62/2013 Version incorporating amendments as at 27 June 2020*

It can be seen in Figure 23 that there are six 22kV distribution feeders connected to the zone substation "CTN". There are five areas that are connected along the distribution feeder CTN006, including: Feeder B, Feeder A, Donald Area, Litchfield, and Donald South. The zone substation "CTN" is connected to the upstream terminal station "BETS" located at Bendigo via a 66kV transmission line, while the terminal station "BETS" is connected to the 220kV transmission network in Victoria. The geographical and network topology of the 66kV BETS-CTN transmission line is shown in Figure 24.

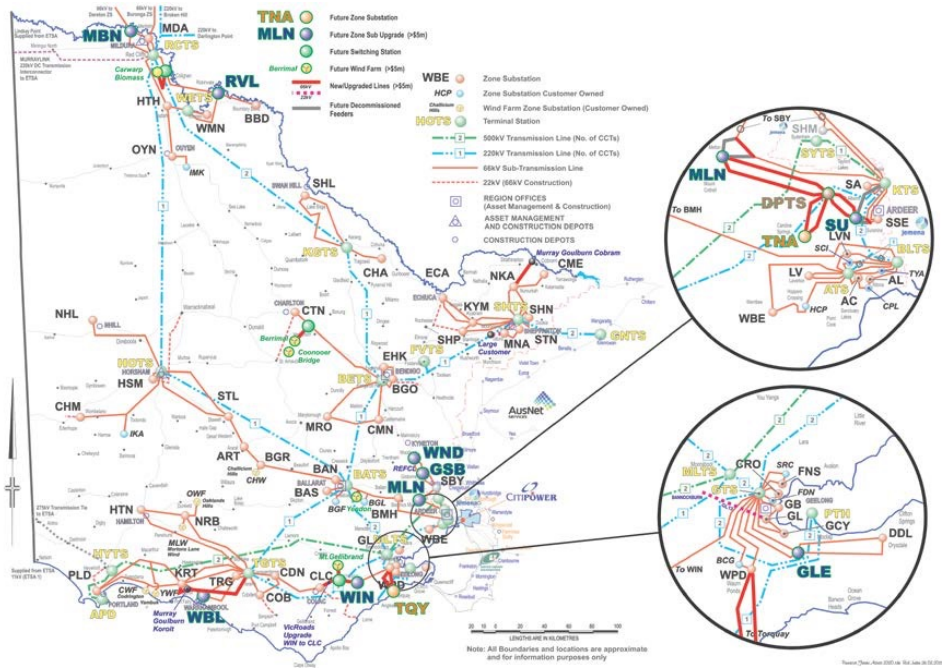

Figure 24. 66kV BETS-CTN and BETS-MRO transmission line topology [10]

As can be seen from Figure 24, the 66kV BETS-CTN transmission line passes two climatic zones of ESCI project [11], which includes "***Coonooer Bridge***" and "***Bendigo***". The map of ESCI climatic zones in Victoria is shown in Figure 25. The bushfire risk information from these two climatic zones will be used as the input to model the impact of bushfire risk on transmission line online status, which is introduced in the next chapter.

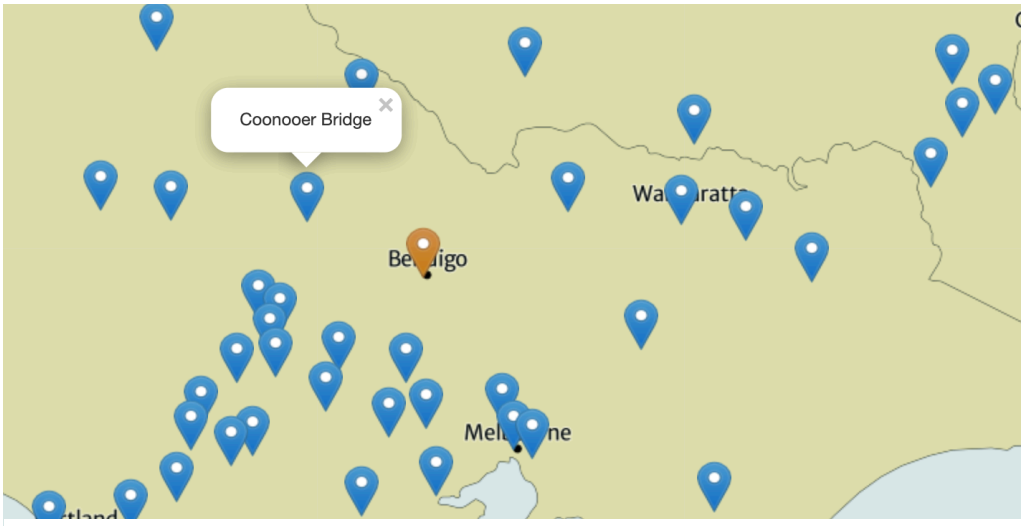

Figure 25. ESCI Climatic Zones Map in Victoria [11]

2.5.2 Tarnagulla community connection with upstream grid

According to the operation diagram provided by Powercor, Tarnagulla area network is connected to the zone substation “MRO” via MRO feeder 007.

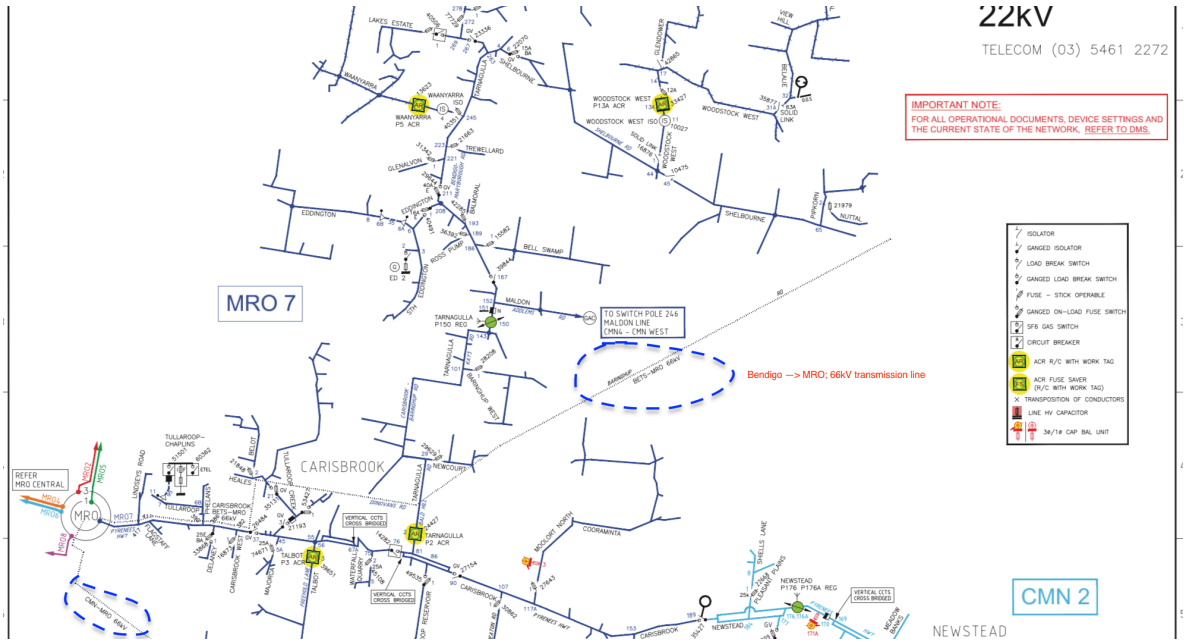

Figure 26. Operation Diagram of Tarnagulla Area Community [12]

It can be seen in Figure 26 that there are seven 22kV distribution feeders connected to the zone substation “MRO”. The zone substation “MRO” is connected to upstream terminal station “BETS” located at Bendigo via a 66kV transmission line, as shown in Figure 24. Also, it can be noted that the zone substation “MRO” is also connected to the adjacent zone substation “CMN” via a 66kV CMN-MRO transmission line, while the zone substation “CMN” is also connected to the upstream terminal station “BETS” via a 66 kV BETS-CMN transmission line, as shown in Figure 24. In this light, the Tarnagulla area community can be supplied via two pathways:

1) 66kV BETS-MRO transmission Line and MRO feeder 007,

2) 66kV BETS-CMN transmission line, 66kV CMN-MRO transmission line and MRO feeder 007.

All of the three 66kV transmission lines locate within the ESCI climate zone “**Bendigo**”. According to the Powercor’s annual distribution network planning report [13], the Tarnagulla area may be solely supplied by BETS-MRO transmission line. However, the sub-transmission line loop could be used as a backup contingency plan when BETS-MRO line is unavailable. Therefore, both BETS-MRO transmission line and the BETS-CMN-MRO loop are considered in the equivalent network model for Tarnagulla area for capacity adequacy assessment.

2.5.3 Equivalent network topology of Donald and Tarnagulla network

The objective of the capacity adequacy assessment is to determine whether there is sufficient generation and transmission capacity to supply the community’s demand. In this light, only the transmission line, 66kV/22kV substation transformer and the distribution feeder are modelled in the *equivalent network topology of Donald and Tarnagulla area, without modelling the internal distribution* network. According to Project 5 report, different islanding points are identified along the distribution

feeders in these two areas. The equivalent network topology of Donald and Tarnagulla network and the potential islanding points are shown in Figure 27.

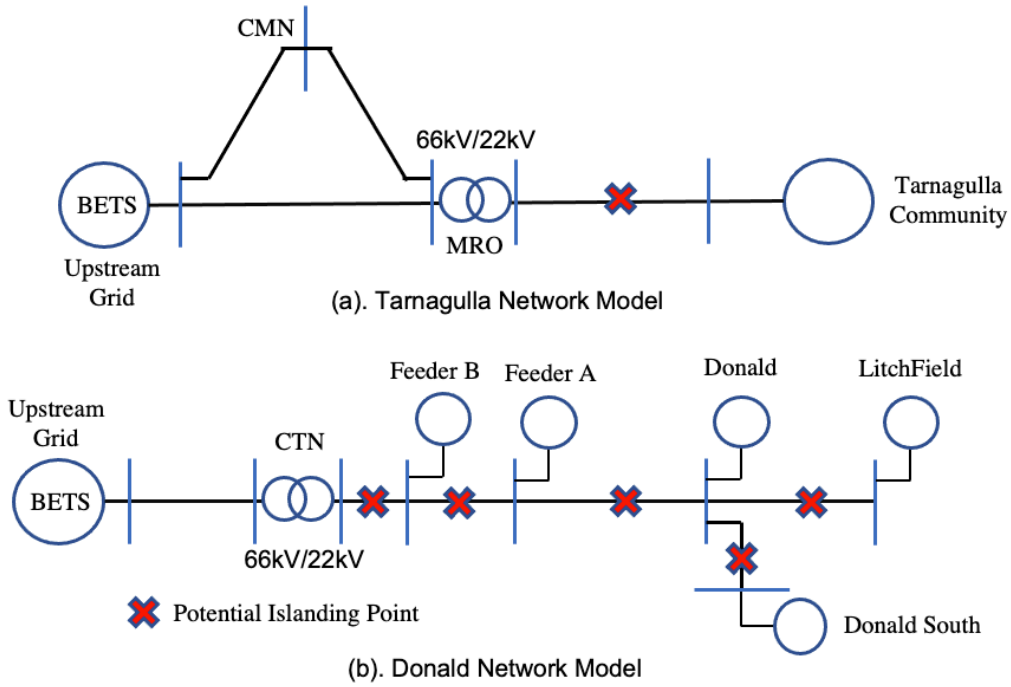

Figure 27. Equivalent network topology of Donald and Tarnagulla area for capacity adequacy assessment

2.6 Summary

In this chapter, the network modelling and necessary input data analysis is introduced. The smart meter and feeder data are processed for the development of dynamic simulation model and the assessment of capacity adequacy in Donald and Tarnagulla area. It should be highlighted that the smart meter time series data consists of import/export data for each NMI are conversed into demand / generation time series, which can enable better understanding the dispatch and coordination between battery and solar PV. Then, dynamic models of the Donald and Tarnagulla microgrid networks are developed that will enable simulating and assessing the impacts of various dynamic and transient events across both networks in grid-connected and off-grid modes. The performances of static model and the developed dynamic model are compared via a couple of demonstration case studies. In the end, the equivalent network models in Donald and Tarnagulla area considering their connection with upstream grid are introduced for capacity adequacy assessment and further bushfire impact analysis.

3 Disturbance modelling

In this chapter, the modelling and analysis for disturbances are introduced, which include the extreme demand/generation ramping events forecast, the failure probability of network components, and the impact modelling of bushfire risk on the supply availability from upstream grid.

3.1 Extreme event identification from smart meter data

This section provides analysis and visualisation of extreme events identified in the smart meter data. Only those time series for which we both (i) have time series data and (ii) know the transformer mapping are included in this analysis.

The insights from this project may slightly deviate from datasets used in previous projects (in particular Projects 4 and 5). The reason for this is that we have been provided additional data (such as transformer mappings) that were not considered in previous projects, which may lead to us including a slightly different set of NMIs in the analysis. We have also conducted the conversion from import & export time series to demand & generation time series, as detailed in Section 2.1. However, we have found that our results largely match those used in previous projects. For example, our estimated peak net demand for Donald is 2.41 MW, while in Project 5, a value of 2.36 MW was used; our estimated peak net demand for Tarnagulla is 0.16 MW, while in Project 5, a value of 0.17 MW was used.

Following the conversion of import and export time series to demand and generation time series (Section 2.1), and using the mapping of NMIs to transformers that was made available, it was possible to generate demand and generation time series at the level of (i) each town (Donald and Tarnagulla), (ii) each transformer, and (iii) each individual customer. For each level, a number of extreme events could be identified, such as:

- Maximum and minimum demand
- Maximum and minimum generation
- Maximum and minimum net demand (sum of demand and generation)
- Zero or net negative demand (times where the towns as a whole were generating more than consuming)
- Ramp rates – both ramp up and down – across either 30 minute or 1-hour intervals – for demand, generation, and net demand

3.1.1 Donald and Tarnagulla towns

The distributions of demand, generation, net demand, and ramps for each town are shown in Figure 28[4]. As can be seen, Tarnagulla has a significant number of net export events (generation exceeds demand). Donald has much fewer, but there are a number of intervals in which Donald is net exporting as well. Example data for some individual days are shown for Tarnagulla in Figure 29 and Figure 30. In both figures, any intervals that contain an extreme value (as per the list above) are highlighted with vertical red lines. In Figure 29, it can be seen that maximum (or minimum) demand, generation, or net demand does not typically align across all transformers. In other words, different transformers may experience extreme events at different times, due to diversity of load at each transformer. In Figure 30, it can be seen that the same is true for ramps – these do not typically align across transformers either. As a result, a transformer-by-transformer analysis may be valuable.

[4] For generation, this figure only shows intervals having > 5kW, to avoid the y-axis being skewed by the large number of zero-generation intervals

3.1.2 Transformer level analysis

A more detailed transformer-by-transformer analysis, showing distribution of net demand values (positive or negative) for the full year for each individual transformer are shown in Figure 31(Donald) and Figure 32 (Tarnagulla). Vertical dotted red lines indicate transformer ratings, which do not appear to be exceeded at any time, for any transformer.

Donald, having a much larger number of transformers, displays much greater diversity in terms of the shape of net demand distribution for its transformers. This means it may be worth exploring forecasting models that forecast net demand for each transformer in Donald individually.

Distributions of ramp rates (again, defined as difference in demand between one interval and the next) are shown in Figure 33 (Donald) and Figure 34 (Tarnagulla). Also here, there is significantly greater diversity across transformers in Donald.

	Donald	Tarnagulla
Demand	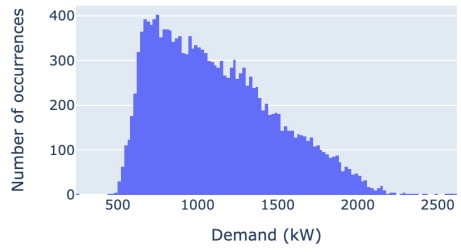	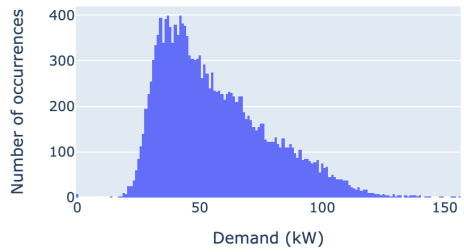
Generation (absolute values)	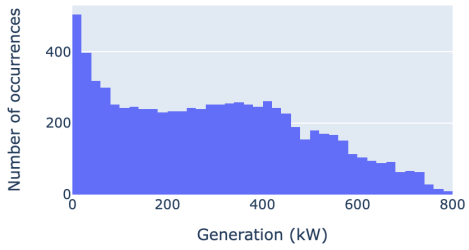	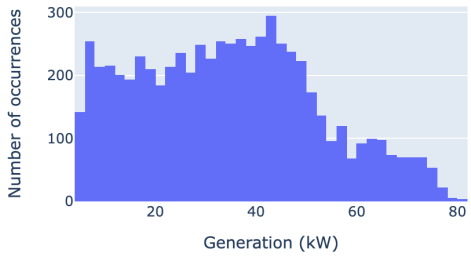
Net demand (sum of demand and generation)	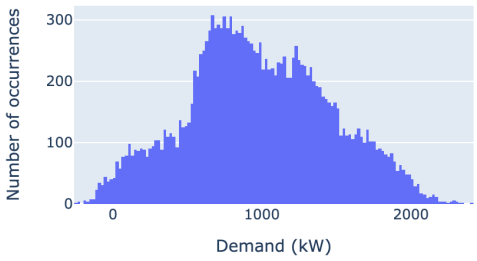	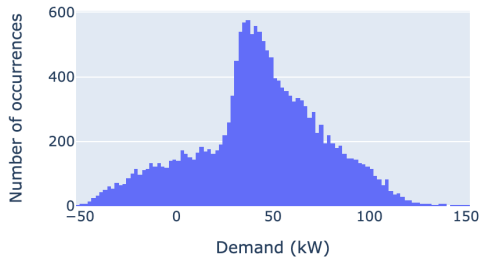
Ramps (differences between consecutive intervals)	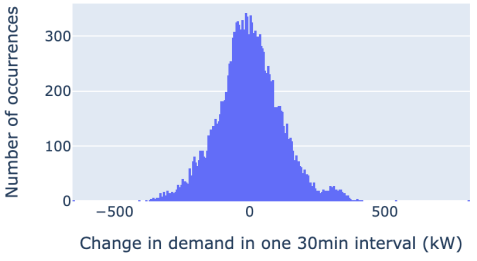	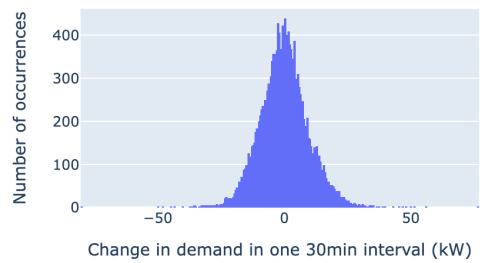

Figure 28. Distribution of demand, generation, net demand, and ramps for Donald and Tarnagulla towns

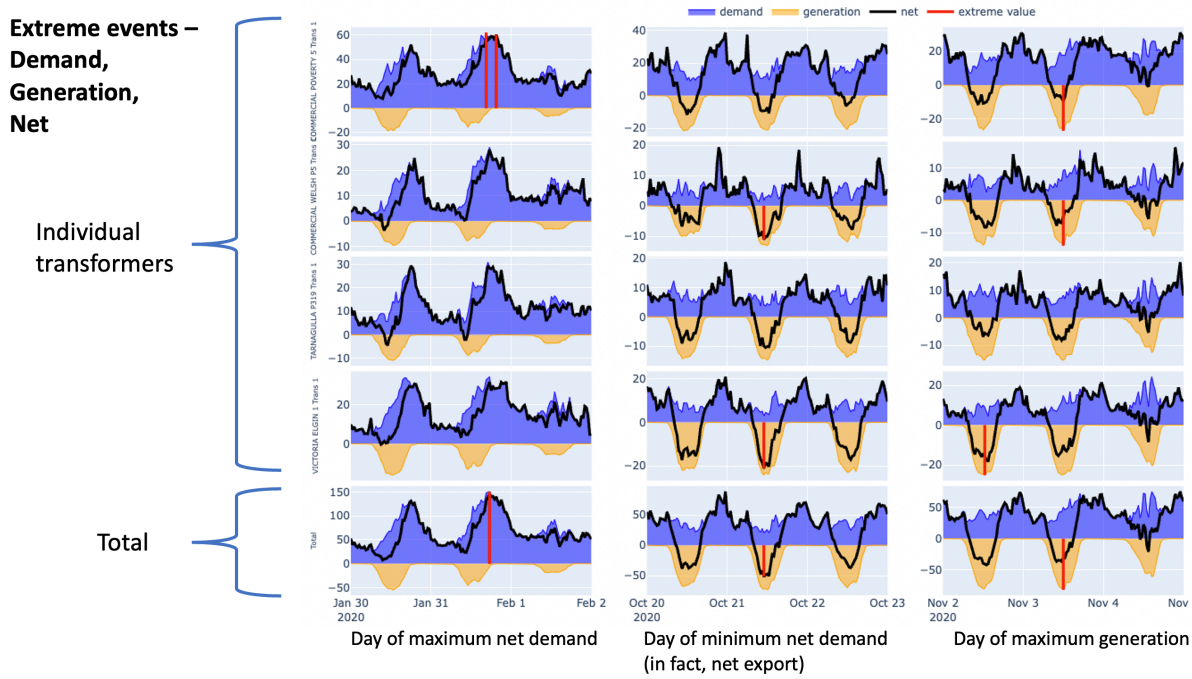

Figure 29. Extreme values - Tarnagulla - demand, generation, and net demand

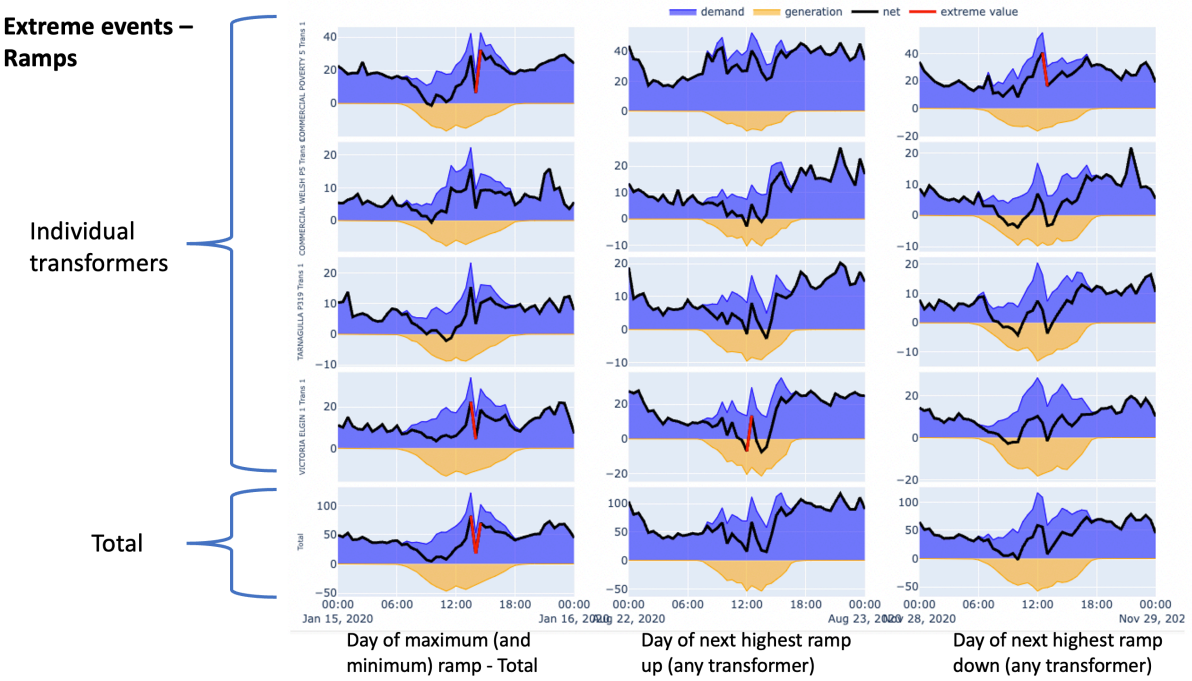

Figure 30. Extreme values - Tarnagulla - ramp rates

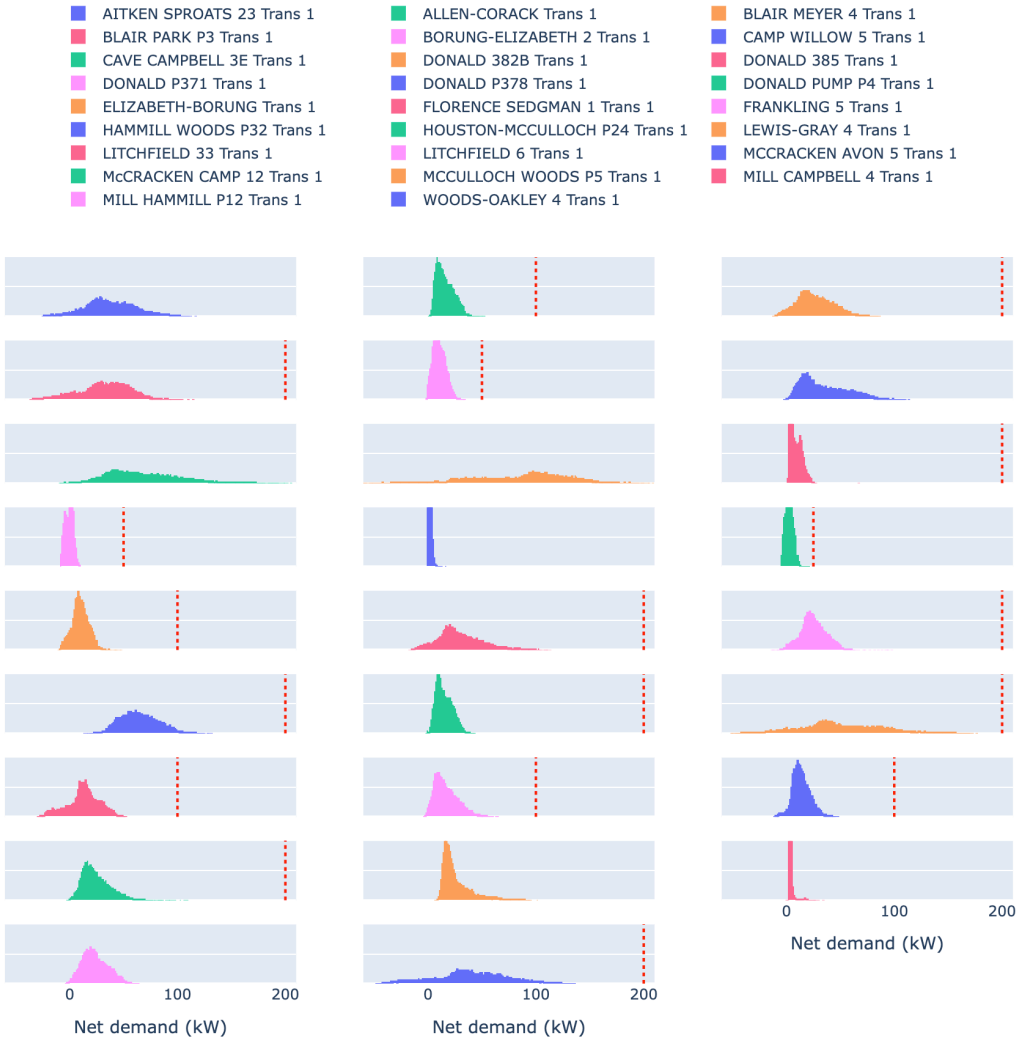

Figure 31. Distribution of net demand for transformers in Donald.

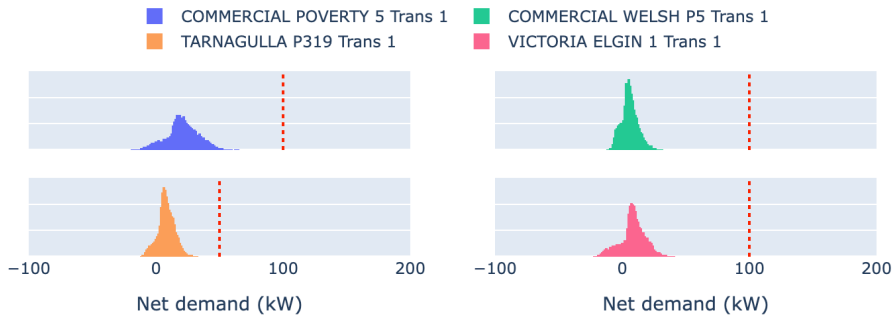

Figure 32. Distribution of net demand for transformers in Tarnagulla

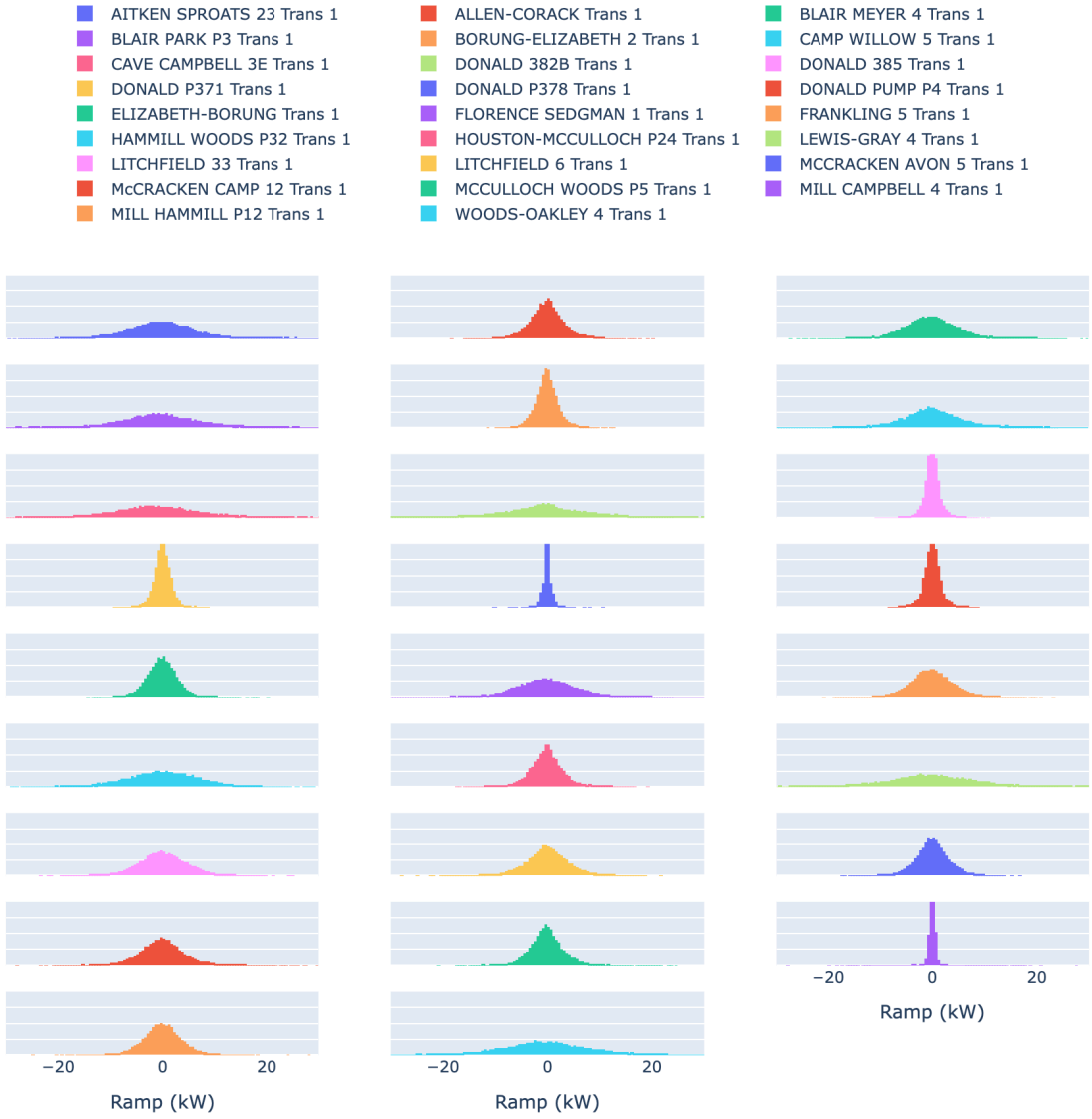

Figure 33. Distribution of ramps for transformers in Donald

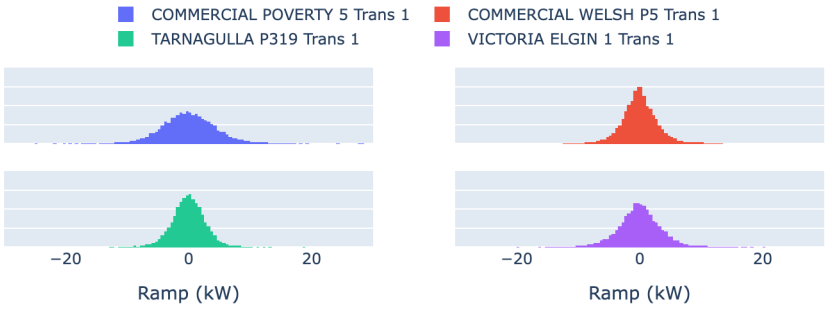

Figure 34. Distribution of ramps for transformers in Tarnagulla

3.1.3 Continuous and discrete disturbances

A range of credible network disturbances have been selected to test the resilience of each microgrid. These disturbances can be broadly categorised into:

- **Continuous disturbances**, e.g., dynamic changes in PV generation or customer demand
- **Discrete disturbances**, e.g., transient faults, islanding, loss of a network component

The continuous disturbances have been identified based on the largest changes in load and generation levels that are derived from the smart meter data analysis. The largest ramp values on transformer level across 30 min intervals are summarised below:

Donald		**Tarnagulla**	
Largest load ramp up	: 60.27 kW at TF-T05a[1]	Largest load ramp up	: 24.33 kW at TF-C[3]
Largest load ramp down	: 63.70 kW at TF-T05a[1]	Largest load ramp down	: 24.74 kW at TF-C[3]
Largest gen. ramp up	: 43.38 kW at TF-R04a[2]	Largest gen. ramp up	: 10.92 kW at TF-V[4]
Largest gen. ramp down	: 35.18 kW at TF-R04a[2]	Largest gen. ramp down	: 8.26 kW at TF-V[4]
[1]CAVE CAMPBELL 3E, [2]DONALD 382B		*[3]COMMERCIAL POVERTY 5, [4]VICTORIA ELGIN 1*	

The discrete disturbances include an islanding event, tripping of a transformer and short-circuit faults.

The disturbance events and the network locations where they are applied are listed below.

ID	Disturbance	Mode	Location
D1	Load Ramp Up	Grid connected	Largest transformer in the microgrid
D2	Generation Ramp Down	Grid connected	Largest transformer in the microgrid
D3	Islanding Event	Grid connected	Point of Common Coupling (PCC)
D4	Transformer Loss	Grid connected	Largest transformer in the microgrid
D5	1Ph-G Fault (10ms) (Asym)	Grid connected	Mid-point across the MV feeder
D6	3Ph-N-G Fault (150ms) (Sym)	Grid connected	Largest transformer in the microgrid
D7	Transformer Loss	Off-grid	Point of Common Coupling (PCC)

Table 3-1a: Network Disturbances

The following plots show the maximum generation and load ramping values for the mapped transformers for each town.

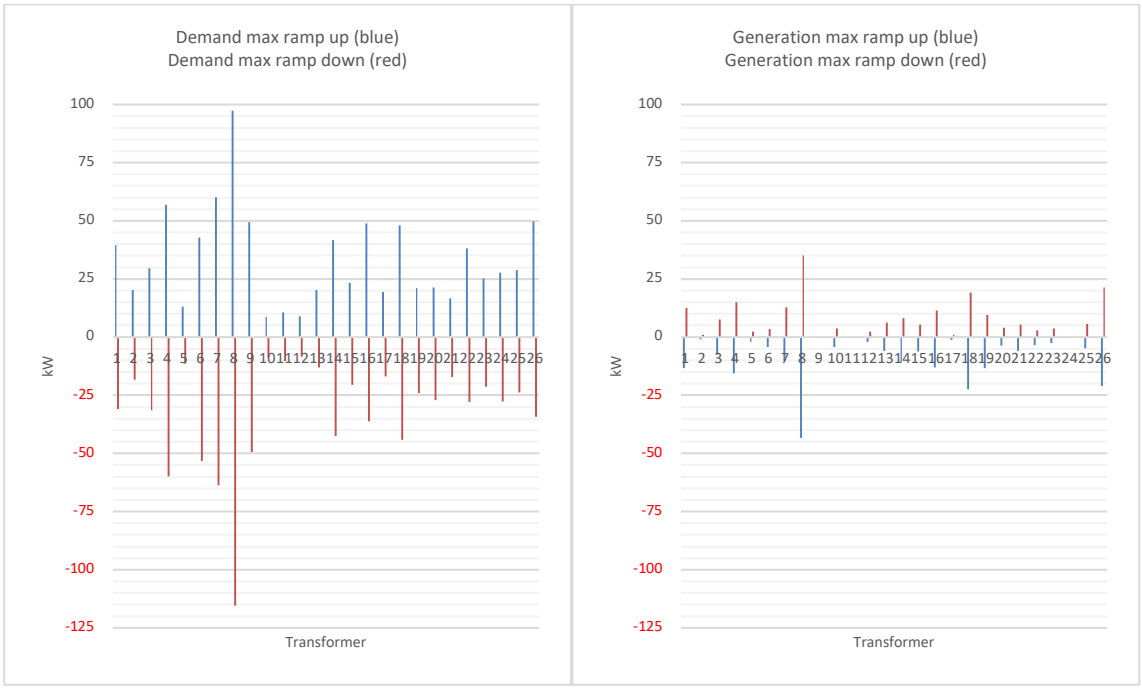

Figure 35. Donald Ramping Events

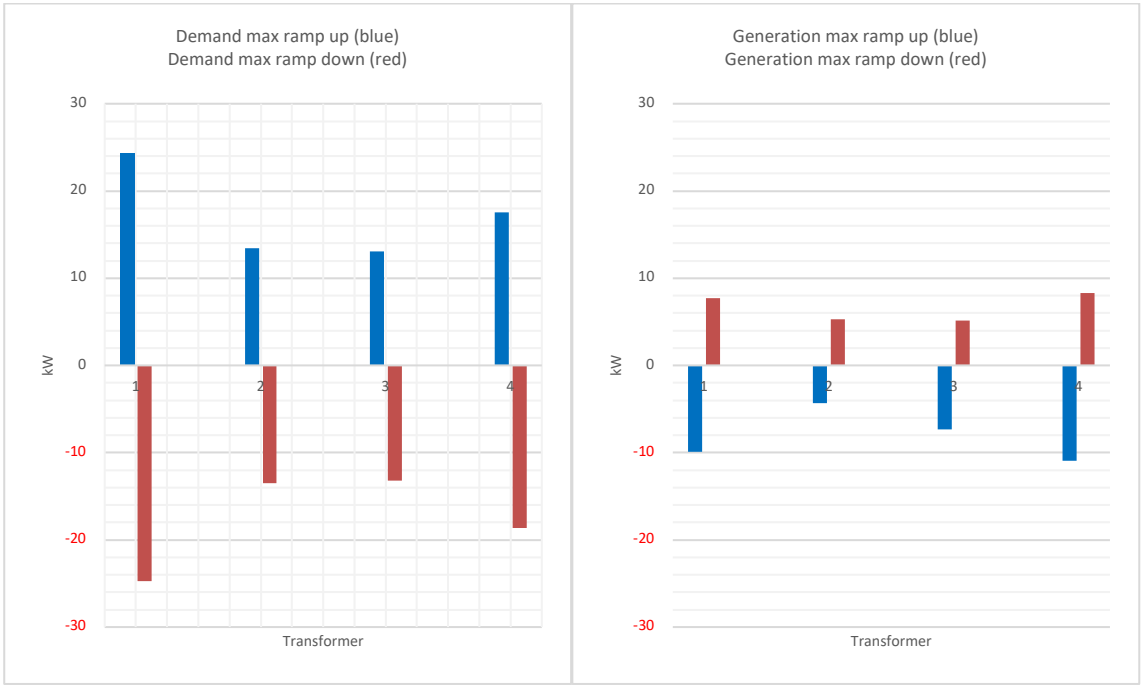

Figure 36. Tarnagulla Ramping Events

Transformer legend:

No	Tx Name (Donald)
1	AITKEN SPROATS 23
2	ALLEN-CORACK
3	BLAIR MEYER 4
4	BLAIR PARK P3
5	BORUNG-ELIZABETH 2
6	CAMP WILLOW 5
7	CAVE CAMPBELL 3E
8	DOLD 382B
9	DOLD 385
10	DOLD P371

No	Tx Name (Donald)
11	DOLD P378
12	DOLD PUMP P4
13	ELIZABETH-BORUNG
14	FLORENCE SEDGMAN 1
15	FRANKLING 5
16	HAMMILL WOODS P32
17	HOUSTON-MCCULLOCH P24
18	LEWIS-GRAY 4
19	LITCHFIELD 33
20	LITCHFIELD 6

No	Tx Name (Donald)
21	MCCRACKEN AVON 5
22	McCRACKEN CAMP 12
23	MCCULLOCH WOODS P5
24	MILL CAMPBELL 4
25	MILL HAMMILL P12
26	WOODS-OAKLEY 4

No	Tx Name (Tarnagulla)
1	COMMERCIAL POVERTY 5 Trans 1
2	COMMERCIAL WELSH P5 Trans 1
3	TARNAGULLA P319 Trans 1
4	VICTORIA ELGIN 1 Trans 1

3.2 Forecasting

3.2.1 Point forecasts

A number of forecasting models were implemented and evaluated, for both demand and generation, for each of Donald and Tarnagulla. The forecasting models included:

1. **Periodic persistence**, also referred to sometimes as "seasonal naïve". This is a very simple model often used as a baseline for comparison with advanced models. In a periodic persistence model, the forecasted period takes on the same values as the preceding period; in other words, "tomorrow will be the same as today".
2. **SARIMA:** This is a standard statistical model often used in the forecasting community. It combines auto-regressive (AR) and moving-average (MA) models into a single forecasting approach. Since both demand and generation have obvious daily seasonality, the model is extended from standard ARIMA to SARIMA. Following an extensive evaluation of model parameters, the following type of model was chosen: ARIMA(1,0,1)(1,0,0)[48] (seasonality of 48 being due to half-hourly intervals).
3. **Multiple linear regression:** This is a supervised machine learning model in which the output is modelled as a linear function of multiple inputs.
4. **Support vector regression:** This is a supervised machine learning model that tries to find the optimal hyperplane amongst a given set of inputs that can be used to predict the output.
5. **Random forest regression:** This is a supervised machine learning model in which an ensemble of classifiers (decision trees) is used to determine the most likely output, given a set of inputs.

The input features for generation forecasts included weather data (temperature, pressure, humidity, wind speed, and cloud cover) – see Section 2.2.

The input features for demand forecasts included the same weather data, but additionally included features that might help to explain demand, such as time lagged variables (same interval [1, 2, 7, 14] days previously), day of week, and week of year.

When generating historical forecasts for forecast model evaluation, only true forecasts of input features were used; in other words, for any forecast no information was provided that would not have been available at the time the forecast was generated. All forecasts compared to date consist of half-hourly intervals, 24 hours ahead. All forecast evaluations are averaged over all available days in the dataset.

The metrics used for forecast evaluation are mean absolute error (MAE) and root mean square error (RMSE).

The full forecast results are provided in Figure 37(a). For demand forecasting, the statistical SARIMA model performs poorly. This may be due to the fact that such models perform best when there are highly regular patterns in the data, and demand is often not this regular. For generation forecasting, multiple linear regression and support vector regression perform poorly. This may be due to the fact that there is an inherently non-linear relationship between some input variables and generation (for example, temperature).

Across both demand and generation, and for both Donald and Tarnagulla, random forest regression provides the lowest errors. This forecasting model will be used for all subsequent analyses.

The impact of converting import and export datasets into demand and generation datasets (as discussed in Section 2.3) was also explored and Figure 37(b) shows the results. As can be seen, when forecasting import and export individually (and then aggregating), a forecast improvement of 5.29% is possible,

versus only forecasting net demand directly. However, when forecasting demand and generation individually (and then aggregating), a forecast improvement of 6.45% is possible. Finally, when forecasting demand and generation for each transformer individually (and the aggregating), a forecast improvement of 11.3% is possible. This is likely due to the large diversity of transformers, as discussed in Section 3.1.2.

Some examples of forecasts generated using random forest regression are shown in Figure 38 (demand) and Figure 39 (generation).

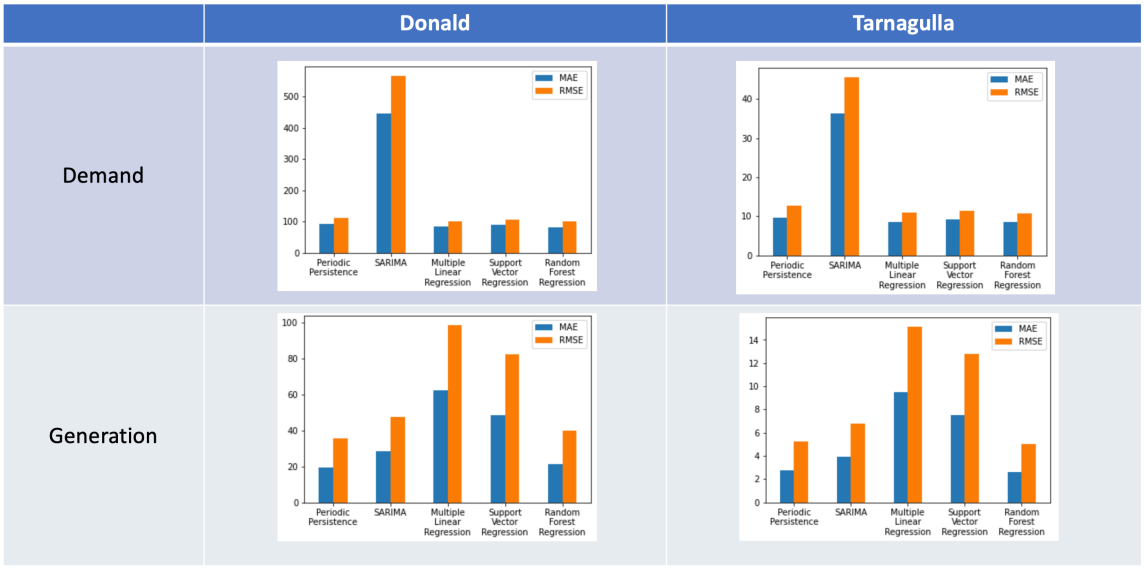

(a) Forecasting results for all forecasting models

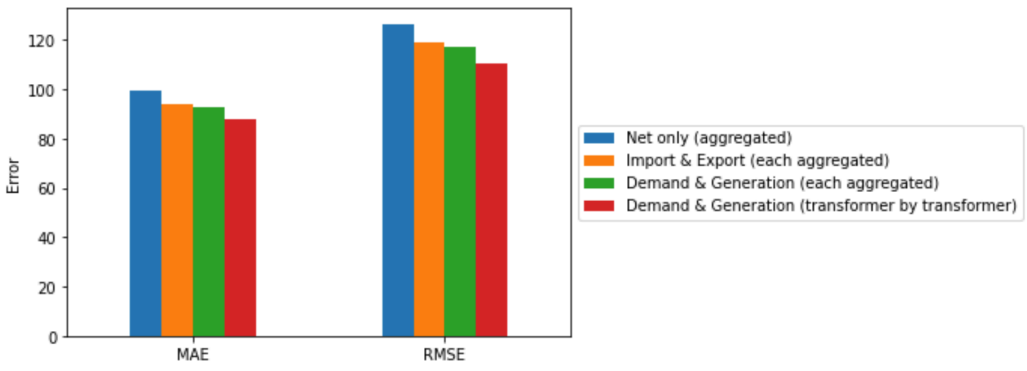

Figure 37. (b) Forecasting result comparison for difference forecasting approaches

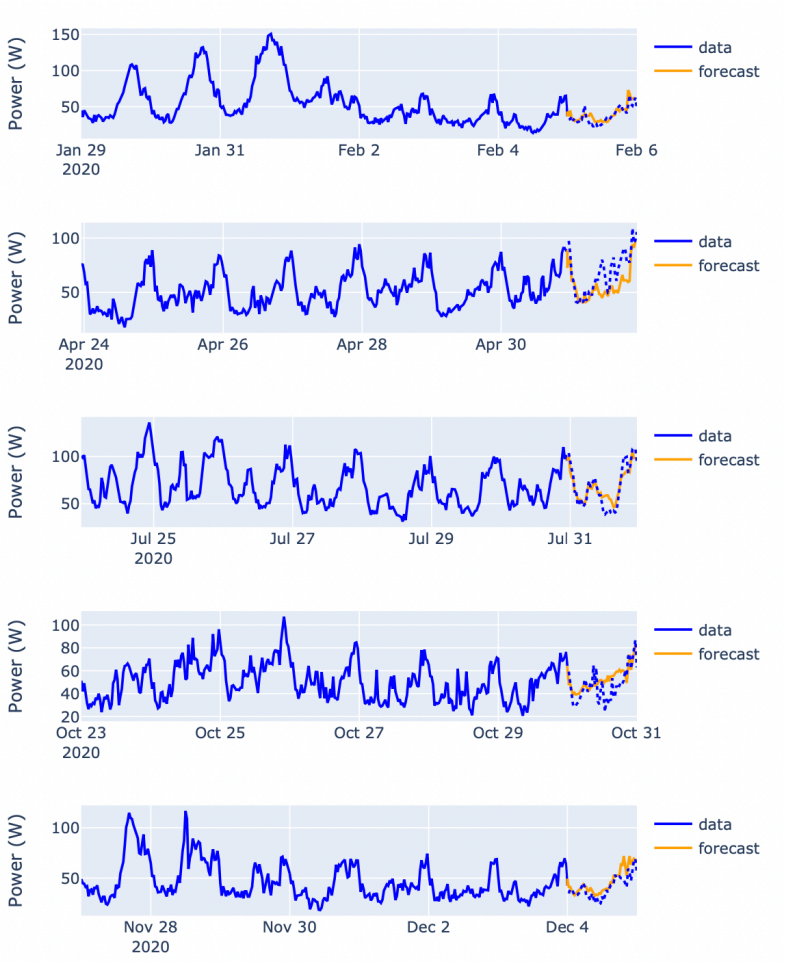

Figure 38. Randomly selected examples of demand forecasts for Tarnagulla

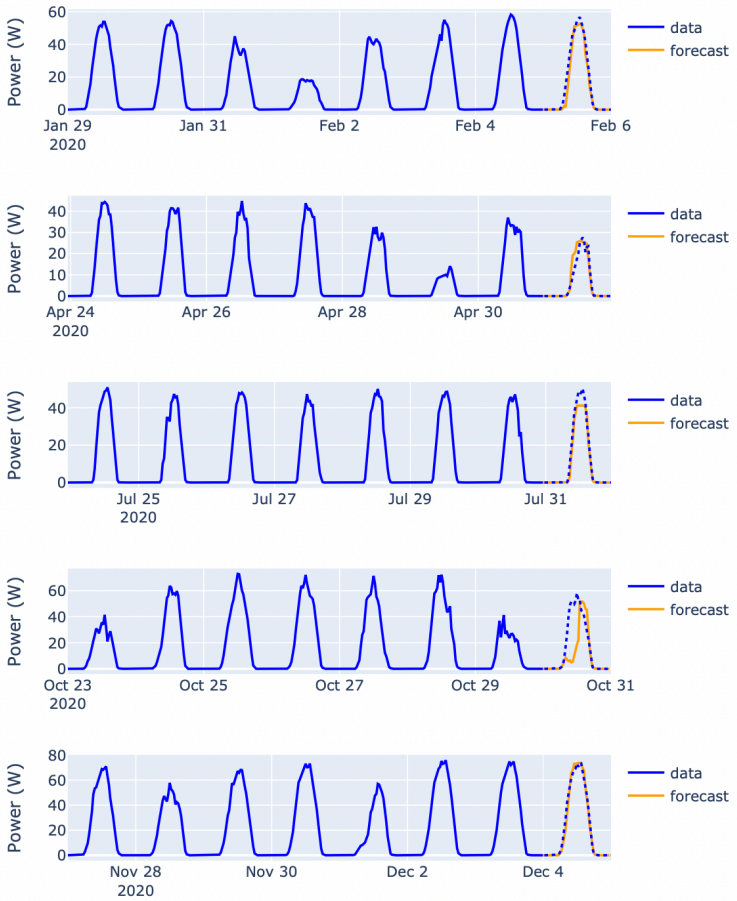

Figure 39. Randomly selected examples of generation forecasts for Tarnagulla

3.2.2 Probabilistic forecasts – Method 1: Historical forecast errors

The forecasting models developed in Section 3.2.1 generated point forecasts – in other words, a single forecast value for each interval in the forecast horizon (24 hours).

However, it can be valuable instead to generate probabilistic forecasts – in other words, for each interval in the forecast horizon there is an understanding of the distribution of possible values that may occur. This can help to understand and visualise anticipated forecast accuracy and to better prepare for extreme events based on how likely they are to occur.

There are several ways in the forecasting community that probabilistic forecasts may be generated, and this is an area of ongoing research with no single approach considered the standard or best way. For the purposes of this project, we explored two different methods to generate probabilistic forecasts, as described in this and the next subsections.

For the first method, we leveraged the fact that – having generated individual daily forecasts for an entire year – we had a detailed understanding of our forecasting errors for that year. Forecasting errors may change from one interval to the next, but they may also broadly change from one time of year to another. For example, solar generation may be easier to forecast in summer, when many days

are clear, but much harder in winter, when weather variability introduces significantly higher chance of errors.

In this probabilistic forecasting method, when generating the forecast for a particular day, we consider it reasonable to use the errors from within a margin of some number of days (we use 30) before and after that day in the historical set. Our dataset covers 2020 – so if we were to generate a forecast for 10 April 2022 (just as an example), we can use the forecasting errors from the individual daily forecasts on the 2020 dataset within 30 days before and 30 days after 10 April 2020 to approximate likely forecast error and generate an error distribution for each interval.

Figure 40 shows the distributions of values for demand and generation for Tarnagulla, across the whole 2020 dataset. For demand, night-time intervals (particularly 2am – 6am) have a very narrow distribution since they are likely to have very similar values across much of the year. Later afternoon values, on the other hand, have quite dispersed distributions since there is considerably more variability regarding the range of values for demand at this time. Likewise, for solar generation, mornings and evenings should be fairly easy to forecast accurately, while daytime intervals can take on a very wide range of values, and are thus more difficult to forecast accurately.

Figure 41 shows the error distributions of the point forecasts (as described in Section 3.2) that exist across the full 2020 dataset. As expected, intervals with highest forecast errors coincide with intervals in Figure 40 that have a wide range of possible values.

This understanding of forecast error distributions can subsequently be applied in the probabilistic forecasting approach described above to generate the example forecasts shown in Figure 42 (Tarnagulla) and Figure 43 (Donald).

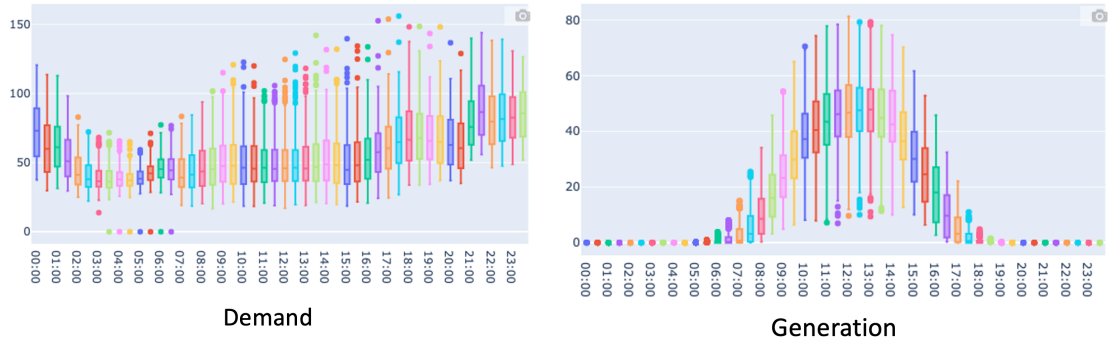

Figure 40. Distributions of actual values of demand and generation for Tarnagulla

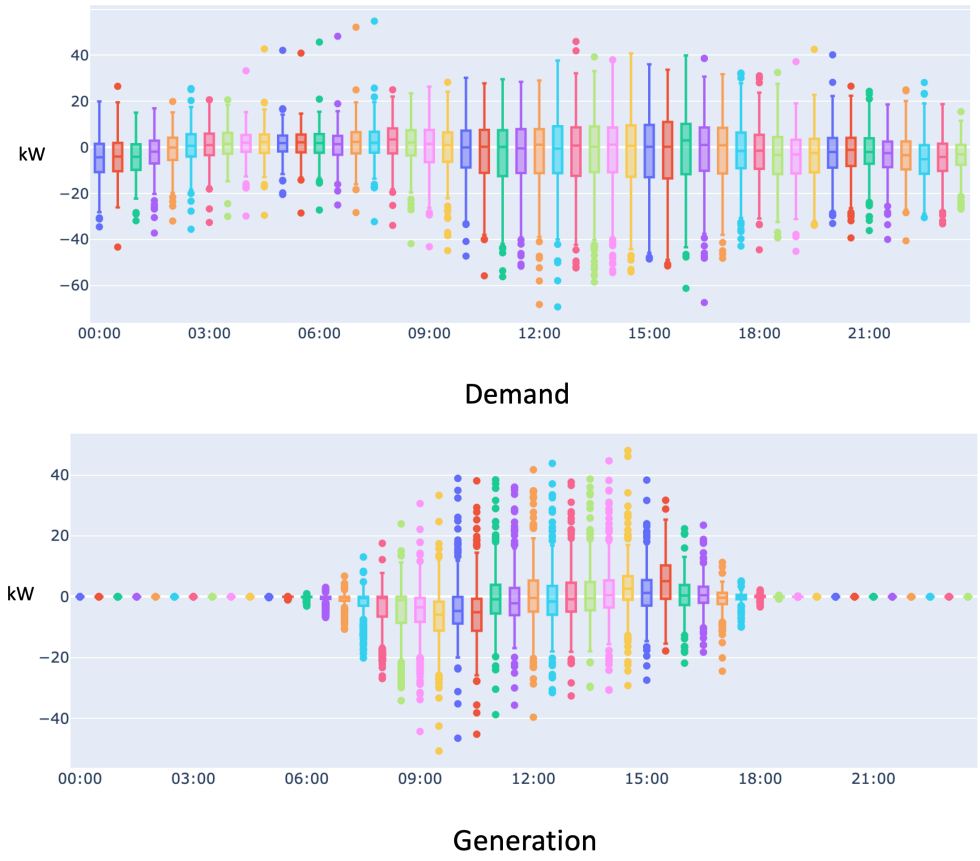

Figure 41. Distribution of forecast errors (across full 2020 dataset) for Tarnagulla

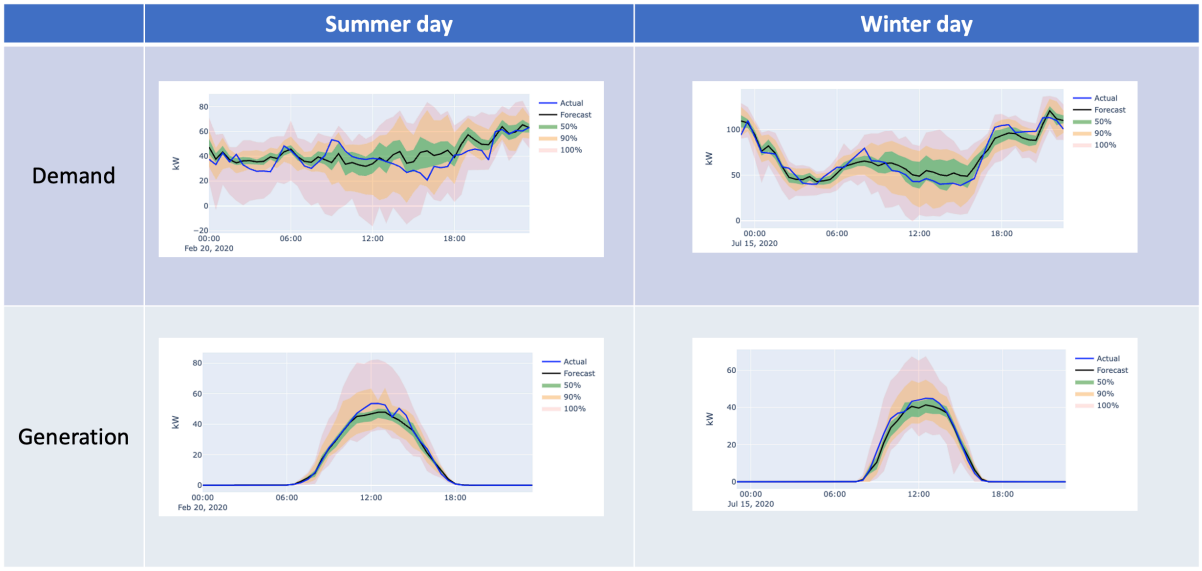

Figure 42. Examples of probabilistic forecasts for Tarnagulla

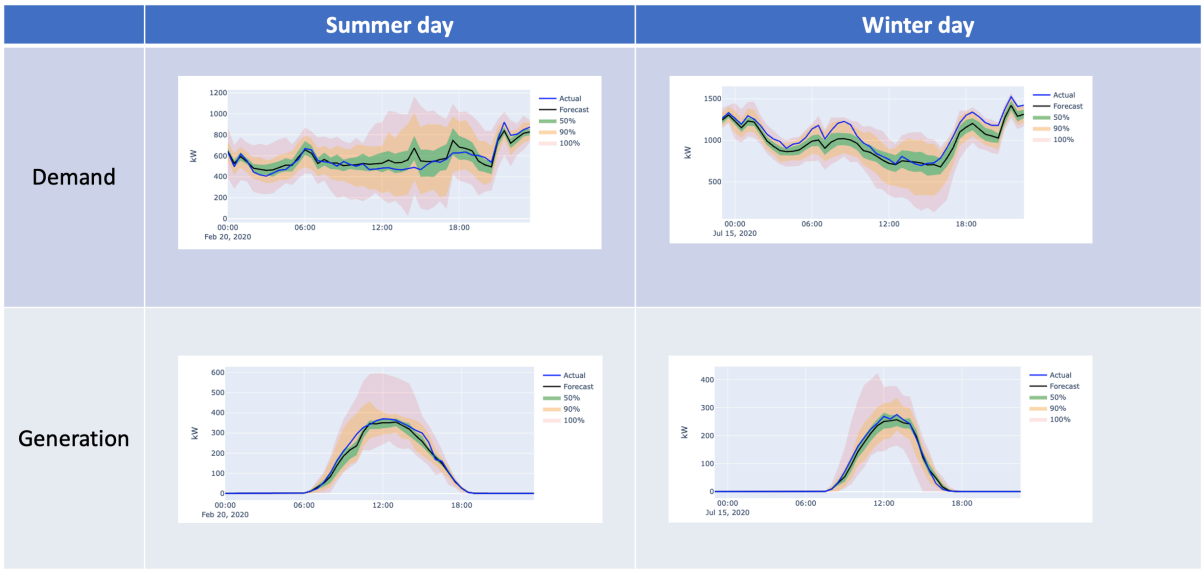

Figure 43. Examples of probabilistic forecasts for Donald

3.2.3 Probabilistic forecasts – Method 2: Markov Chain Monte Carlo

The probabilistic forecasts using the first method described in Section 3.2.2 provide a quick and easy way to determine and visualise, for each interval, the likely forecast accuracy and the range of possible values that may be obtained in that interval. However, these forecasts do not preserve the temporal dependency that exists between adjacent intervals. For example, if at 13:00 a forecast overshoots the actual value by a significant amount, then it is extremely unlikely that one interval later, at 13:30, it will undershoot it by a significant amount.

This temporal dependence can be captured by another approach to probabilistic forecasting called Markov Chain Monte Carlo simulation. In this approach, many different scenarios are generated based on probability distributions of transitioning from one state to another. The change in value from one interval to the next is based on the distributions of historical data. In other words, if at 13:00 the forecasted amount of generation is 100kW, then using historical data we can determine a distribution of the most likely values that may be reached at 13:30 – and most likely the value in the next interval will be close to 100kW too.

To generate realistic demand and generation profiles for Donald and Tarnagulla in this way, we adapted a method that has previously been used to generate simulated wind generation data[5]. The basic principles of this method are to:

1. Discretize demand / generation into a small set of discrete values
2. Go through the entire dataset, keeping track of every time there is a transition from one state to another (i.e., build a transition matrix)

[5] Papaefthymiou, G., & Klockl, B. (2008). MCMC for wind power simulation. *IEEE transactions on energy conversion*, *23*(1), 234-240.

Each row in the transition matrix then represents the probability distribution for which next state may be reached from this state.

For demand and solar generation, there is an obvious daily seasonality, so for every interval there is a unique transition matrix that determines the distribution of intervals that are likely to be reached in the next state. Consider for example solar generation. If at 11:00, 100kW are being generated, there is a high chance that at 11:30 this value will be higher. However, if at 15:00, 100kW are being generated, there is a high chance that at 15:30 this value will be lower. Hence it was necessary to generate individual transition matrices for each interval.

Figure 44 shows some example transition matrices (presented as heat maps) for 3 different intervals of the day. Each heat map show likelihood of transition from one discrete state (y-axis) to another discrete state (x-axis). In the morning the higher values are below the diagonal since solar generation is likely to rise; in the afternoon the higher values are above the diagonal since they are likely to fall.

Figure 45 shows real and simulated profiles for generation in Tarnagulla, while Figure 46 shows real and simulated profiles for demand in Tarnagulla. When it comes to the distributions of possible values, it can be seen that the simulated data closely matches the real data, and has similar statistical properties.

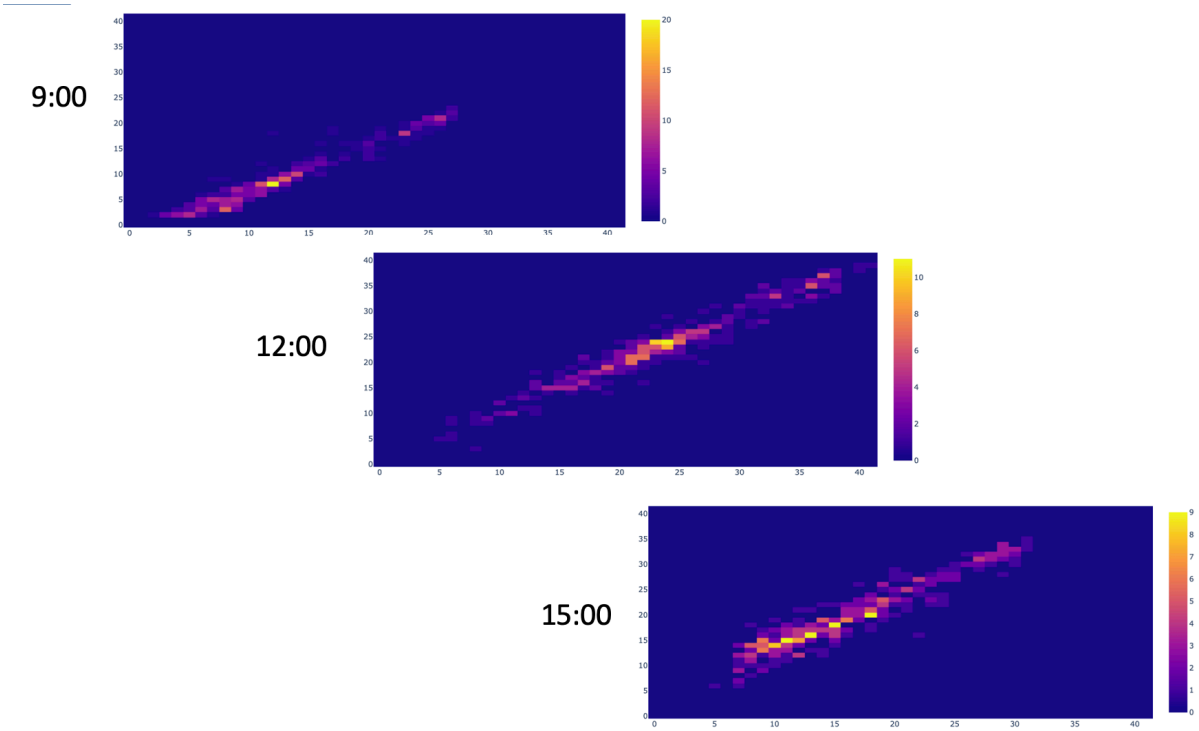

Figure 44. Transition matrices for solar power generation in Tarnagulla, for three intervals

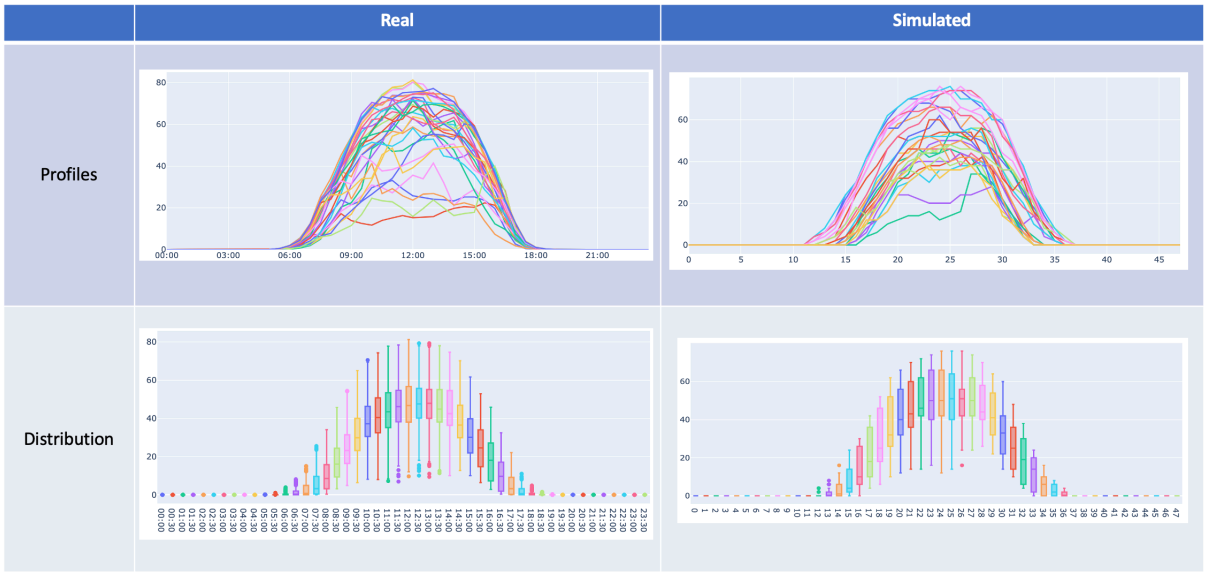

Figure 45. Real and simulated profiles and value distributions for solar generation (Tarnagulla)

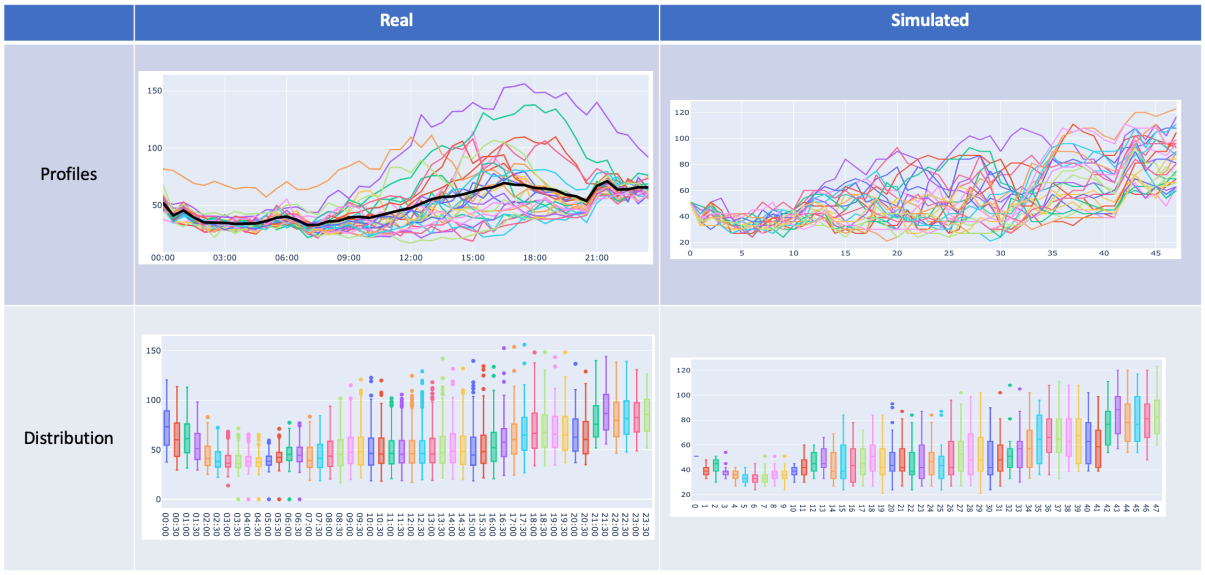

Figure 46. Real and simulated profiles and value distributions for demand (Tarnagulla)

3.3 Bushfire impact modelling on upstream electricity supply

The impacts of bushfires on the transmission system have typically been fast moving in heavily forested areas adjacent to the transmission easements. Long transmission lines may cross different regions with separate and different wildfire risk conditions due to their microclimates. The forest fire danger index (FFDI) is a commonly used metric that indicates the risk of bushfire ignition in different regions in Australia. FFDI includes measures of dryness—based on rainfall and evaporation—wind speed, temperature and humidity but does not include the contribution to bushfire risk from fuel types, ignition, such as lightning, or fuel management practices [14]. The impact of bushfire on the electricity supply of Donald and Tarnagulla can be modelled based on constructing the fragility curve of the sub-transmission line failure rate under different bushfire risk weather.

A. Bushfire risk in Donald and Tarnagulla area

The levels of bushfire weather risk defined based on the value range of FFDI that are currently used in Victoria is shown in Figure 47:

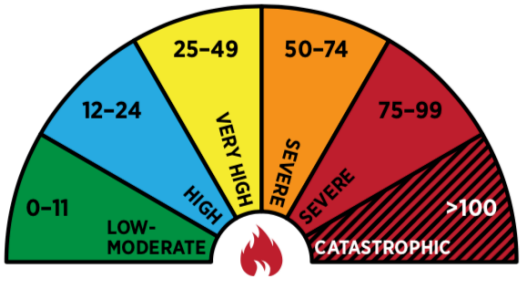

Figure 47. Relationship between FFDI values and bushfire danger ratings for Victoria to show how higher FFDI values are used to indicate more dangerous weather conditions for bushfires (FFDI values in silver boxes). [14]

Daily time series of historical FFDI (1980 to 2020) and projected FFDI under different emission and temperature rise scenarios (RCP 4.5 and RCP 8.5, from 2021 to 2050) are accessed from the ESCI data portal. For Donald area, the FFDI time series from **"Bendigo"** and **"Coonooner Bridge"** climatic zone are used to determine the online status of the CTN-BETS transmission line. For Tarnagulla area, the FFDI time series from "**Bendigo**" climatic zone are used to determine the online status of the MRO-BETS transmission line.

Historical and projections of the number of days and maximum consecutive days that the FFDI thresholds (FFDI > 25, FFDI > 50, FFDI > 75), corresponding approximately to 'very high', 'severe' and 'extreme' bushfire risk (Figure 47), are calculated for climatic zones along the transmission paths linking Donald and Tarnagulla area to the upstream grid, which includes the FFDI statistics from Bendigo and Coonooer Bridge. The time series of FFDI are shown in Figure 48 and Figure 49.

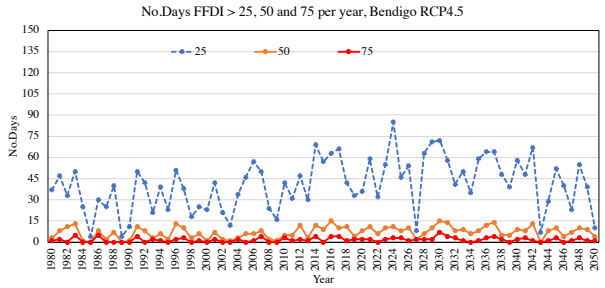

(a)

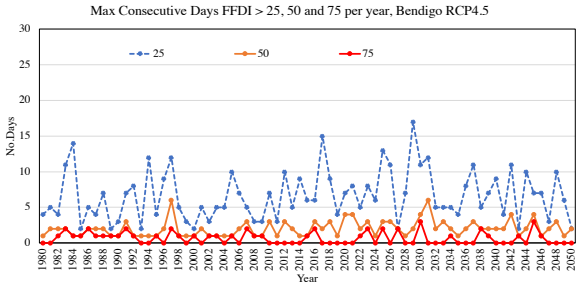

(b)

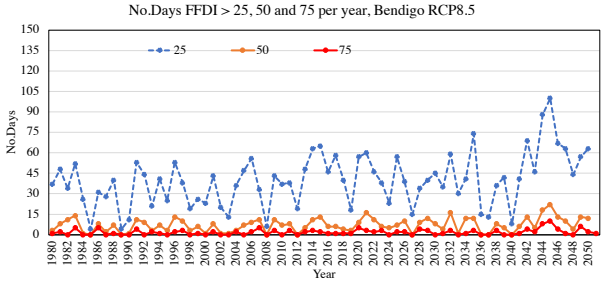

(c)

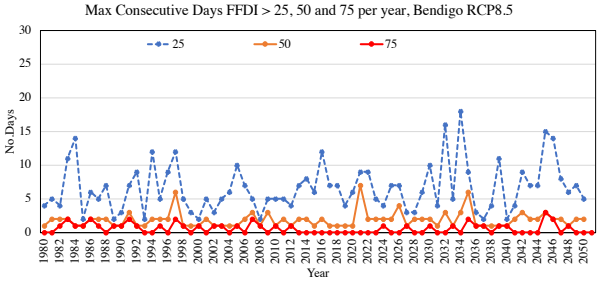

(d)

Figure 48. Time-series of historical and projected FFDI for Bendigo climatic zone for three different thresholds, corresponding approximately to 'very high (FFDI > 25)', 'severe(FFDI > 50)' and 'extreme (FFDI > 75)' bushfire risk

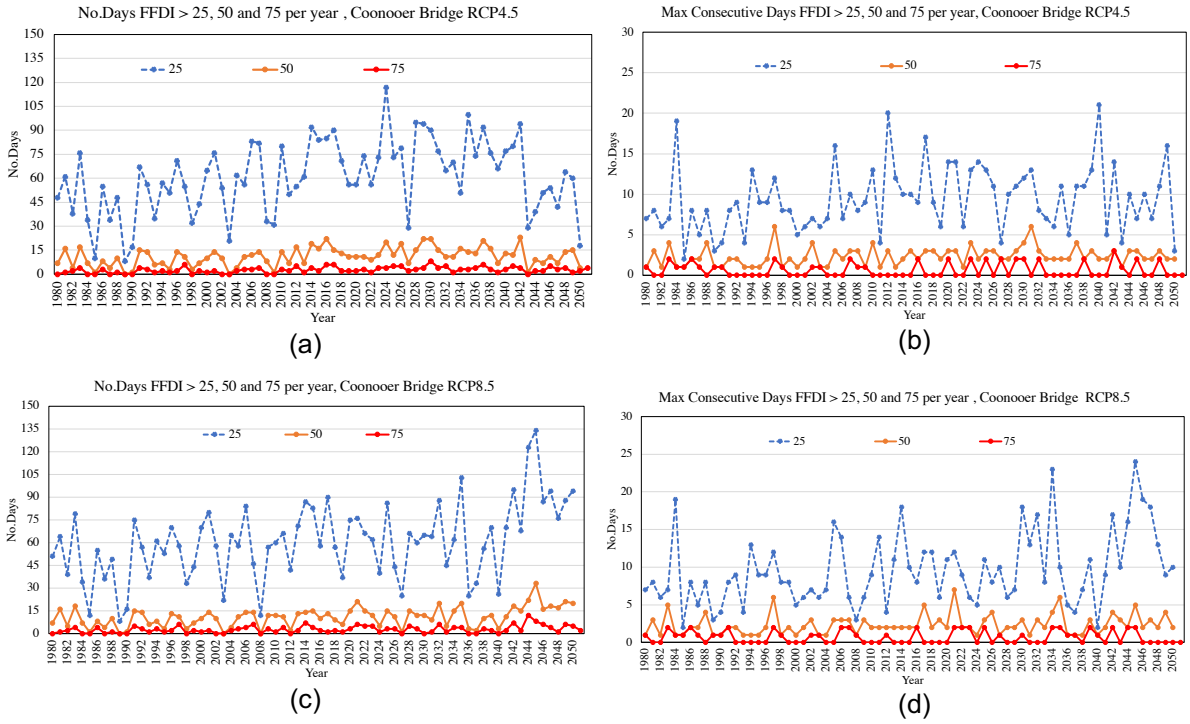

Figure 49. Time-series of historical and projected FFDI for Coonooer Bridge climatic zone for three different thresholds, corresponding approximately to 'very high (FFDI > 25)', 'severe(FFDI > 50)' and 'extreme (FFDI > 75)' bushfire risk

As can be seen from Figure 48 and Figure 49, for all FFDI values and all locations there appears an increase in frequency through the century with, for example, the average frequency of FFDI days above different thresholds in both Bendigo and Coonooer Bridge climatic zones under RCP 8.5 scenario increased significantly over the time, as shown in Figure 48 (c,d) and Figure 49 (c,d). Although there is not a significant increase in the average frequency of FFDI days above different thresholds in those two areas under RCP 4.5 scenario, there is an increase in the more extreme FFDI indices through the assessment period, as shown in Figure 48 (a,b) and Figure 49 (a,b).

B. Construct fragility curve of sub-transmission line failure rate

During extreme high bushfire period, the probability of poles flashover and thus the probability of bushfire ignition could increase, which would lead to forced line trip under this condition. Thus, the failure probability of a sub-transmission line would increase with the bushfire risk [14] as well as the repair/restoration time of a sub-transmission line. In this light, the concept of "fragility curve" is introduced to characterise the potential relationship between the line failure probability and the bushfire risk (which is represented by the value of FFDI). Since there is no official record of the relationship between line failure rate against bushfire risk weather in Australia [15], the fragility curve of the line failure rate and restoration time under different bushfire risk method is constructed via parametric method. The parametric method to construct the fragility curve can be summarised as following (taking line failure rate as example, the fragility curve construction for line restoration time is the same):

Assume that the nominal line failure rate is p_0, the line failure rate will keep constant when the FFDI value is lower than 11[6]. When $FFDI > 11$, the sensitivity of line failure rate to a single unit of FFDI value increase is assumed to be s, and the corresponding line failure rate p_{FFDI} under a certain value of FFDI larger than 11 can be calculated using the formula as following:

$$p_{FFDI} = s \cdot (FFDI - 11) \cdot p_0 + p_0 \quad (1)$$

It should be noted that s is the only unknown parameter in Eq. (1) therefore different values for s are assumed in case studies. Also, it should be noted that the FFDI value used to calculate the failure rate and the restoration time of a sub-transmission line on each day should be the maximum FFDI value within the climatic zones that the sub-transmission line passes through. Also, it should be noted that failure probability of the line should not exceed 1 at any time, therefore the aggregated fragility curve of a line can be expressed as:

$$p(FFDI) = \begin{cases} p_0, & FFDI \leq 11 \\ \min\{s \cdot (FFDI - 11) \cdot p_0 + p_0, 1\}, & FFDI > 11 \end{cases} \quad (2)$$

A typical set of fragility curves for line failure rate against different FFDI values are shown in Figure .

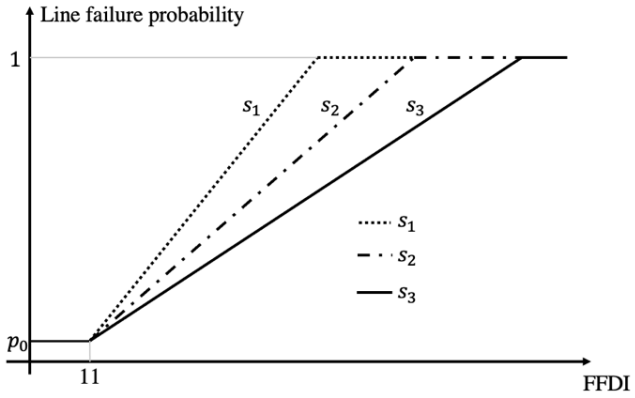

Figure 54. Fragility curve of line failure probability vs. FFDI value under different sensitivities

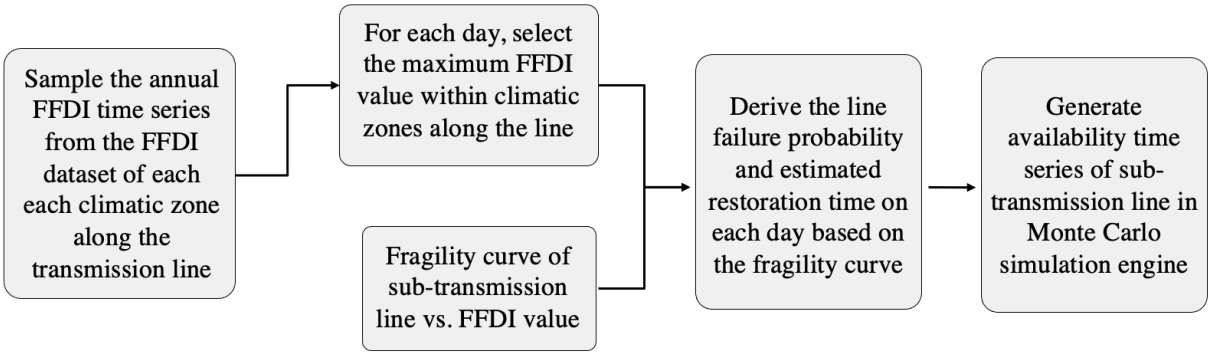

Figure 55. Procedure to generate sub-transmission line availability time series based on fragility

[6] According to Country Fire Authority Australia, FFDI < 11 corresponds to low-moderate bushfire risk and thus it is considered as outside of the fire danger period. Website: https://www.cfa.vic.gov.au/warnings-restrictions/total-fire-bans-and-ratings

Based on the daily FFDI time series in different climatic zones that each sub-transmission line passes through, the failure probability and the estimated restoration time of each sub-transmission line on each day can be derived. Then, the daily failure probability and estimated restoration time are used as the input to a Monte Carlo simulation to sample the availability time series of the sub-transmission line. The procedure is illustrated in Figure .

3.4 Bushfire impact modelling for off-grid community

The major impact of bushfires in a grid-connected community is the increasing unavailability of the upstream transmission line. For an off-grid (aka islanded) community, the fuel supply of distributed generators may be impacted during a prolonged bushfire event, which would reduce the reliability and resilience of rural communities. In this light, renewables-based systems may even have an advantage here. However, in the lack of information on the duration of fuel supply disruption, parametric sensitivity studies are conducted to simulate the impact of bushfire on the fuel supply chain of the off-grid community. It is assumed that when no bushfire event occurs, the fuel of generators can be restored without any delay. However, if a bushfire event occurs, the fuel supply depends on the different bushfire clearance times. The bushfire clearance time and the local fuel storage capacity are the two varying parameters in this case study.

3.5 Network component failure rates

The capacity adequacy of the rural area community is influenced mainly by the (un)availability of the supply feeder (at both transmission and distribution level), various equipment forced outage and the dispatch strategy of the community. The capacity adequacy of the community is also dependent on the emergency response strategies to cope with capacity shortage events. Expected energy not supplied (EENS) is selected as the capacity adequacy metric, which refers to the expected amount of demand not covered annually. The capacity adequacy assessment has been performed in grid- connected and off-grid mode considering one-year timeframe under the corresponding required solar PV, diesel generator and battery capacity identified in Project 5 report [17]. The failure rates and repair duration of different network, generation, and storage facilities are adopted from Table 38 in Project 5 report [16], which is summarised in Table 3-2 below.

Table 3-2. Input Reliability Parameters

Component	Reliability Parameters	
	Failure frequency (1/year)	Repair duration (hours/year)
Busbar	0.00225	0.325
Feeders/Transmission Lines	0.0285/km	2.04
Transformer	0.02	5.72
Battery	0.0312	50
DG	0.1	37

3.6 Summary

This section provided the considerations on modelling the eligible continuous and descete disturbances that may occur to the towns, including generation/load ramp events, forecast errors, faults, component failures, bushfire-induced outages and fuel disruption events.

Special effort was placed on the construction of forecasting models for the PV generation and demand in the two towns. The random forest regression proved to be more accurate for the PV generation and demand signals compared several state-of-the-art forecasting methods. Additionally, probabilistic forecast error models were built to assist in quantifying disturbances due to generation-load mismatch. Moroever, it was shown that the forecast error was reduced when the proposed (estimated) seperate PV generation and demand signals were used as input, instead of the direct import/export signals from smart meter data.

4 Capacity Adequacy Analysis

4.1 Capacity adequacy assessment methodology

The capacity adequacy of the rural area community is influenced mainly by the (un)availability of the supply feeder (at both transmission and distribution level), various equipment forced outage and the dispatch strategy of the community. The capacity adequacy of the community is also dependent on the emergency response strategies to cope with capacity shortage events. Expected energy not supplied (EENS) is selected as the capacity adequacy metric, which refers to the expected amount of demand not covered annually. The capacity adequacy assessment has been performed in grid- connected and off-grid mode considering one-year timeframe under the corresponding required solar PV, diesel generator and battery capacity identified in Project 5 report [16].

The capacity adequacy assessment framework includes two main modules: 1) **System dispatch engine** is used to determine the charging/discharging schedule of storage and the power import/export from upstream grid; 2) **Monte-Carlo simulation engine** is used to sample the outage status of system components, including the outage of substations, transmission and distribution feeders, diesel generators and the disconnection status of transmission feeder during high bushfire risk periods. Based on the emergency response strategy adopted by the system, the system dispatch engine and the Monte-Carlo simulation engine is coordinated in different ways to calculate the EENS value of the community, where the emergency response strategies and the coordination scheme of the system dispatch engine and the Monte-Carlo simulation engine will be introduced in the following text.

The load following dispatch has been considered for this study. In the load following dispatch, a generator operates to produce only enough power to meet the primary electrical load demand. Lower-priority objectives such as charging the battery bank or serving any deferrable electrical load are left to renewable sources. The backup generator can still ramp up and sell power to the utility grid if it is economically feasible. It should be noted that the dispatch algorithm is assumed to have no advance knowledge of unexpected outages.

The emergency response strategies considered in this study includes:

1) *Enabling emergency power import (for grid-connected community) from upstream grid when there is a capacity shortage within the community and the transmission feeder has spare capacity beyond the scheduled amount of import power.*
2) *Enabling emergency discharge and rescheduling of battery to minimize the potential load shedding when capacity shortage event occurs (for both grid-connected and off-grid community).*
3) *Enabling different scheduling leading time (for off-grid community) when determining the charging and discharging profile of batteries. The scheduling will be based on load-following under perfect RES output and demand forecast assumption while with no information of potential outage events.*

When no emergency discharge nor rescheduling of battery is considered, the charging/discharging profile of batteries and the power import/export schedule is pre-determined using the system dispatch engine, where the net load profile after subtracting solar and battery power and the power import/export schedule will be used as the input for capacity adequacy analysis. The flowchart for capacity adequacy assessment is shown in Figure 50 when no emergency response from battery is considered.

When the emergency response from battery is considered, the system dispatch engine and the Monte-simulation engine will be coordinated in a rolling-horizon manner. The community's status is checked at each time step to determine whether a loss of load event would occur. When there is no capacity

shortage event occurs, the state of charge (SOC) and charge/discharge schedule at each time step of BESS will be scheduled using system dispatch engine, with a pre-defined scheduling horizon ΔT. Then, BESS SOC and charge/discharge power at each time step will be recorded as the input to calculate the capacity mismatch at each time step. If a load shedding event is identified at any time step, the battery will be discharged to minimize the load shedding and the SOC will be updated accordingly as the input for the re-scheduling at the next time step, using the system dispatch engine.
The flowchart for capacity adequacy assessment is shown in Figure 51 when emergency response from storage is considered.

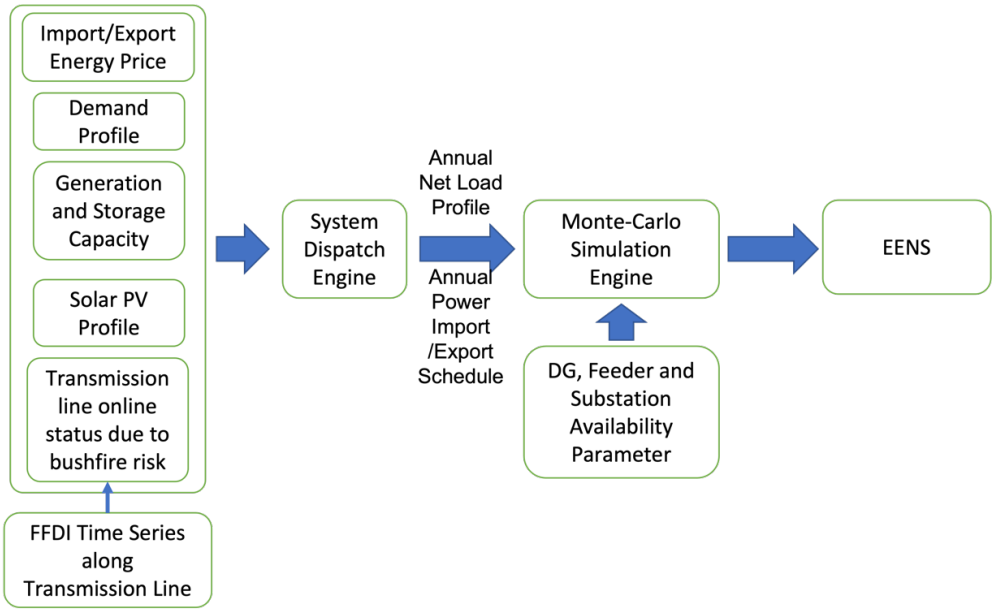

Figure 50. Capacity Adequacy Assessment Procedure without Emergent Response from Battery

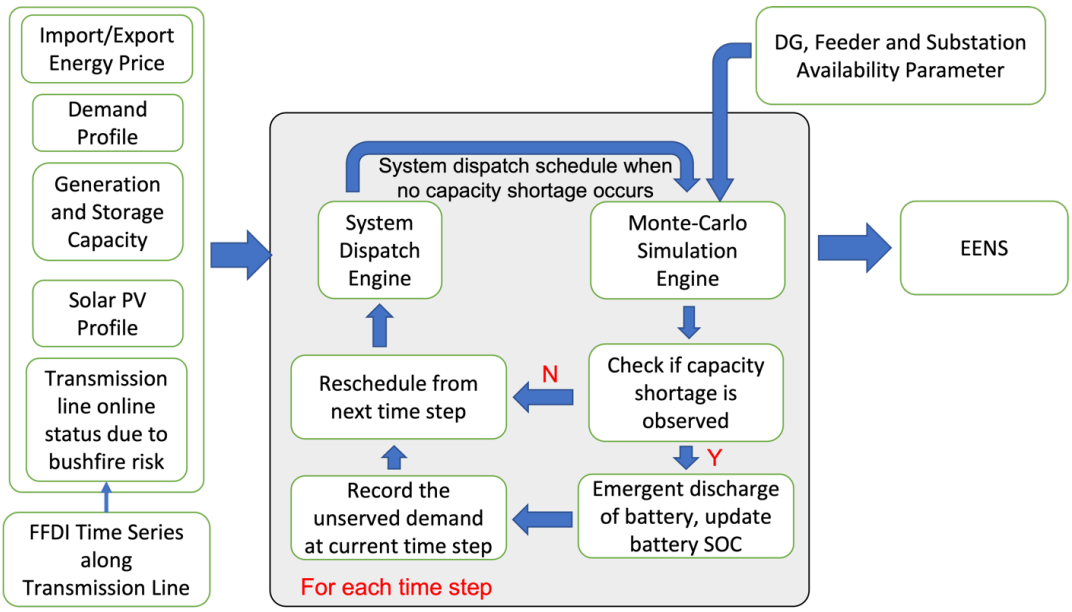

Figure 51. Capacity Adequacy Assessment Procedure with Emergent Response from Battery

4.2 Donald and Tarnagulla area capacity adequacy assessment

For both areas, the capacity adequacy under grid-connected scenario is analysed when

- different mitigation strategies mentioned in Section 4.1 are applied
- considering (or not) the impact of bushfire on upstream supply availability based on fragility curve with different line failure rate sensitivity with FFDI increase
- considering (or not) the impact of bushfire-induced fuel supply chain disruption under different local diesel storage capacity and different fuel supply disruption duration

The sensitivity of line failure rate with FFDI increase are assumed to be 1%, 2% and 5% respectively. The fuel supply disruption event is assumed to occur within the fortnight with highest bushfire risk in these areas, which corresponds to 20th Jan to 2nd Feb.

4.2.1 Donald area under grid-connected scenario

The network topology for Donald area grid-connected case is shown in Figure 52, corresponding to scenario 32 identified in Project 5 Donald area islanding scenario analysis that has found to be the most economic grid-connected option [16]. The required generation capacity is summarised in Table 4-1 and the peak load information for each area along the Donald area feeder CTN006 is summarised in Table 4-2.

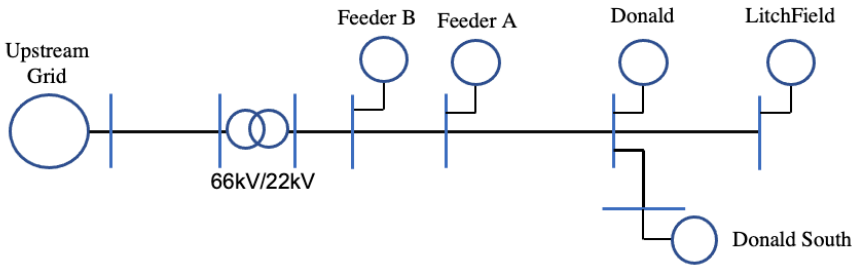

Figure 52. Donald area network topology for grid-connected scenario

Table 4-1 Required Generation Information for Donald Area Grid-connected scenario 32(S32)

Scenario S32						
Network Name	Grid	Feeder B	Feeder A	Donald	Donald South	Litchfield
Network Topology	1	1	1	1	1	1
Load (MW)	3.14					
Required Generation						
Solar PV (kW)	1688					
DG (kW)	2430					
Battery Storage (kWh)	155					
Converter (kW)	392					

Table 4-2 Peak Load Information for Areas along Feeder CTN006

Region	Load	Lines	Busbars	Loads	Shunts
Feeder B	0.42MW	166	181	74	2
Feeder A	0.1MW	104	110	43	2
Donald	2.36MW	116	130	50	0
LitchField	0.29MW	172	177	71	2
Donald South	0.06MW	42	43	20	0

The capacity adequacy for Donald grid-connected scenario when no bushfire impact is shown in Figure 53. The expected not energy supplied (EENS) in MWh and the EENS in % of the annual energy consumption for Donald area is shown on the left and right vertical axis using the bar plot and the orange line respectively. The results are tested under different capacity shortage mitigation strategies for grid-connected community, including enabling emergent power import from upstream grid and enabling emergent discharge from BESS. It can be seen that both capacity shortage mitigation strategies can improve the capacity adequacy, while enabling emergent BESS discharge can improve the EENS more significantly than emergent power import.

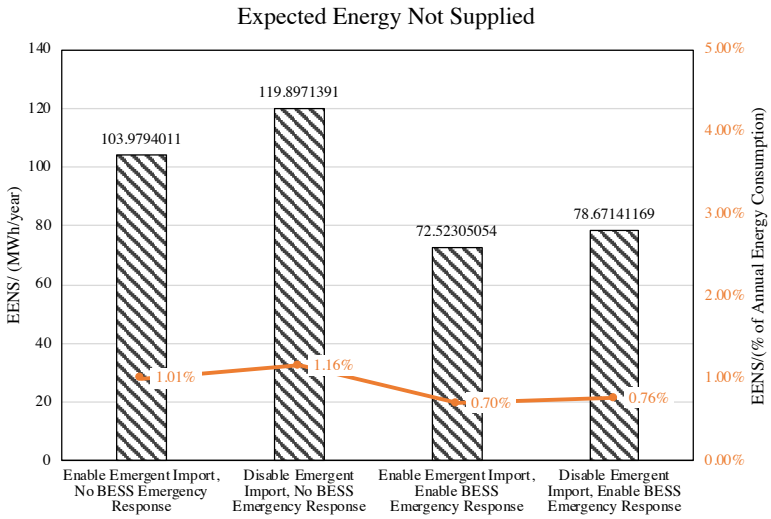

Figure 53. EENS for grid-connected Donald area with no bushfire impact considered

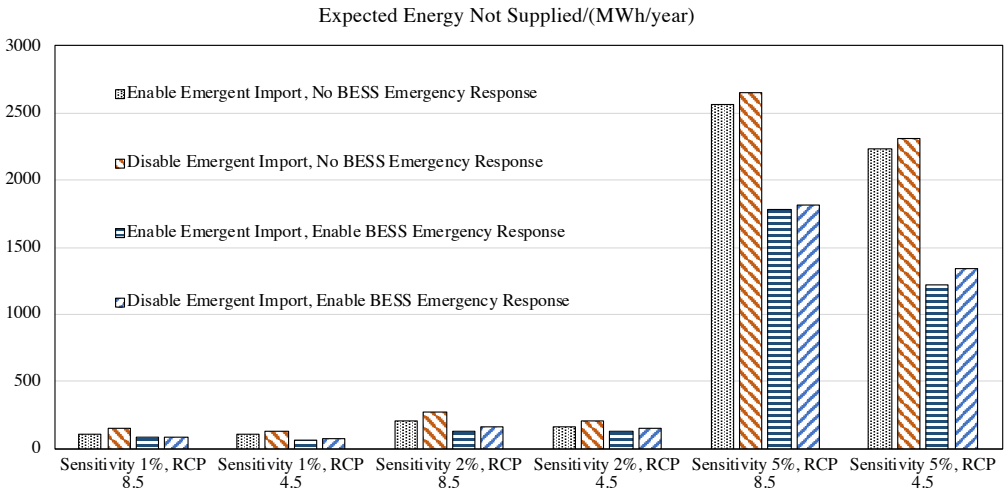

Figure 54. EENS(in MWh) of grid-connected Donald area considering bushfire Impact on line failure rate, under different line failure sensitivity and RCP scenario

The capacity adequacy for Donald grid-connected scenario when only considering the bushfire impact on the line failure availability is shown in Figure 54 and Figure 55 respectively. The EENS is represented in MWh (Figure 54) and % of the annual energy consumption (Figure 55). Different line failure sensitivity with FFDI increase is used to explore the impact of bushfire on capacity adequacy of grid-connected community, where 1%, 2% and 5% sensitivity is used in this work. It can be seen that the EENS of the grid-connected community increases significantly as the line failure rate sensitivity with FFDI increases

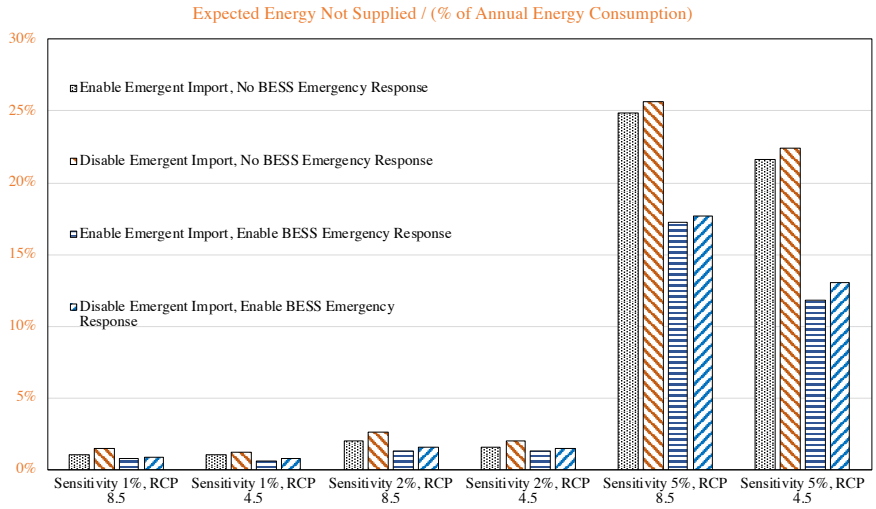

Figure 55. EENS(in % of annual energy consumption) of grid-connected Donald Area considering bushfire impact on line failure rate, under different line failure sensitivity and RCP scenario

from 1% to 5%, which represents a giant compromise of grid-connected community capacity adequacy as the bushfire impact on upstream supply availability becomes more severe. Also, it can be seen that the EENS under RCP 8.5 is higher than that under RCP 4.5, under the same mitigation control strategies and same line failure rate sensitivity assumption.

Parametric analysis exploring the impact of fuel supply disruption on the community's capacity adequacy follows:

- Different fuel supply disruption duration is assumed, including 1 day, 5 days and 10 days
- Different local diesel storage capacity is assumed based on the energy/power ratio, including 1 day, 5 days and 10 days
- The local diesel storage is assumed to be fully restored before fuel disruption period

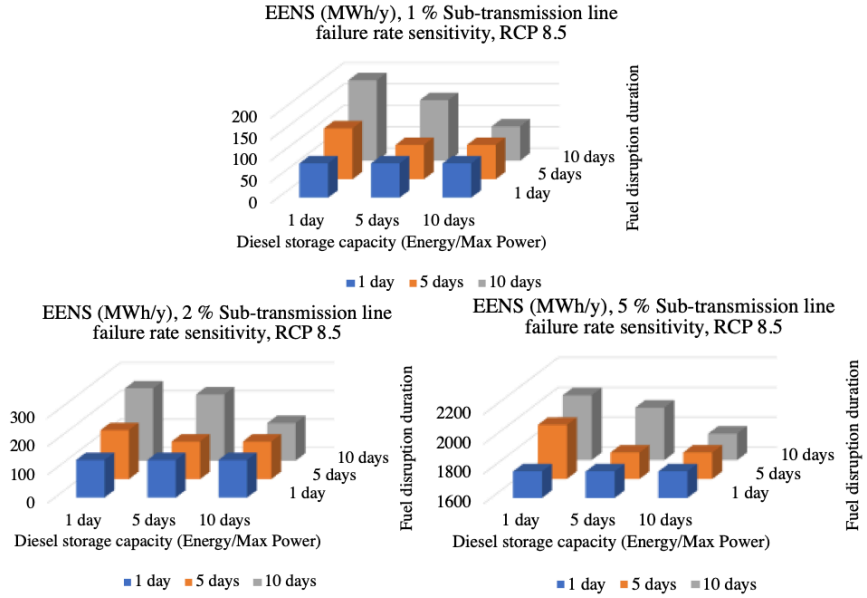

Figure 56. Capacity adequacy of grid-connected Donald area considering bushfire-induced fuel supply disruption and bushfire impact on line failure rate, RCP 8.5

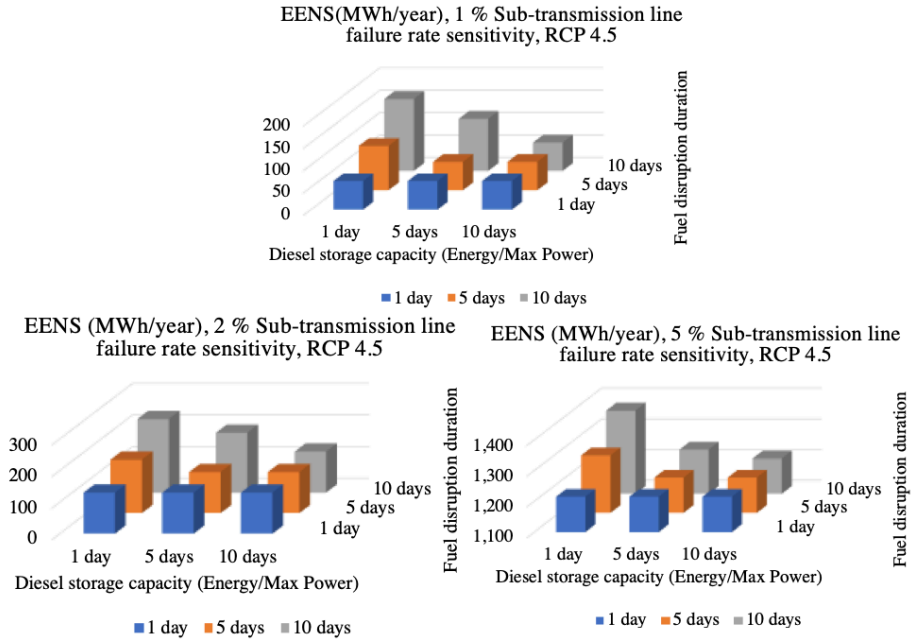

Figure 57.Capacity adequacy of groid- connected Donald area considering bushfire-induced fuel supply disruption and bushfire impact on line failure rate, RCP 4.5

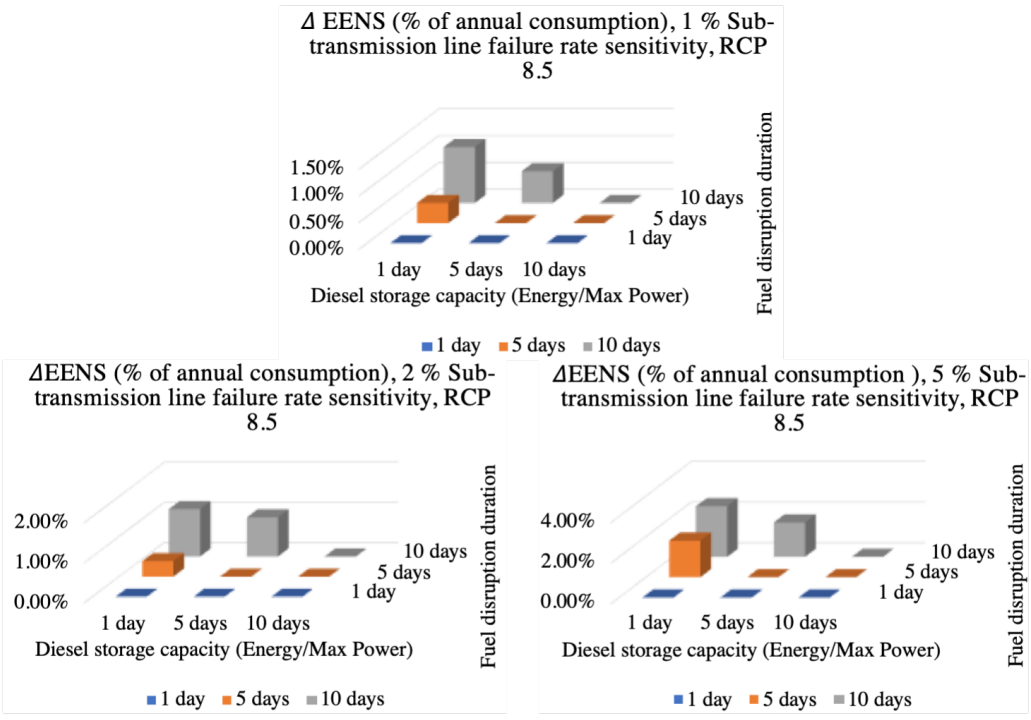

Figure 58. ΔEENS (% of annual energy consumption) for grid-connected Donald area when considering fuel supply disruption or not, RCP 8.5

The capacity adequacy for Donald area when considering bushfire impact on upstream supply availability and the fuel supply disruption is shown in Figure 56 and Figure 57 when enabling emergency power import and BESS discharge. The changes in EENS (in % of annual energy consumption) when considering fuel supply disruption or not are shown in Figure 58 and Figure 59. By observing the trend in Figure 56 and Figure 57, a clear decrease on capacity adequacy level can be observed when the bushfire-induced fuel supply disruption duration is longer than the local diesel storage capacity, and the negative impact of fuel disruption becomes more significant as the disruption duration becomes longer. However, it is also evident that no significant additional risk is introduced by bushfire-induced fuel supply disruption when the disruption duration is shorter than the local diesel storage capacity (measured in energy/power ratio). By observing the trend in Figure 58 and Figure 59, it can also be concluded that the capacity adequacy level is more impacted when the line failure rate sensitivity with FFDI increases under a given local diesel storage capacity and the same fuel supply disruption duration.

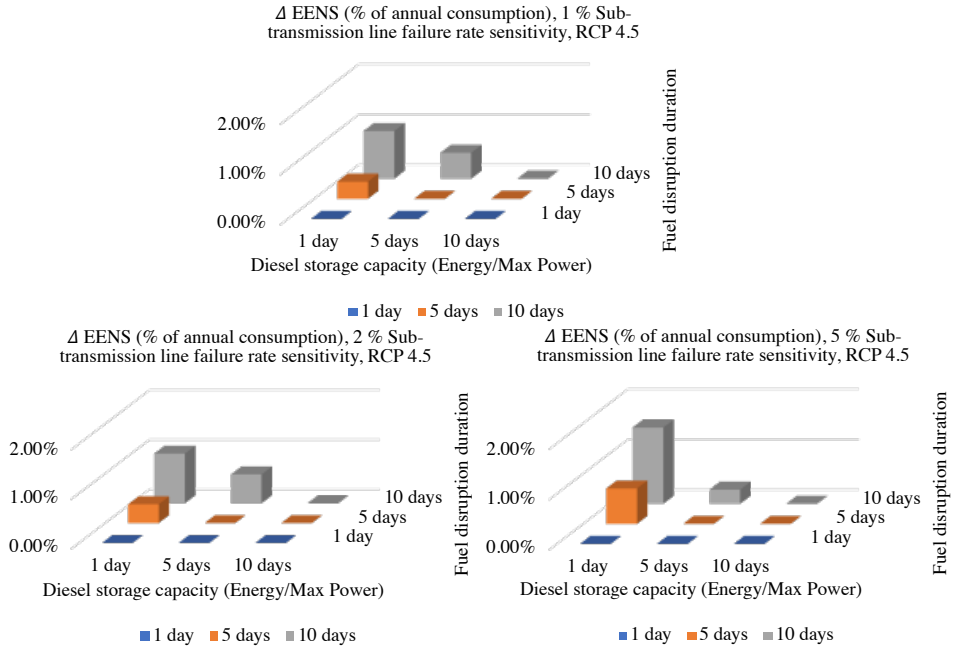

Figure 59. ΔEENS (% of annual energy consumption) for grid-connected Donald area when considering fuel supply disruption or not, RCP 4.5

4.2.2 Tarnagulla area under grid-connected scenario

The required generation capacity for Tarnagulla area under grid connected scenario is summarised in Table 4-1 which is adopted from the sizing results from Project 5 [16].

Table 4-3 Tarnagulla Grid-Connected Scenario Information

Peak Load	0.17MW
Required Generation	
Solar PV(kW)	201
Diesel Generator(kW)	70
Battery(kWh)	0
Converter (kW)	0

The capacity adequacy for Tarnagulla grid-connected scenario when no bushfire impact is considered is shown in Figure 60. The expected not energy supplied (EENS) in MWh and the EENS in % of the

annual energy consumption for Donald area is shown on the left and right vertical axis using the bar plot and the orange line respectively. Since there is not battery required for Tarnagulla grid connected scenario, only one capacity shortage mitigation strategy is tested in this case, which is enabling emergent power import. It can be seen that enabling emergent power import from upstream grid does improve the overall community capacity adequacy by more than 2 times based on the percent of annual energy consumption.

The capacity adequacy for Donald grid-connected scenario when only considering the bushfire impact on the line failure availability is shown in Figure 61. The EENS is represented in MWh using bar plot and in % of the annual energy consumption using the orange line. Under different line failure rate sensitivity with FFDI, the trend of EENS is quite similar to the case in Donald area as explained in Section 4.2.1.

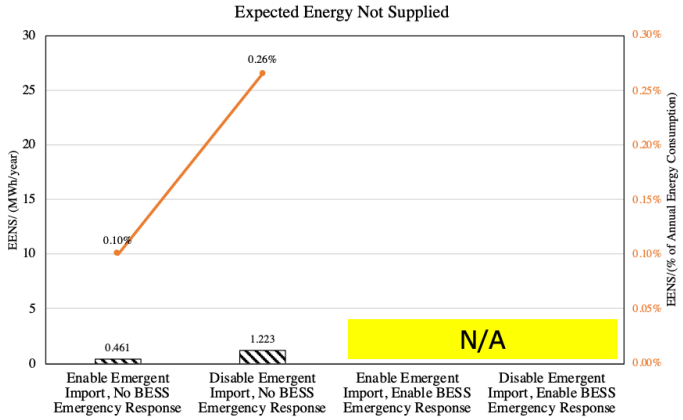

Figure 60. EENS for grid-connected Tarnagulla area with no bushfire impact considered

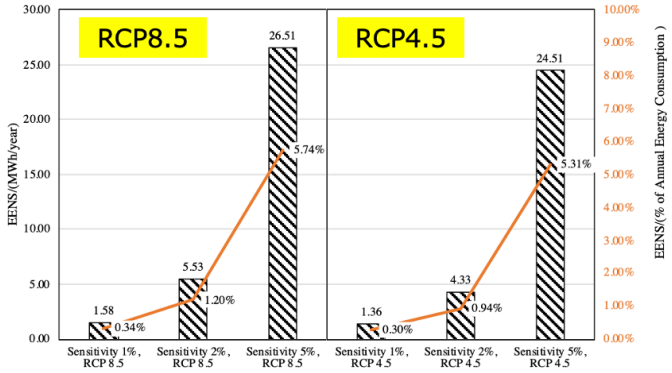

Figure 61. EENS(in MWh and in % of annual energy consumption) of grid-connected Tarnagulla Area considering bushfire impact on line failure rate, under different line failure sensitivity and RCP scenario

Same parametric analysis introduced in Section 2.1, is conducted to explore the impact of fuel supply disruption on the community's capacity adequacy. The capacity adequacy for Donald area when considering bushfire impact on upstream supply availability and the fuel supply disruption is shown in Figure 60 and Figure 61 when enabling emergency power import and BESS discharge. The changes in EENS (in % of annual energy consumption) when considering fuel supply disruption or not are shown in Figure 62 and Figure 63. Similar impacts by bushfire-induced fuel supply disruption on capacity adequacy can be observed for Tarnagulla grid-connected community as Donald grid-connected area as introduced in Section 4.2.1.

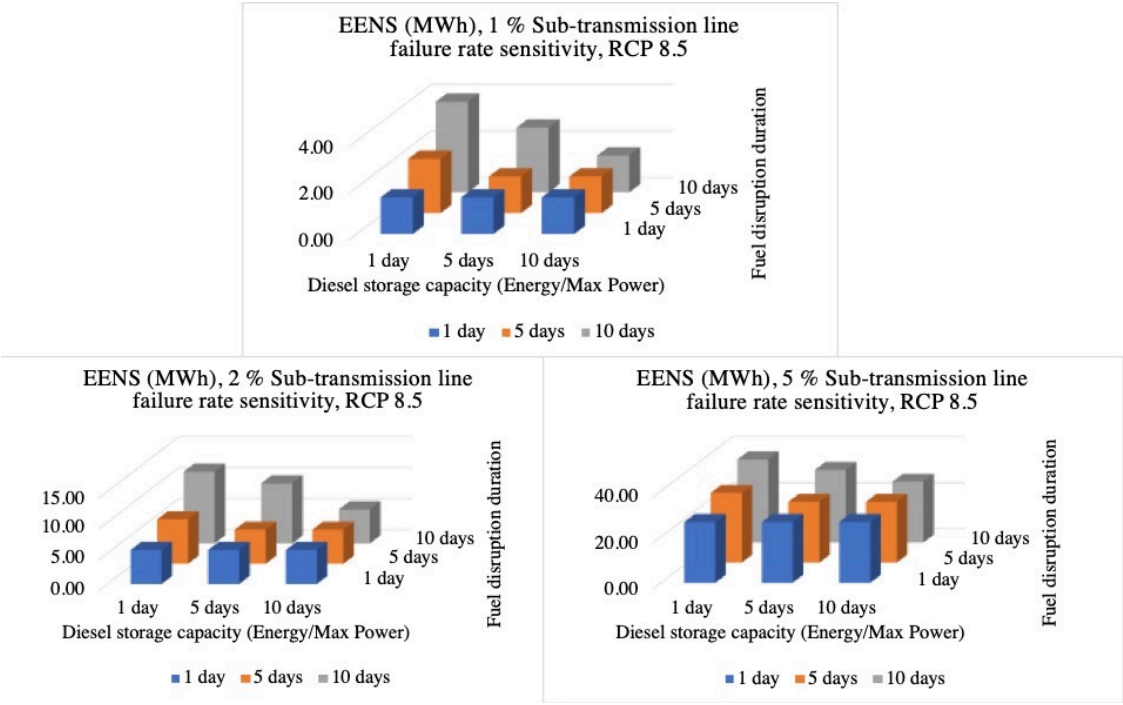

Figure 62. Capacity adequacy of grid-connected Tarnagulla area considering bushfire-induced fuel supply disruption and bushfire impact on line failure rate, RCP 8.5

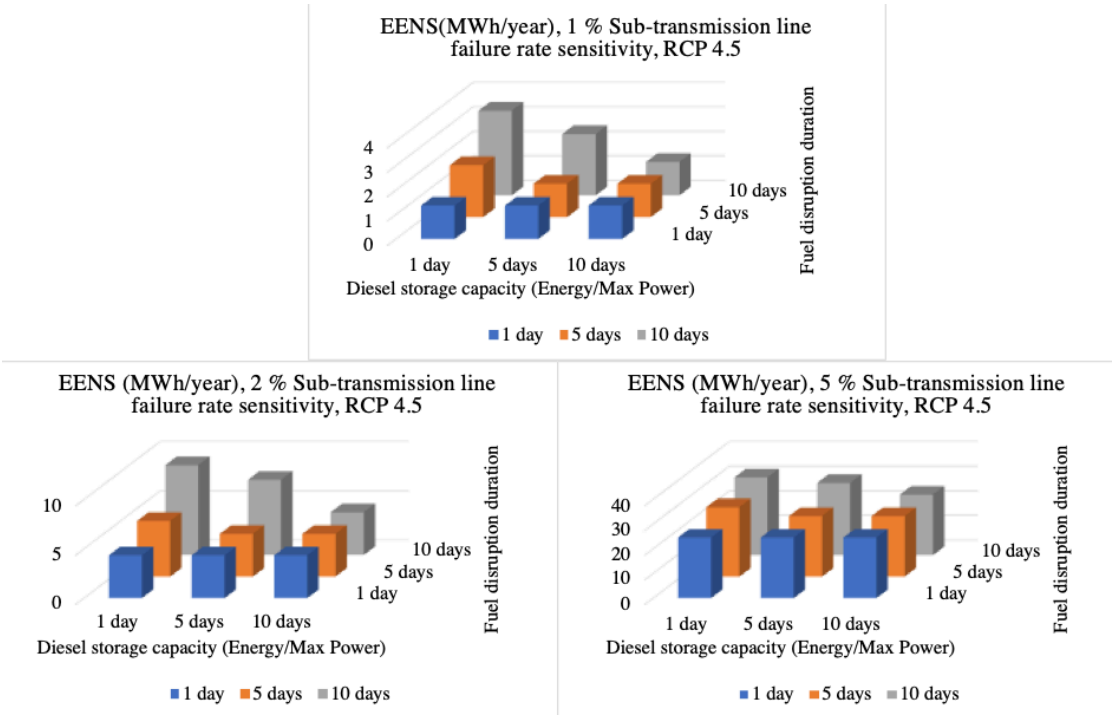

Figure 63. Capacity adequacy of grid-connected Tarnagulla area considering bushfire-induced fuel supply disruption and bushfire impact on line failure rate, RCP 4.5

4.2.3 Donald area under off-grid scenario

The network topology for Donald area off-grid case is shown in Figure 64, corresponding to scenario 16 identified in Project 5 Donald area islanding scenario analysis. The off-grid scenario has the same internal distribution network topology as the grid-connected scenario considered in this work, which can enable to consistent comparison of the impact of bushfire impact on grid-connected or off-grid community adequacy [16]. The required generation capacity is summarised in Table 4-4 and the peak load information for each area along the Donald area feeder CTN006 is summarised in Table 4-5:

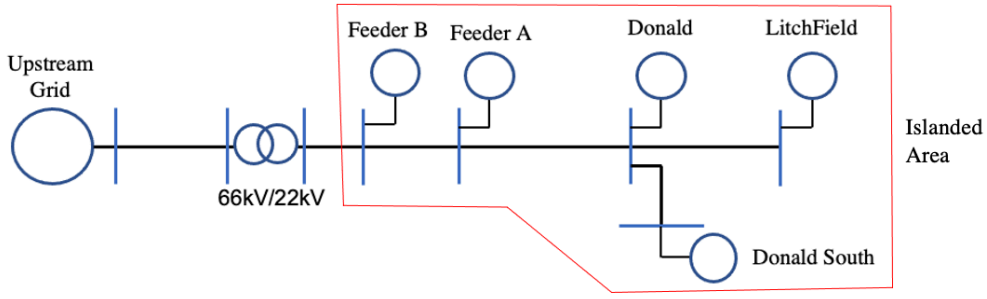

Figure 64. Donald area network topology for off-grid scenario

Table 4-4 Required Generation Information for Donald Area Off-grid Scenario 16 (S16) in Project 5

Scenario S16					
Network Name	Feeder B	Feeder A	Donald	Donald South	Litchfield
Network Topology	1	1	1	1	1
Load (MW)	3.14				
Required Generation					
Solar PV (kW)	1688				
DG (kW)	2430				
Battery Storage (kWh)	155				
Converter (kW)	392				

Table 4-5 Peak Load Information for Areas along Feeder CTN006

Region	Load	Lines	Busbars	Loads	Shunts
Feeder B	0.42MW	166	181	74	2
Feeder A	0.1MW	104	110	43	2
Donald	2.36MW	116	130	50	0
LitchField	0.29MW	172	177	71	2
Donald South	0.06MW	42	43	20	0

The capacity adequacy for Donald off-grid community when no bushfire impact is considered is shown in Figure 65. Different BESS scheduling leading time {1 day, 2 days and 1 week} are applied to explore its impact on off-grid community adequacy. The capacity adequacy is also evaluated when emergency BESS charge is enabled or not. In Figure 65, EENS value of grid connected scenario with no emergent import nor BESS response is shown using the red dashed line. As can be seen from Figure 65, increasing the schedule leading time can improve the capacity adequacy of the off-grid community in general. The capacity adequacy levels under all different schedule leading times, when emergent BESS response is enabled, are higher than those when emergent BESS response is not considered. Also, the

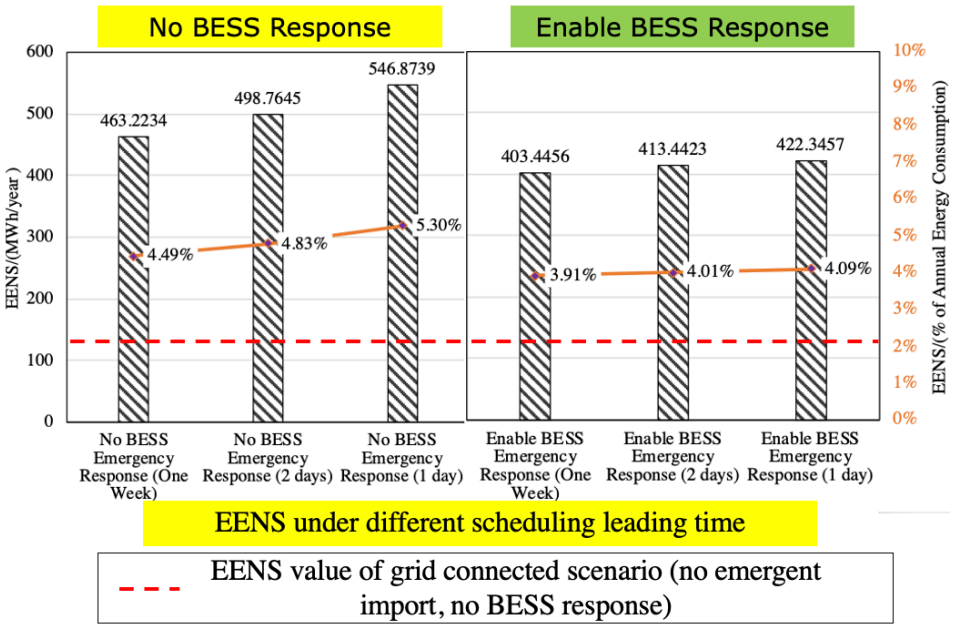

Figure 65. Capacity adequacy of Donald off-grid scenario when no bushfire impact is considered

improvement on capacity adequacy by increasing the schedule leading time becomes more significant when no BESS response is considered, compared to the case when BESS response is enabled.

The impact of bushfire-induced fuel supply disruption on Donald off-grid is analysed under different solar, BESS and DG penetration levels, given different combination of local diesel storage capacity and different assumed fuel disruption duration. When the local diesel storage capacity (in energy/power ratio) is longer than the fuel disruption duration, the bushfire disruption will have no impact on the fuel supply continuity of the off-grid community. In this light, the fuel supply disruption scenario under tested can be summarised using Table 4-6,where the 'N' represents that the bushfire caused no fuel supply constraints.

Table 4-6 Fuel Supply Disruption Scenarios for off-grid System

		Diesel Supply Disruption Duration		
		1 day	**5 days**	**10 days**
Local Diesel Storage Capacity	**1 day**	N	S1D5	S1D10
	5 days	N	N	S5D10
	10 days	N	N	N

The required generation capacity shown in Table 4-4 is used as the base case capacity in the analysis of bushfire impact on off-grid scenario community capacity adequacy. The capacity of DG, solar and BESS capacity are adjusted based on the percentage of based case value, where the percentage under tested for each type of technology is shown below:

- DG: 50%, 100% and 150% of base case capacity are considered
- Solar: 100%, 125%, 150%,175% and 200% of base case capacity are considered
- BESS: 100% and 150% of base case capacity are considered

The EENS results for each fuel supply disruption scenario under different DG, solar and BESS capacity combination are shown in Figure 66(a)~(d). In each plot, different planes correspond to different DG capacity. The X and Y axis of each plot represent the BESS capacity and PV capacity in percent of the base case value respectively and the EENS value is shown on the Z-axis in MWh. Also, it should be noted that the capacity adequacy level for grid-connected scenario under the portfolio shown in Table 4-1 with no bushfire impact is represented using the purple plane with red edge in Figure 66(a). As can be seen from Figure 66(a), the capacity level of Donald off-grid system is higher than the grid-connected community under most combinations of DG, solar and BESS penetration. As can be observed from all subplots in Figure 66, the increase of diesel generator capacity can greatly improve the capacity adequacy level when PV and BESS capacity is low, while the improvement increases at a decreasing rate with PV and BESS capacity increase.

In order to observe the trend of bushfire-induced fuel supply disruption more clearly, the changes in EENS when considering fuel supply disruption constraints or not under different fuel supply disruption scenario are shown in the subplots in Figure 67. The changes in EENS is represented by the percent of annual energy consumption in Donald area. Comparing the corresponding subplot in Figure 66 and Figure 67, it can be seen that higher diesel generator capacity can be more impacted by fuel supply disruption despite the improvement on capacity adequacy level. It can also be seen from subplots in Figure 67, installing more PV and BESS can mitigate the impact of fuel supply disruption on capacity

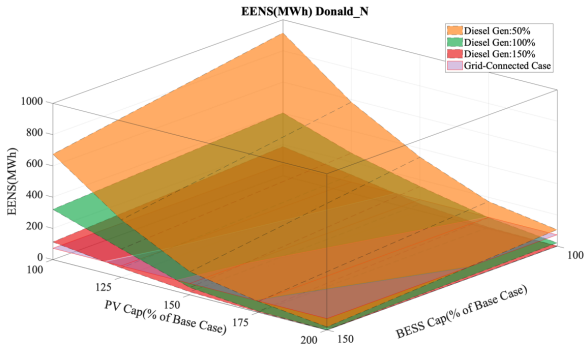

(a) Bushfire caused no fuel supply constraint

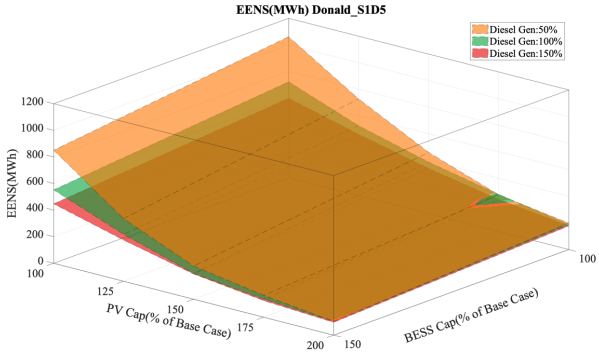

(b) S1D5: 1-day local diesel storage, bushfire caused 5 days fuel disruption

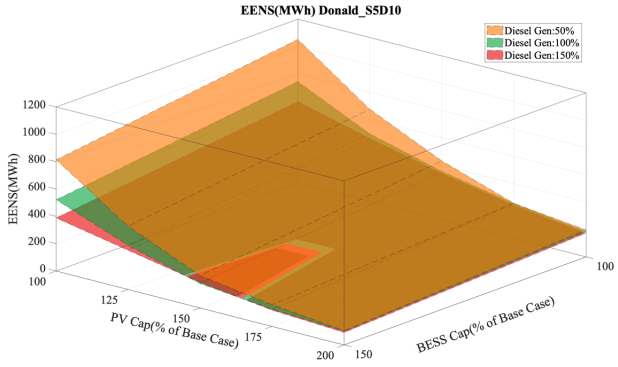

(c) S5D10: 1-day local diesel storage, bushfire caused 10 days fuel disruption period

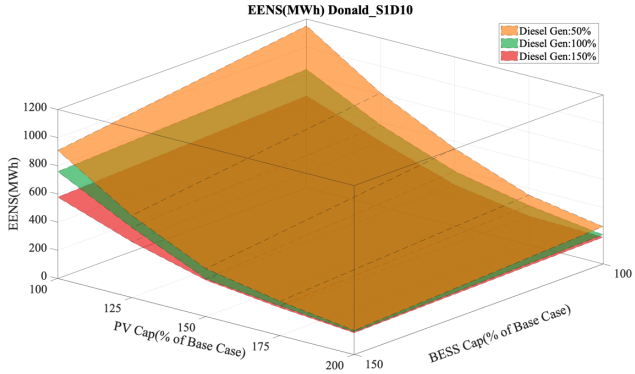

(d) S1D10: 1-day local diesel storage, bushfire caused 10 days fuel disruption period

Figure 66. EENS of Donald off-grid scenario considering bushfire-induced fuel supply disruption impact

adequacy. Nonetheless, this kind of mitigation impact decreases as the fuel supply disruption event becomes more severe, e.g., from S1D5 to S1D10, comparing the results shown in Figure 67 (b) and (d).

Not applicable

(a) Bushfire caused no fuel supply constraint

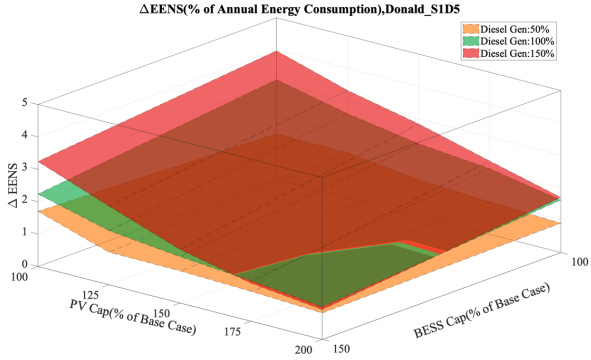

(b) S1D5: 1-day local diesel storage, bushfire caused 5 days fuel disruption

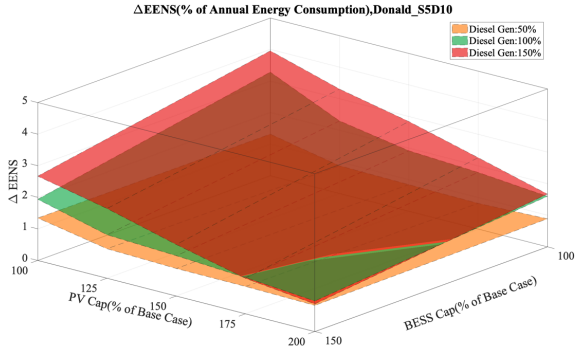

(c) S5D10: 5-day local diesel storage bushfire caused 10 days fuel disruption period

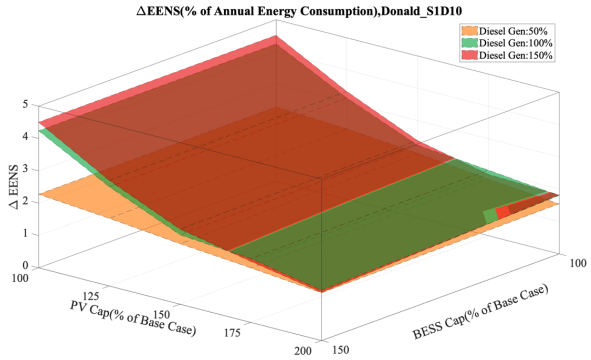

(d) S1D10: 1-day local diesel storage, bushfire caused 10 days fuel disruption period

Figure 67. ΔEENS of Donald off-grid scenario when considering bushfire-induced fuel supply disruption or not

4.2.4 Tarnagulla area under off-grid scenario

The required generation capacity for Tarnagulla area under off-grid scenario is shown in Table 4-7, which is adopted from the sizing results of Project 5 [16].

Table 4-7 Tarnagulla off-grid scenario information

Peak Load	0.17MW
Required Generation	
Solar PV(kW)	134
Diesel Generator(kW)	170
Battery(kWh)	12
Converter (kW)	26.7

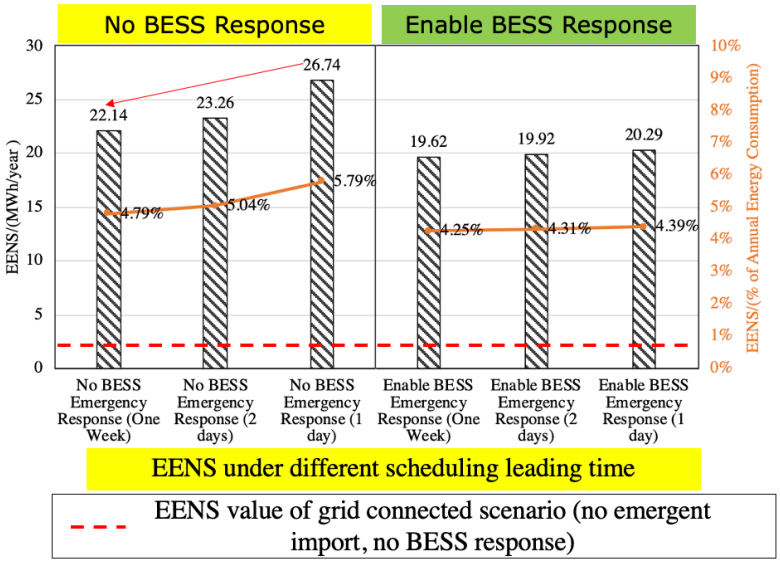

Figure 68. Capacity adequacy of Tarnagulla off-grid scenario when no bushfire impact is considered

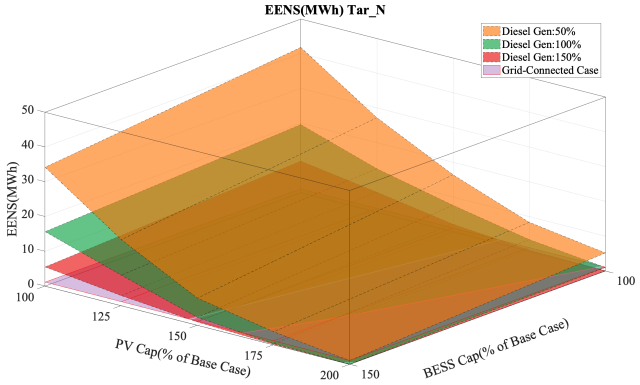

(a) Bushfire caused no fuel supply constraint

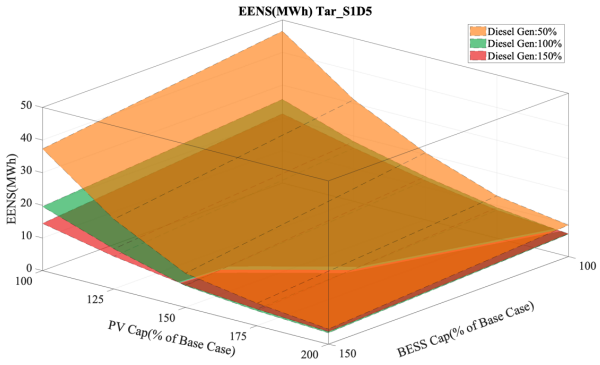

(b) S1D5: 1-day local diesel storage, bushfire caused 5 days fuel disruption

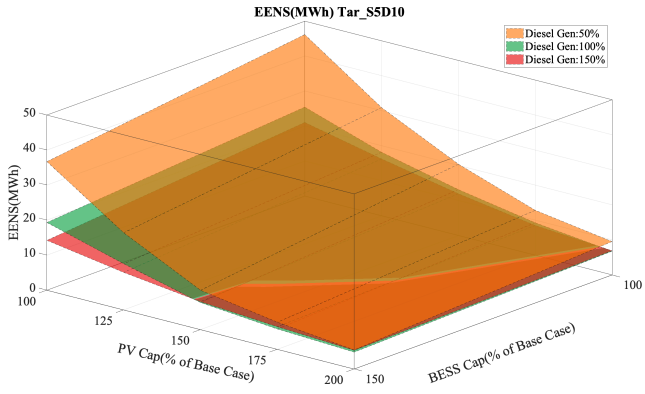

(c) S5D10: 5-day local diesel storage, bushfire caused 10 days fuel disruption period

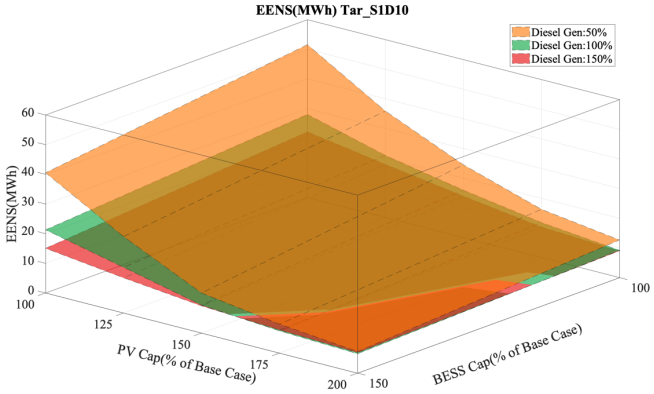

(d) S1D10: 1-day local diesel storage, bushfire caused 10 days fuel disruption period

Figure 69. EENS of Tarnagulla off-grid scenario considering bushfire-induced fuel supply disruption impact

The capacity adequacy for Tarnagulla off-grid community when no bushfire impact is considered is shown in Figure 68. The plot settings of Figure 68 are the same with Figure 65, and the EENS value of grid connected scenario with no emergent import nor BESS response is shown using the red dashed line. The impacts of enabling BESS emergent response and different schedule leading time on the off-grid Tarnagulla area capacity adequacy are the same with the trend for Donald area as shown in Figure 65.

The EENS results for each fuel supply disruption scenario under different DG, solar and BESS capacity combination are shown in Figure 69(a)~(d). The changes in EENS when considering fuel supply disruption constraints or not under different fuel supply disruption scenario are shown in the subplots in Figure 70. The plot settings of Figure 69 and Figure 70 are kept the same with Figure 66 and Figure 67 respectively.

Not applicable

(a) Bushfire caused no fuel supply constraint

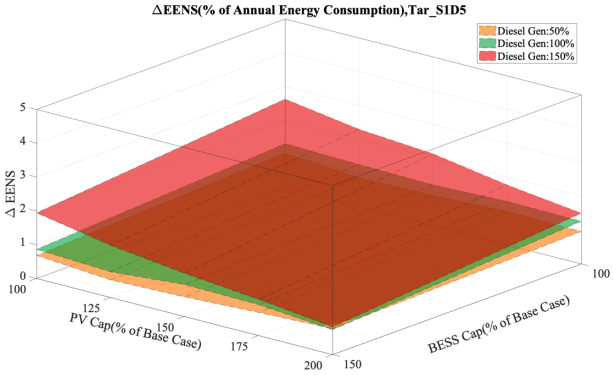

(b) S1D5: 1-day local diesel storage, bushfire caused 5 days fuel disruption

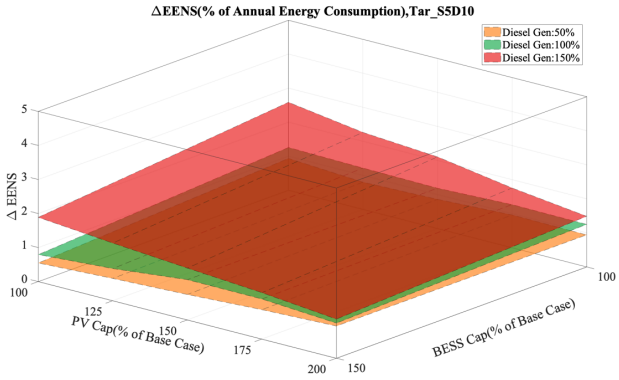

(c) S5D10: 5-day local diesel storage, bushfire caused 10 days fuel disruption period

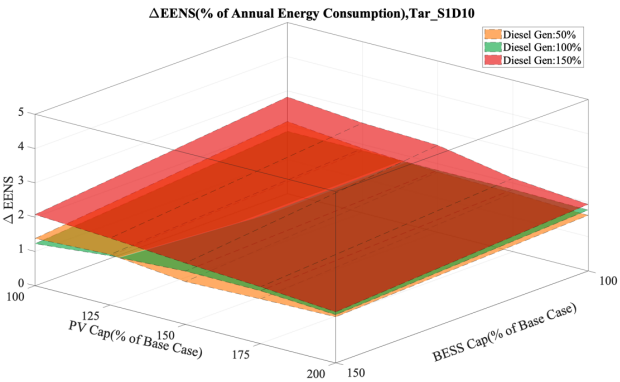

(d) S1D10: 1-day local diesel storage, bushfire caused 10 days fuel disruption period

Figure 70. ΔEENS of Tarnagulla off-grid scenario when considering bushfire-induced fuel supply disruption or not

4.3 Off-grid generation portfolio – SAPS rules

Based on the newly published *Stand-Alone Power System (SAPS) Capacity Adequacy Rules [17],* the off-grid system capacity adequacy level should not be worse than that when it is grid-connected. As can

be seen from Figure 65 and Figure 68, the off-grid scenario capacity adequacy levels of both Donald and Tarnagulla area under the sizing results of project 5 are both much higher than grid-connected scenario under the required generation portfolio from project 5. In this light, the generation capacity of off-grid scenario of these two areas needs to be increased in order to fulfill the SAPS capacity adequacy rules.

4.3.1 Off-grid community sizing without bushfire-induced fuel disruption

Currently, the impact of extreme events (e.g., bushfire) has not been considered in the community capacity adequacy level planning. Thus, the off-grid community sizing procedure without considering bushfire-induced fuel disruption impact is first introduced to determine the required off-grid community generation portfolios of Tarnagulla and Donald area. The procedure is detailed as following:

Step 1) Identify DG/PV/BESS portfolios such that the capacity adequacy level of off-grid community is no less than grid-connected community (under the specific generation portfolio as shown in Table 4-1 and Table 4-3)

Step 2) For each identified portfolio, calculate the total net present cost $NPC_{tot} = NPC_{inv} + NPC_{vcr}$. Where NPC_{inv} represents the infrastructure investment cost, NPC_{vcr} represent the cost for energy not supplied based on the value of customer reliability (VCR). The VCR value is **AU$16.96/kWh** adopted from the value used in project 5 [16].

Step 3) Identify the portfolio generates the least total NPC.

The sizing results for Tarnagulla and Donald area are tabulated and highlighted using red dashed line in Table 4-8 and Table 4-9 respectively:

Table 4-8 Off-grid Tarnagulla area sizing without considering bushfire impact

1 DG Cap(% of Base Cap)	2 BESS Cap(% of Base Cap)	3 PV Cap(% of Base Cap)	4 Investment NPC(AU$M)	5 Reliablity NPC(No Disruption)	6 Total NPC(AU$M)
0.5000	1.5000	1.7500	8.3828	15.9862	24.3690
0.5000	1.5000	2	9.2268	4.4518	13.6786
1	1	1.7500	9.4225	16.2563	25.6788
1	1	2	10.2665	4.8202	15.0867
1	1.5000	1.5000	8.9373	10.5855	19.5228
1	1.5000	1.7500	9.7813	1.6067	11.3880
1	1.5000	2	10.6253	0.1418	10.7670
1.5000	1	1.5000	9.9770	10.4550	20.4320
1.5000	1	1.7500	10.8210	1.9092	12.7302
1.5000	1	2	11.6650	0.3225	11.9875
1.5000	1.5000	1.2500	9.4918	13.5137	23.0055
1.5000	1.5000	1.5000	10.3358	4.2774	14.6131
1.5000	1.5000	1.7500	11.1798	0.6202	11.8000
1.5000	1.5000	2	12.0238	0.0536	12.0773

Table 4-9 Off-grid Donald area sizing without considering bushfire impact

1 DG Cap(% of Base Cap)	2 BESS Cap(% of Base Cap)	3 PV Cap(% of Base Cap)	4 Investment NPC(AU$M)	5 Reliablity NPC(No Disruption)	6 Total NPC(AU$M)
0.5000	1.5000	2	0.7100	0.2447	0.9547
1	1	2	0.7824	0.2344	1.0168
1	1.5000	1.7500	0.7408	0.0781	0.8190
1	1.5000	2	0.8078	0.0069	0.8147
1.5000	1	1.7500	0.8133	0.0928	0.9061
1.5000	1	2	0.8803	0.0157	0.8960
1.5000	1.5000	1.5000	0.7717	0.2080	0.9797
1.5000	1.5000	1.7500	0.8387	0.0302	0.8688
1.5000	1.5000	2	0.9057	0.0026	0.9083

4.3.2 Off-grid community sizing with bushfire-induced fuel disruption

As can be seen from the case studies in Sections 2.1 to 2.4, it can be observed that the bushfire-induced fuel supply disruption can have great impact on off-grid community capacity adequacy level. It could be necessary to understand how the bushfire impact can mitigate the investment decision.

4.3.2.1 Scenario-based probabilistic off-grid sizing procedure

A scenario-based off-grid community probabilistic sizing procedure that can incorporate bushfire-induced fuel disruption impact on capacity adequacy is adopted to determine the off-grid generation portfolio investment. The formulation of probabilistic sizing procedure is based on assigning probabilities to different disruption duration scenarios to enable the selection of the "statistically" best solution regarding a given attribute (e.g., net present cost considering both investment and value of unserved energy) across scenarios through a linear composition of its values weighted with the respective scenario probabilities. However, it should be noted that the results could be sensitive to the probabilities assigned to different scenarios. The procedure of the scenario-based probabilistic sizing procedure is explained as following:

Step 1) Identify DG/PV/BESS portfolios such that the capacity adequacy level of off-grid community is no less than grid-connected community (under the specific generation portfolio as shown in Table 4-1 and Table 4-3)

Step 2) For each identified portfolio, calculate the infrastructure investment net present cost NPC_{inv}

Step 3) Calculate the total NPC (NPC_{tot}) considering investment cost and weighted NPC_{vcr} under different fuel supply disruption scenario probability. To do this, assumptions are made to specify the probabilities of bushfire-induced fuel supply disruption duration [no disruption; 1 day disruption; 5 days disruption; 10 days disruption]:

$$[p_0, p_{1d}, p_{5d}, p_{10d}] = [0.9; 0.06; 0.03; 0.01]$$

The values of $[p_0, p_{1d}, p_{5d}, p_{10d}]$ represent the probability of fuel-supply disruption occurrence of different duration, for example, $p_0 = 0.01$ represents that a 10-day bushfire-induced fuel-supply disruption could occur one time in every 100 years. Then, the total NPC can be calculated using the formula:

$$NPC_{tot} = NPC_{inv} + p_0 * NPC_{vcr,0} + p_{1d} * NPC_{vcr,1d} + p_{5d} * NPC_{vcr,5d} + p_{10d} * NPC_{vcr,10d}$$

Step 4) Identify the portfolio generates the least total NPC

Different set of probabilities $[p_0, p_{1d}, p_{5d}, p_{10d}]$ are assumed to explore the sensitivity of investment decision to different fuel supply disruption duration scenario occurrence probability, the probabilities under tested including:

a) $[p_0, p_{1d}, p_{5d}, p_{10d}] = [0.9, 0.1, 0, 0]$;
b) $[p_0, p_{1d}, p_{5d}, p_{10d}] = [0.9, 0, 0.1, 0]$;
c) $[p_0, p_{1d}, p_{5d}, p_{10d}] = [0.9, 0, 0, 0.1]$;
d) $[p_0, p_{1d}, p_{5d}, p_{10d}] = [0.9, 0.06, 0.03, 0.01]$;

The sizing results for Donald and Tarnagulla off-grid scenario under different combination probability of fuel supply disruption duration are tabulated in Table 4-10 and Table 4-11.

Table 4-10 Donald off-grid Scenario Sizing Results under Different $[p_0, p_{1d}, p_{5d}, p_{10d}]$

$[p_0, p_{1d}, p_{5d}, p_{10d}]$	DG Cap(% of Base Cap)	Local Fuel Storage Cap(days)	BESS Cap(% of Base Cap)	PV Cap(% of Base Cap)	NPC_{inv}(AU$M)	$NPC_{vcr,0}$	$NPC_{vcr,1d}$	$NPC_{vcr,5d}$	$NPC_{vcr,10d}$	$NPC_{vcr,total}$	Total NPC
[0.9, **0.1**, 0, 0]	1	**1**	1.5	2	10.625	0.12759	0.0142	0	0	0.14179	10.767
[0.9, 0, **0.1**, 0]	1	**5**	1.5	2	10.641	0.12759	0	0.0142	0	0.14179	10.783
[0.9, 0 , 0, **0.1**]	1	**10**	1.5	2	10.673	0.12759	0	0	0.0142	0.14179	10.815
[**0.9, 0.06 , 0.03, 0.01**]	1	**10**	1.5	2	10.673	0.12759	0.0085	0.0043	0.00141	0.1418	10.815

Table 4-11 Tarnagulla off-grid Scenario Sizing Results under Different $[p_0, p_{1d}, p_{5d}, p_{10d}]$

$[p_0, p_{1d}, p_{5d}, p_{10d}]$	DG Cap(% of Base Cap)	Local Fuel Storage Cap(days)	BESS Cap(% of Base Cap)	PV Cap(% of Base Cap)	NPC_{inv}(AU$M)	$NPC_{vcr,0}$	$NPC_{vcr,1d}$	$NPC_{vcr,5d}$	$NPC_{vcr,10d}$	$NPC_{vcr,total}$	Total NPC
[0.9, **0.1**, 0, 0]	1	**1**	1.5	2	0.808	0.0062	0.0007	0	0	0.0069	0.8149
[0.9, 0, **0.1**, 0]	1	**5**	1.5	2	0.809	0.0062	0	0.0007	0	0.0069	0.8159
[0.9, 0 , 0, **0.1**]	1	**10**	1.5	2	0.811	0.0062	0	0	0.0007	0.0069	0.8179
[**0.9, 0.06 , 0.03, 0.01**]	1	**10**	1.5	2	0.811	0.0062	0.0004	0.0002	0.0001	0.0069	0.8179

It can be seen from both tables that the required DG, PV and BESS capacity kept constant as the probabilities of fuel supply disruption with different duration varies, only the required local fuel storage capacity increases as p_{1d}, p_{5d}, p_{10d} are set to a non-zero value respectively. This is due to the investment on additional local fuel storage can lead to more savings on $NPC_{vcr,total}$ compared to the slight infrastructure investment NPC increase. A full table that displays the NPC of each identified portfolio in **Step 1)** under each combination of probability can be seen from an interactive visualisation tool developed in MATLAB, which will be introduced at the end of this section.

It should also be noted that the value of customer reliability can also change with the duration of outage events. Most available research have only focused on exploring the cost of outages with an outage duration shorter than 24 hours [18],[19], no research has ever investigated how the cost of outages may vary with an outage duration longer than 5 days or 10 days. It can be inferred that the cost of outages will increase when the outage duration lasts for days. In this light, the VCR under different fuel-supply disruption duration is scaled up with different factors:

$$VCR_{\{0,1d,5d,10d\}} = 16.96 * [1, 1.1, 1.5, 2]\ AU\$/kWh$$

and the sizing results under different $[p_0, p_{1d}, p_{5d}, p_{10d}]$ are summarized in Table 4-12 and Table 4-13:

Table 4-12 Donald off-grid Scenario Sizing Results under Different $[p_0, p_{1d}, p_{5d}, p_{10d}]$

$[p_0, p_{1d}, p_{5d}, p_{10d}]$	DG Cap(% of Base Cap)	Local Fuel Storage Cap(days)	BESS Cap(% of Base Cap)	PV Cap(% of Base Cap)	NPC_{inv}(A U$M)	$NPC_{vcr,0}$	$NPC_{vcr,1d}$	$NPC_{vcr,5d}$	$NPC_{vcr,10d}$	$NPC_{vcr,total}$	Total NPC
[0.9, **0.1**, 0, 0]	1	**1**	1.5	2	10.625	0.12759	0.0159	0	0	0.14349	10.768
[0.9, 0, **0.1**, 0]	1	**5**	1.5	2	10.641	0.12759	0	0.0212	0	0.14879	10.791
[0.9, 0 , 0, **0.1**]	1	**10**	1.5	2	10.673	0.12759	0	0	0.0284	0.15419	10.829
[**0.9, 0.06 , 0.03, 0.01**]	1	**10**	1.5	2	10.673	0.12759	0.0094	0.0064	0.0028	0.147	10.82

Table 4-13 Tarnagulla off-grid Scenario Sizing Results under Different $[p_0, p_{1d}, p_{5d}, p_{10d}]$

$[p_0, p_{1d}, p_{5d}, p_{10d}]$	DG Cap(% of Base Cap)	Local Fuel Storage Cap(days)	BESS Cap(% of Base Cap)	PV Cap(% of Base Cap)	NPC_{inv}(A U$M)	$NPC_{vcr,0}$	$NPC_{vcr,1d}$	$NPC_{vcr,5d}$	$NPC_{vcr,10d}$	$NPC_{vcr,total}$	Total NPC
[0.9, **0.1**, 0, 0]	1	**1**	1.5	2	0.8078	0.0062	0.0008	0	0	0.0070	0.8148
[0.9, 0, **0.1**, 0]	1	**5**	1.5	2	0.8089	0.0062	0	0.0010	0	0.0072	0.8162
[0.9, 0 , 0, **0.1**]	1	**10**	1.5	2	0.8112	0.0062	0	0	0.0014	0.0076	0.8189
[**0.9, 0.06 , 0.03, 0.01**]	1	**10**	1.5	2	0.8112	0.0062	0.0005	0.0003	0.0001	0.0071	0.8183

It can be seen that the sizing results do not change under the new assumed $VCR_{\{0,1d,5d,10d\}}$.

4.3.2.2 Min/Max regret sizing procedure

The scenario-based sizing procedure is usually used as a risk-neutral decision-making framework, and it can only be used when the assumption of different disruption scenarios probabilities can be properly estimated. If the system planners are extreme risk-averse, then the min-max regret framework can be adopted to size the off-grid community. This general methodology, which is widely used in the area of *game theory*, models the decision-making issue under uncertainty using 2-layer optimisations (minmax). Although it needs a more sophisticated formulation than stochastic programming, it does not require the explicit assignment of weights to each scenario, which system designers view to be a benefit.

Min-max regret is a variant of generic nested min-max optimisation in which the value attribute is replaced with a regret. Regrets are based on an ex-post assessment of the decision maker's perceptions of its actions, which are often represented in monetary terms. The preferred alternative is the one that minimises a decision maker's regret upon discovering that the decision he made was not optimum in light of the ultimate outcome [20]. The procedure of the min-max regret decision framework in the off-grid sizing procedure are explained as following:

Step 1) Identify DG/PV/BESS portfolios such that the capacity adequacy level of off-grid community is no less than grid-connected community (under the specific generation portfolio as shown in Table 4-1 and Table 4-3)

Step 2) For each identified portfolio i, calculate the infrastructure investment net present cost NPC_{inv}^{i}

Step 3) For each identified portfolio i, calculate the total NPC (NPC_{tot}) under each fuel supply disruption scenario, including the investment cost and the NPC_{vcr} under each fuel supply disruption scenario. The total NPC under each fuel supply disruption duration [no disruption; 1 day disruption; 5 days disruption; 10 days disruption] is denoted as $[NPC_{tot,nodis}^{i}, NPC_{tot,1d\ Dis}^{i}, NPC_{tot,5d\ Dis}^{i}, NPC_{tot,10d\ Dis}^{i}]$, which can be calculated using:

$$NPC_{tot,nodis}^{i} = NPC_{inv}^{i} + NPC_{vcr,0}^{i}$$

$$NPC_{tot,1d\ Dis}^{i} = NPC_{inv}^{i} + NPC_{vcr,1d}^{i}$$

$$NPC^{i}_{tot,5d\ Dis} = NPC^{i}_{inv} + NPC^{i}_{vcr,5d}$$
$$NPC^{i}_{tot,10d\ Dis} = NPC^{i}_{inv} + NPC^{i}_{vcr,10d}$$

Step 4) For each portfolio, calculate the regret under under each fuel supply disruption scenario $[Reg^{i}_{tot,nodis}, Reg^{i}_{tot,1d\ Dis}, Reg^{i}_{tot,5d\ Dis}, Reg^{i}_{tot,10d\ Dis}]$ and the maximum regret $MaxReg^{i}$ using the equations below:

$$Reg^{i}_{tot,nodis} = NPC^{i}_{tot,nodis} - NPC^{min}_{tot,nodis}$$
$$Reg^{i}_{tot,1d\ Dis} = NPC^{i}_{tot,1d\ Dis} - NPC^{min}_{tot,1d\ Dis}$$
$$Reg^{i}_{tot,5d\ Dis} = NPC^{i}_{tot,5d\ Dis} - NPC^{min}_{tot,1d\ Dis}$$
$$Reg^{i}_{tot,10d\ Dis} = NPC^{i}_{tot,10d\ Dis} - NPC^{min}_{tot,10d\ Dis}$$
$$MaxReg^{i} = \max\{Reg^{i}_{tot,nodis}, Reg^{i}_{tot,1d\ Dis}, Reg^{i}_{tot,5d\ Dis}, Reg^{i}_{tot,10d\ Dis}]\ \}$$

Step 5) Identify DG/PV/BESS portfolios which gives the minimum $MaxReg^{i}$.

The NPC tables including investment cost and the NPC_{vcr} under each fuel supply disruption scenario of Donald and Tarnagulla area when the values of $VCR_{\{0,1d,5d,10d\}}$ are not scaled up is shown in Table 4-14 and Table 4-15, while the regret tables and the optimal portfolio (highlighted in red rectangular) of Donald and Tarnagulla area are shown in Table 4-16 and Table 4-17.

Table 4-14. Donald Area Investment NPC, NPC_VCR and Total NPC under Different Disruption Duration Scenarios(AU$M)

1 DG Cap	2 Fuel Tank	3 BESS Cap	4 PV Cap	5 Investment NPC	6 VCR_NPC(Nodis)	7 VCR_NPC(1d Dis)	8 VCR_NPC(5d Dis)	9 VCR_NPC(10d Dis)	10 Tot NPC(Nodis)	11 Tot NPC(1d Dis)	12 Tot NPC(5d Dis)	13 Tot NPC(10d Dis)
0.5000	1	1.5000	1.7500	8.3828	15.9862	15.9862	37.7793	55.8757	24.3690	24.3690	46.1621	64.2586
0.5000	5	1.5000	1.7500	8.3908	15.9862	15.9862	15.9862	36.4278	24.3770	24.3770	24.3770	44.8186
0.5000	10	1.5000	1.7500	8.4069	15.9862	15.9862	15.9862	15.9862	24.3930	24.3930	24.3930	24.3930
0.5000	1	1.5000	2	9.2268	4.4518	4.4518	23.7690	39.4094	13.6786	13.6786	32.9958	48.6362
0.5000	5	1.5000	2	9.2348	4.4518	4.4518	4.4518	24.0124	13.6867	13.6867	13.6867	33.2472
0.5000	10	1.5000	2	9.2509	4.4518	4.4518	4.4518	4.4518	13.7027	13.7027	13.7027	13.7027
1	1	1	1.7500	9.4225	16.2563	16.2563	64.2913	64.3665	25.6788	25.6788	73.7138	73.7890
1	5	1	1.7500	9.4385	16.2563	16.2563	16.2563	58.8332	25.6948	25.6948	25.6948	68.2718
1	10	1	1.7500	9.4706	16.2563	16.2563	16.2563	16.2563	25.7269	25.7269	25.7269	25.7269
1	1	1	2	10.2665	4.8202	4.8202	43.2602	47.5928	15.0867	15.0867	53.5267	57.8593
1	5	1	2	10.2825	4.8202	4.8202	4.8202	42.7349	15.1027	15.1027	15.1027	53.0174
1	10	1	2	10.3146	4.8202	4.8202	4.8202	4.8202	15.1348	15.1348	15.1348	15.1348
1	1	1.5000	1.5000	8.9373	10.5855	10.5855	44.4200	61.4639	19.5228	19.5228	53.3572	70.4012
1	5	1.5000	1.5000	8.9533	10.5855	10.5855	10.5855	40.7815	19.5388	19.5388	19.5388	49.7348
1	10	1.5000	1.5000	8.9854	10.5855	10.5855	10.5855	10.5855	19.5709	19.5709	19.5709	19.5709
1	1	1.5000	1.7500	9.7813	1.6067	1.6067	31.1868	48.2504	11.3880	11.3880	40.9680	58.0317
1	5	1.5000	1.7500	9.7973	1.6067	1.6067	1.6067	28.7096	11.4040	11.4040	11.4040	38.5069
1	10	1.5000	1.7500	9.8294	1.6067	1.6067	1.6067	1.6067	11.4361	11.4361	11.4361	11.4361
1	1	1.5000	2	10.6253	0.1418	0.1418	23.8477	36.9824	10.7670	10.7670	34.4730	47.6077
1	5	1.5000	2	10.6413	0.1418	0.1418	0.1418	23.0140	10.7831	10.7831	10.7831	33.6553
1	10	1.5000	2	10.6734	0.1418	0.1418	0.1418	0.1418	10.8152	10.8152	10.8152	10.8152
1.5000	1	1	1.5000	9.9770	10.4550	10.4550	77.9502	66.9861	20.4320	20.4320	87.9272	76.9631
1.5000	5	1	1.5000	10.0010	10.4550	10.4550	10.4550	77.8730	20.4561	20.4561	20.4561	87.8740
1.5000	10	1	1.5000	10.0491	10.4550	10.4550	10.4550	10.4550	20.5042	20.5042	20.5042	20.5042
1.5000	1	1	1.7500	10.8210	1.9092	1.9092	55.5756	46.9744	12.7302	12.7302	66.3966	57.7954
1.5000	5	1	1.7500	10.8450	1.9092	1.9092	1.9092	55.5390	12.7542	12.7542	12.7542	66.3840
1.5000	10	1	1.7500	10.8931	1.9092	1.9092	1.9092	1.9092	12.8024	12.8024	12.8024	12.8024
1.5000	1	1	2	11.6650	0.3225	0.3225	40.6655	43.6049	11.9875	11.9875	52.3305	55.2698
1.5000	5	1	2	11.6890	0.3225	0.3225	0.3225	39.9332	12.0115	12.0115	12.0115	51.6223
1.5000	10	1	2	11.7371	0.3225	0.3225	0.3225	0.3225	12.0597	12.0597	12.0597	12.0597
1.5000	1	1.5000	1.2500	9.4918	13.5137	13.5137	71.0420	90.9367	23.0055	23.0055	80.5337	100.4285
1.5000	5	1.5000	1.2500	9.5158	13.5137	13.5137	13.5137	65.8096	23.0295	23.0295	23.0295	75.3254
1.5000	10	1.5000	1.2500	9.5639	13.5137	13.5137	13.5137	13.5137	23.0777	23.0777	23.0777	23.0777
1.5000	1	1.5000	1.5000	10.3358	4.2774	4.2774	43.3945	59.2909	14.6131	14.6131	53.7302	69.6266
1.5000	5	1.5000	1.5000	10.3598	4.2774	4.2774	4.2774	42.8781	14.6372	14.6372	14.6372	53.2379
1.5000	10	1.5000	1.5000	10.4079	4.2774	4.2774	4.2774	4.2774	14.6853	14.6853	14.6853	14.6853
1.5000	1	1.5000	1.7500	11.1798	0.6202	0.6202	28.4496	45.3149	11.8000	11.8000	39.6293	56.4946
1.5000	5	1.5000	1.7500	11.2038	0.6202	0.6202	0.6202	27.1641	11.8240	11.8240	11.8240	38.3679
1.5000	10	1.5000	1.7500	11.2519	0.6202	0.6202	0.6202	0.6202	11.8722	11.8722	11.8722	11.8722
1.5000	1	1.5000	2	12.0238	0.0536	0.0536	21.8937	35.3965	12.0773	12.0773	33.9174	47.4203
1.5000	5	1.5000	2	12.0478	0.0536	0.0536	0.0536	20.6991	12.1014	12.1014	12.1014	32.7469
1.5000	10	1.5000	2	12.0959	0.0536	0.0536	0.0536	0.0536	12.1495	12.1495	12.1495	12.1495

Table 4-15. Tarnagulla Area Investment NPC, NPC_VCR and Total NPC under Different Disruption Duration Scenarios(AU$M)

1 DG Cap	2 Fuel Tank	3 BESS Cap	4 PV Cap	5 Investment NPC	6 VCR_NPC(Nodis)	7 VCR_NPC(1d Dis)	8 VCR_NPC(5d Dis)	9 VCR_NPC(10d Dis)	10 Tot NPC(Nodis)	11 Tot NPC(1d Dis)	12 Tot NPC(5d Dis)	13 Tot NPC(10d Dis)
0.5000	1	1.5000	2	0.7100	0.2447	0.2447	1.0574	1.6677	0.9547	0.9547	1.7673	2.3777
0.5000	5	1.5000	2	0.7105	0.2447	0.2447	0.2447	1.2460	0.9552	0.9552	0.9552	1.9566
0.5000	10	1.5000	2	0.7117	0.2447	0.2447	0.2447	0.2447	0.9563	0.9563	0.9563	0.9563
1	1	1	2	0.7824	0.2344	0.2344	1.5747	2.1181	1.0168	1.0168	2.3571	2.9006
1	5	1	2	0.7836	0.2344	0.2344	0.2344	1.5612	1.0180	1.0180	1.0180	2.3447
1	10	1	2	0.7858	0.2344	0.2344	0.2344	0.2344	1.0202	1.0202	1.0202	1.0202
1	1	1.5000	1.7500	0.7408	0.0781	0.0781	1.0455	1.7111	0.8190	0.8190	1.7863	2.4519
1	5	1.5000	1.7500	0.7419	0.0781	0.0781	0.0781	1.3248	0.8201	0.8201	0.8201	2.0667
1	10	1.5000	1.7500	0.7442	0.0781	0.0781	0.0781	0.0781	0.8223	0.8223	0.8223	0.8223
1	1	1.5000	2	0.8078	0.0069	0.0069	0.7847	1.4939	0.8147	0.8147	1.5925	2.3017
1	5	1.5000	2	0.8089	0.0069	0.0069	0.0069	1.0989	0.8158	0.8158	0.8158	1.9078
1	10	1.5000	2	0.8112	0.0069	0.0069	0.0069	0.0069	0.8181	0.8181	0.8181	0.8181
1.5000	1	1	1.7500	0.8133	0.0928	0.0928	1.9749	2.3619	0.9061	0.9061	2.7882	3.1752
1.5000	5	1	1.7500	0.8150	0.0928	0.0928	0.0928	1.9580	0.9078	0.9078	0.9078	2.7730
1.5000	10	1	1.7500	0.8183	0.0928	0.0928	0.0928	0.0928	0.9112	0.9112	0.9112	0.9112
1.5000	1	1	2	0.8803	0.0157	0.0157	1.6084	2.0750	0.8960	0.8960	2.4887	2.9553
1.5000	5	1	2	0.8820	0.0157	0.0157	0.0157	1.5947	0.8976	0.8976	0.8976	2.4766
1.5000	10	1	2	0.8853	0.0157	0.0157	0.0157	0.0157	0.9010	0.9010	0.9010	0.9010
1.5000	1	1.5000	1.5000	0.7717	0.2080	0.2080	1.5652	2.1028	0.9797	0.9797	2.3369	2.8745
1.5000	5	1.5000	1.5000	0.7733	0.2080	0.2080	0.2080	1.8225	0.9814	0.9814	0.9814	2.5958
1.5000	10	1.5000	1.5000	0.7767	0.2080	0.2080	0.2080	0.2080	0.9847	0.9847	0.9847	0.9847
1.5000	1	1.5000	1.7500	0.8387	0.0302	0.0302	1.1641	1.7862	0.8688	0.8688	2.0027	2.6248
1.5000	5	1.5000	1.7500	0.8403	0.0302	0.0302	0.0302	1.4750	0.8705	0.8705	0.8705	2.3153
1.5000	10	1.5000	1.7500	0.8437	0.0302	0.0302	0.0302	0.0302	0.8739	0.8739	0.8739	0.8739
1.5000	1	1.5000	2	0.9057	0.0026	0.0026	0.8706	1.5800	0.9083	0.9083	1.7763	2.4857
1.5000	5	1.5000	2	0.9073	0.0026	0.0026	0.0026	1.2193	0.9099	0.9099	0.9099	2.1266
1.5000	10	1.5000	2	0.9107	0.0026	0.0026	0.0026	0.0026	0.9133	0.9133	0.9133	0.9133

Table 4-16. Regret Table for Donald Area Under Each Identified Portfolio and the Optimal Portfolio Based on Min/Max Regret Decision Framework

1 DG Cap	2 Fuel Tank	3 BESS Cap	4 PV Cap	5 Regret Nodis	6 Regret(1-day Dis)	7 Regret(5-day Dis)	8 Regret(10-day Dis)	9 Max regret
0.5000	1	1.5000	1.7500	13.6019	13.6019	35.3790	53.4434	53.4434
0.5000	5	1.5000	1.7500	13.6100	13.6100	13.5939	34.0035	34.0035
0.5000	10	1.5000	1.7500	13.6260	13.6260	13.6100	13.5779	13.6260
0.5000	1	1.5000	2	2.9116	2.9116	22.2127	37.8210	37.8210
0.5000	5	1.5000	2	2.9196	2.9196	2.9036	22.4321	22.4321
0.5000	10	1.5000	2	2.9356	2.9356	2.9196	2.8875	2.9356
1	1	1	1.7500	14.9117	14.9117	62.9307	62.9738	62.9738
1	5	1	1.7500	14.9278	14.9278	14.9117	57.4566	57.4566
1	10	1	1.7500	14.9598	14.9598	14.9438	14.9117	14.9598
1	1	1	2	4.3196	4.3196	42.7437	47.0441	47.0441
1	5	1	2	4.3357	4.3357	4.3196	42.2023	42.2023
1	10	1	2	4.3677	4.3677	4.3517	4.3196	4.3677
1	1	1.5000	1.5000	8.7557	8.7557	42.5742	59.5860	59.5860
1	5	1.5000	1.5000	8.7717	8.7717	8.7557	38.9196	38.9196
1	10	1.5000	1.5000	8.8038	8.8038	8.7878	8.7557	8.8038
1	1	1.5000	1.7500	0.6210	0.6210	30.1850	47.2165	47.2165
1	5	1.5000	1.7500	0.6370	0.6370	0.6210	27.6918	27.6918
1	10	1.5000	1.7500	0.6691	0.6691	0.6530	0.6210	0.6691
1	1	1.5000	2	0	0	23.6899	36.7925	36.7925
1	5	1.5000	2	0.0160	0.0160	0	22.8402	22.8402
1	10	1.5000	2	0.0481	0.0481	0.0321	0	0.0481
1.5000	1	1	1.5000	9.6650	9.6650	77.1441	66.1479	77.1441
1.5000	5	1	1.5000	9.6890	9.6890	9.6730	77.0589	77.0589
1.5000	10	1	1.5000	9.7371	9.7371	9.7211	9.6890	9.7371
1.5000	1	1	1.7500	1.9631	1.9631	55.6135	46.9802	55.6135
1.5000	5	1	1.7500	1.9872	1.9872	1.9712	55.5688	55.5688
1.5000	10	1	1.7500	2.0353	2.0353	2.0193	1.9872	2.0353
1.5000	1	1	2	1.2204	1.2204	41.5474	44.4547	44.4547
1.5000	5	1	2	1.2445	1.2445	1.2284	40.8071	40.8071
1.5000	10	1	2	1.2926	1.2926	1.2766	1.2445	1.2926
1.5000	1	1.5000	1.2500	12.2384	12.2384	69.7506	89.6133	89.6133
1.5000	5	1.5000	1.2500	12.2625	12.2625	12.2465	64.5103	64.5103
1.5000	10	1.5000	1.2500	12.3106	12.3106	12.2946	12.2625	12.3106
1.5000	1	1.5000	1.5000	3.8461	3.8461	42.9472	58.8114	58.8114
1.5000	5	1.5000	1.5000	3.8701	3.8701	3.8541	42.4227	42.4227
1.5000	10	1.5000	1.5000	3.9182	3.9182	3.9022	3.8701	3.9182
1.5000	1	1.5000	1.7500	1.0329	1.0329	28.8463	45.6795	45.6795
1.5000	5	1.5000	1.7500	1.0570	1.0570	1.0410	27.5527	27.5527
1.5000	10	1.5000	1.7500	1.1051	1.1051	1.0891	1.0570	1.1051
1.5000	1	1.5000	2	1.3103	1.3103	23.1343	36.6051	36.6051
1.5000	5	1.5000	2	1.3343	1.3343	1.3183	21.9317	21.9317
1.5000	10	1.5000	2	1.3824	1.3824	1.3664	1.3343	1.3824

Table 4-17. Regret Table for Tarnagulla Area Under Each Identified Portfolio and the Optimal Portfolio Based on Min/Max Regret Decision Framework

1 DG Cap	2 Fuel Tank	3 BESS Cap	4 PV Cap	5 Regret Nodis	6 Regret(1-day Dis)	7 Regret(5-day Dis)	8 Regret(10-day Dis)	9 Max regret
0.5000	1	1.5000	2	0.1399	0.1399	0.9515	1.5596	1.5596
0.5000	5	1.5000	2	0.1405	0.1405	0.1394	1.1385	1.1385
0.5000	10	1.5000	2	0.1416	0.1416	0.1405	0.1383	0.1416
1	1	1	2	0.2021	0.2021	1.5413	2.0825	2.0825
1	5	1	2	0.2033	0.2033	0.2021	1.5267	1.5267
1	10	1	2	0.2055	0.2055	0.2044	0.2021	0.2055
1	1	1.5000	1.7500	0.0042	0.0042	0.9705	1.6338	1.6338
1	5	1.5000	1.7500	0.0054	0.0054	0.0042	1.2486	1.2486
1	10	1.5000	1.7500	0.0076	0.0076	0.0065	0.0042	0.0076
1	1	1.5000	2	0	0	0.7767	1.4836	1.4836
1	5	1.5000	2	0.0011	0.0011	0	1.0898	1.0898
1	10	1.5000	2	0.0034	0.0034	0.0022	0	0.0034
1.5000	1	1	1.7500	0.0914	0.0914	1.9724	2.3571	2.3571
1.5000	5	1	1.7500	0.0931	0.0931	0.0920	1.9549	1.9549
1.5000	10	1	1.7500	0.0965	0.0965	0.0953	0.0931	0.0965
1.5000	1	1	2	0.0812	0.0812	1.6729	2.1372	2.1372
1.5000	5	1	2	0.0829	0.0829	0.0818	1.6585	1.6585
1.5000	10	1	2	0.0863	0.0863	0.0852	0.0829	0.0863
1.5000	1	1.5000	1.5000	0.1650	0.1650	1.5210	2.0564	2.0564
1.5000	5	1.5000	1.5000	0.1666	0.1666	0.1655	1.7777	1.7777
1.5000	10	1.5000	1.5000	0.1700	0.1700	0.1689	0.1666	0.1700
1.5000	1	1.5000	1.7500	0.0541	0.0541	1.1869	1.8067	1.8067
1.5000	5	1.5000	1.7500	0.0558	0.0558	0.0547	1.4973	1.4973
1.5000	10	1.5000	1.7500	0.0592	0.0592	0.0580	0.0558	0.0592
1.5000	1	1.5000	2	0.0935	0.0935	0.9604	1.6676	1.6676
1.5000	5	1.5000	2	0.0952	0.0952	0.0941	1.3085	1.3085
1.5000	10	1.5000	2	0.0986	0.0986	0.0975	0.0952	0.0986

It is also of great interest to explore the break-even point of fuel supply disruption scenario probabilities when the probabilistic method and the min/max regret-based method will give different results. The break-even point of scenario probabilities is derived using crude searching under different VCR assumptions for different outage duration:

a. $VCR_{\{0,1d,5d,10d\}} = 16.96 * [1,1,1,1]\ AU\$/kWh$
b. $VCR_{\{0,1d,5d,10d\}} = 16.96 * [1,1.1,1.5,2]\ AU\$/kWh$

Under both VCR assumptions, the sizing results of both areas keep the same with those highlighted in Table 4-16 and Table 4-17, where 10-day local fuel storage is always required. The break-even points of scenario probabilities of both areas are summarized in Table 4-18 to Table 4-21.

Table 4-18 Break-even extreme event probability (10-day disruption) for Donald Area, $VCR_{\{0,1d,5d,10d\}} = 16.96 * [1,1,1,1]\ AU\$/kWh$

$[p_0, p_{1d}, p_{5d}, p_{10d}]$	DG Cap(% of Base Cap)	Local Fuel Storage Cap(days)	BESS Cap(% of Base Cap)	PV Cap(% of Base Cap)	NPC_{inv} (AU$M)	$NPC_{vcr,0}$	$NPC_{vcr,10d}$	Total NPC
[0.998, 0 , 0, **0.002**]	1	**10**	1.5	2	10.673	0.14149	0.0003	10.815
[0.999, 0 , 0, **0.001**]	1	**1**	1.5	2	10.625	0.14163	0.03698	10.804

Table 4-19 Break-even extreme event probability (10-day disruption) for Donald Area, $VCR_{\{0,1d,5d,10d\}} = 16.96 * [1,1.1,1.5,2]\ AU\$/kWh$

$[p_0, p_{1d}, p_{5d}, p_{10d}]$	DG Cap(% of Base Cap)	Local Fuel Storage Cap(days)	BESS Cap(% of Base Cap)	PV Cap(% of Base Cap)	NPC_{inv}(AU$M)	$NPC_{vcr,0}$	$NPC_{vcr,10d}$	Total NPC
[0.9992, 0, 0, **0.0008**]	1	**10**	1.5	2	10.673	0.14166	0.0002	10.815
[0.9993, 0, 0, **0.0007**]	1	**5**	1.5	2	10.641	0.14167	0.0322	10.815
[0.9995, 0, 0, **0.0005**]	1	**1**	1.5	2	10.625	0.1417	0.0370	10.804

Table 4-20 Break-even extreme event probability (10-day disruption) for Tarnagulla Area, $VCR_{\{0,1d,5d,10d\}} = 16.96 * [1,1,1,1]\ AU\$/kWh$

$[p_0, p_{1d}, p_{5d}, p_{10d}]$	DG Cap(% of Base Cap)	Local Fuel Storage Cap(days)	BESS Cap(% of Base Cap)	PV Cap(% of Base Cap)	NPC_{inv} (AU$k)	$NPC_{vcr,0}$	$NPC_{vcr,10d}$	Total NPC
[0.997, 0 , 0, **0.003**]	1	**10**	1.5	2	811.2	6.9	0.02	818.08
[0.998, 0 , 0, **0.002**]	1	**1**	1.5	2	807.82	6.9	2.99	817.69

Table 4-21 Break-even extreme event probability (10-day disruption) for Tarnagulla Area, $VCR_{\{0,1d,5d,10d\}} = 16.96 * [1,1.1,1.5,2]\ AU\$/kWh$

$[p_0, p_{1d}, p_{5d}, p_{10d}]$	DG Cap(% of Base Cap)	Local Fuel Storage Cap(days)	BESS Cap(% of Base Cap)	PV Cap(% of Base Cap)	NPC_{inv} (AU$k)	$NPC_{vcr,0}$	$NPC_{vcr,10d}$	Total NPC
[0.998, 0 , 0, **0.002**]	1	**10**	1.5	2	811.2	6.88	0.03	818.1
[0.999, 0 , 0, **0.001**]	1	**1**	1.5	2	807.82	6.89	2.98	817.7

4.3.3 MATLAB-Based Interactive Sizing Tool

A MATLAB-based interactive sizing tool is developed to allow the planners further explore the interplay between the infrastructure cost, probabilities of bushfire-fire induced fuel supply disruption duration as well as VCR under different outage duration. The user interface of the interactive sizing tool using probabilistic method and min/max regret method are shown in Figure 71 and Figure 72.

The users need to specify the path that stores the EENS results of the off-grid community under different bushfire-induced fuel supply disruption scenario and the path to store the full table that displays the NPC of each identified portfolio in Step 1) and the regret table. The optimal sizing results will be displayed on the user interface.

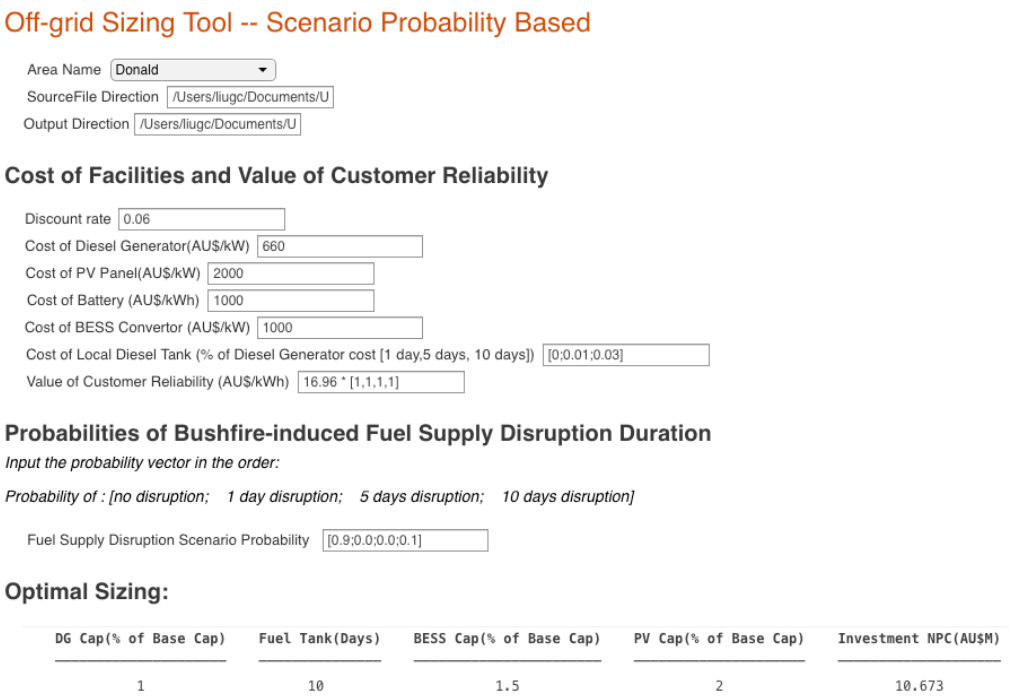

Figure 71. MATLAB-Based interactive sizing tool user interface – Scenario-Based Probablistic Sizing Tool

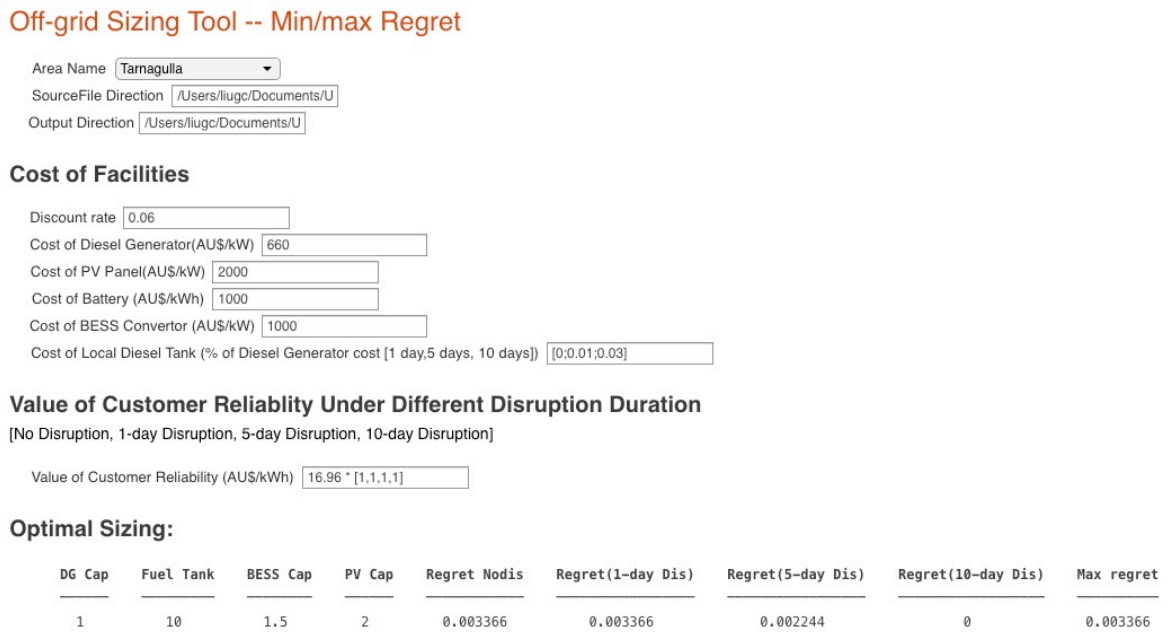

Figure 72. MATLAB-Based interactive sizing tool user interface – Min-Max Regret Sizing Tool

4.4 Summary

- The proposed three capacity outage mitigation strategies can all improve the capacity adequacy level of Donald and Tarnagulla area community, and enabling emergency discharge of BESS has the most significant improvement on capacity adequacy.
- The capacity adequacy level of the grid-connected community can be significantly compromised by the increase line failure rate with FFDI along the transmission path, while the impact of bushfire-fire induced fuel supply disruption has minor negative impact on grid-connected community capacity adequacy. Thus, it is recommended that the network operators to adopt preventive strategies on monitoring the bushfire risk along the transmission path and conduct regular inspection on sub-transmission line health condition in order to avoid forced trip due to flashover during high bushfire risk periods.
- The capacity adequacy level of the off-grid community under the sizing result from project 5 is lower than that when it is grid-connected. Thus, additional generation is required to comply with the SAPS regulation rules, the generation portfolio required for Tarnagulla and Donald off-grid scenario without considering bushfire impact is provided in Table 4-8 and Table 4-9, respectively.
- More local diesel storage capacity is required for off-grid community when considering the trade-off between bushfire-induced fuel supply disruption impact and the overall NPC including both investment cost and loss of load cost.

5 Dynamic Impact Analysis

In order to perform a dynamic impact assessment for each microgrid setting, a range of case studies have been developed that consist of combinations of various **network disturbances** (as identified in Section 3.1.3) applied at various **operating conditions**.

The objective of this analysis, for each town, is to evaluate:

- The microgrid performance against key metrics
- The impact of the microgrid on the broader MV feeder

5.1 Case studies - selected operating conditions

The simulated operating conditions consist of high and low customer net demand at different levels of DER (PV and BESS) penetration.

Load and generation profiles

To determine the high and low net demand levels, two different daily load and generation profiles have been generated for each mapped transformer. The daily profiles have been obtained by extracting, for each 30-min interval, the net demand value that corresponds to the 5th percentile (p5) and 95th percentile (p95) in that interval across full year dataset. The p5 and p95 profiles represent low and high net demand profiles, respectively. In other words:

- **p5** represents a low-load – high-generation condition,
- **p95** represents high-load – low-generation condition.

These daily profiles were then decomposed into individual demand and generation profiles to be fed into the mapped transformers.

The load profiles of the unmapped transformers have been adopted from the mapped transformers and scaled according to the kVA ratings. Similarly, the load profiles for the broader feeder loads have been approximated by using the normalized median load profiles of the mapped transformers for each town.

While these profiles represent daily demand/generation values, the nominal kW capacities of PV and BESS have been determined based on the existing and required installation data, informed by Powercor and Project 5 (Donald: S16 & Tarnagulla: S1), respectively.

DER type	**Existing (kW)** (Powercor)	**Required (kW)** (Project 5)	**Total (kW)** (Project 7)
Donald PV	735.45	1688	**2423.45**
Donald BESS	0	392	**392**
Donald DG	0	2430	2430
Tarnagulla PV	108.44	134	**242.44**
Tarnagulla BESS	0	26.7	**26.7**
Tarnagulla DG	0	170	170

Table 5-1: Base Case Nominal Capacities

The highlighted total PV and BESS kW values in the above table are used as the "**Base case PV**" and "**Base case BESS**" nominal capacities in the rest of the analysis. It should be noted that the BESS/PV kW ratios for Donald and Tarnagulla are 0.16 and 0.11, respectively.

The load and generation profiles for each transformer are shown below.

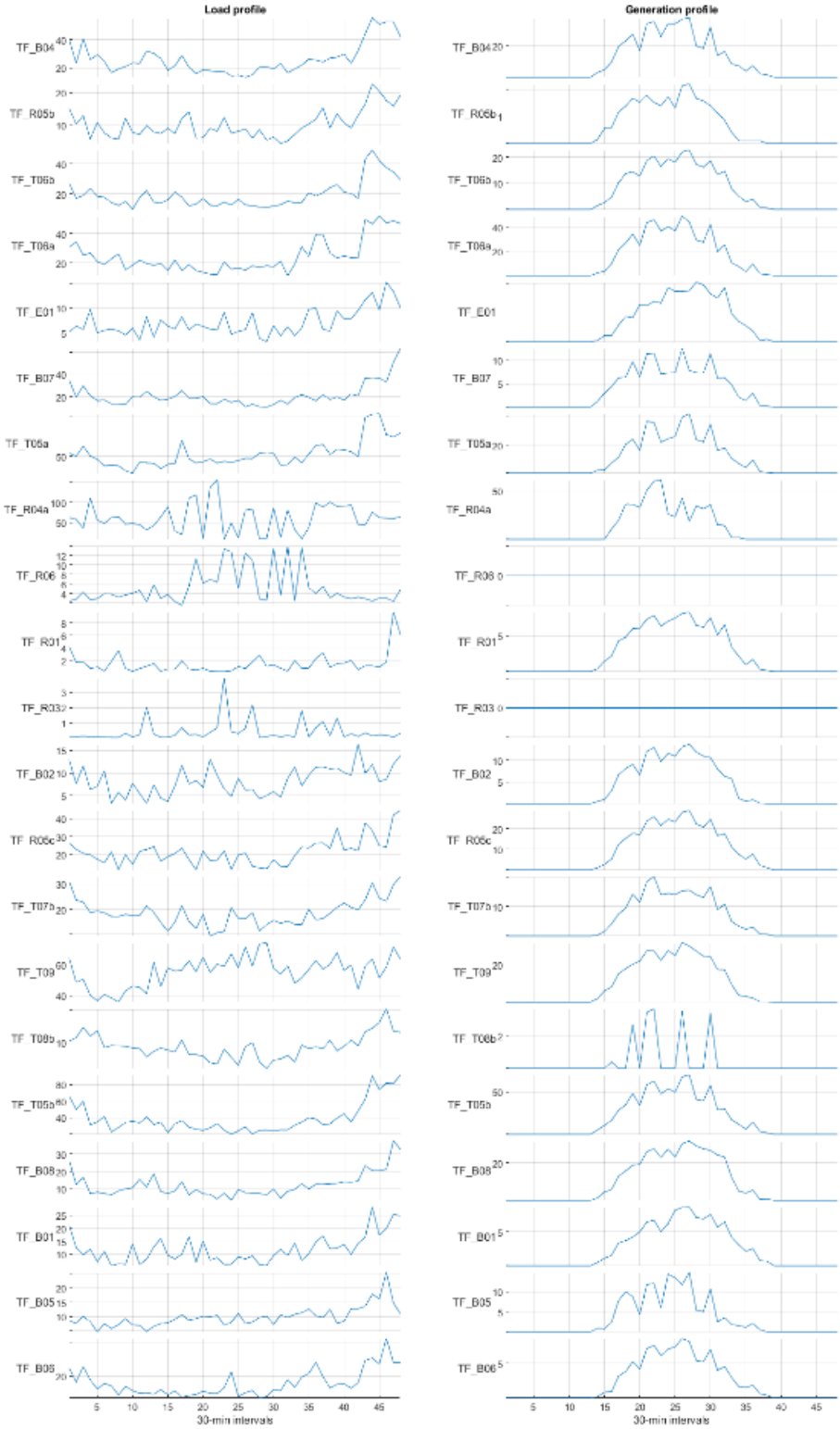

Figure 73: Donald Load & Generation profiles p5 (1)

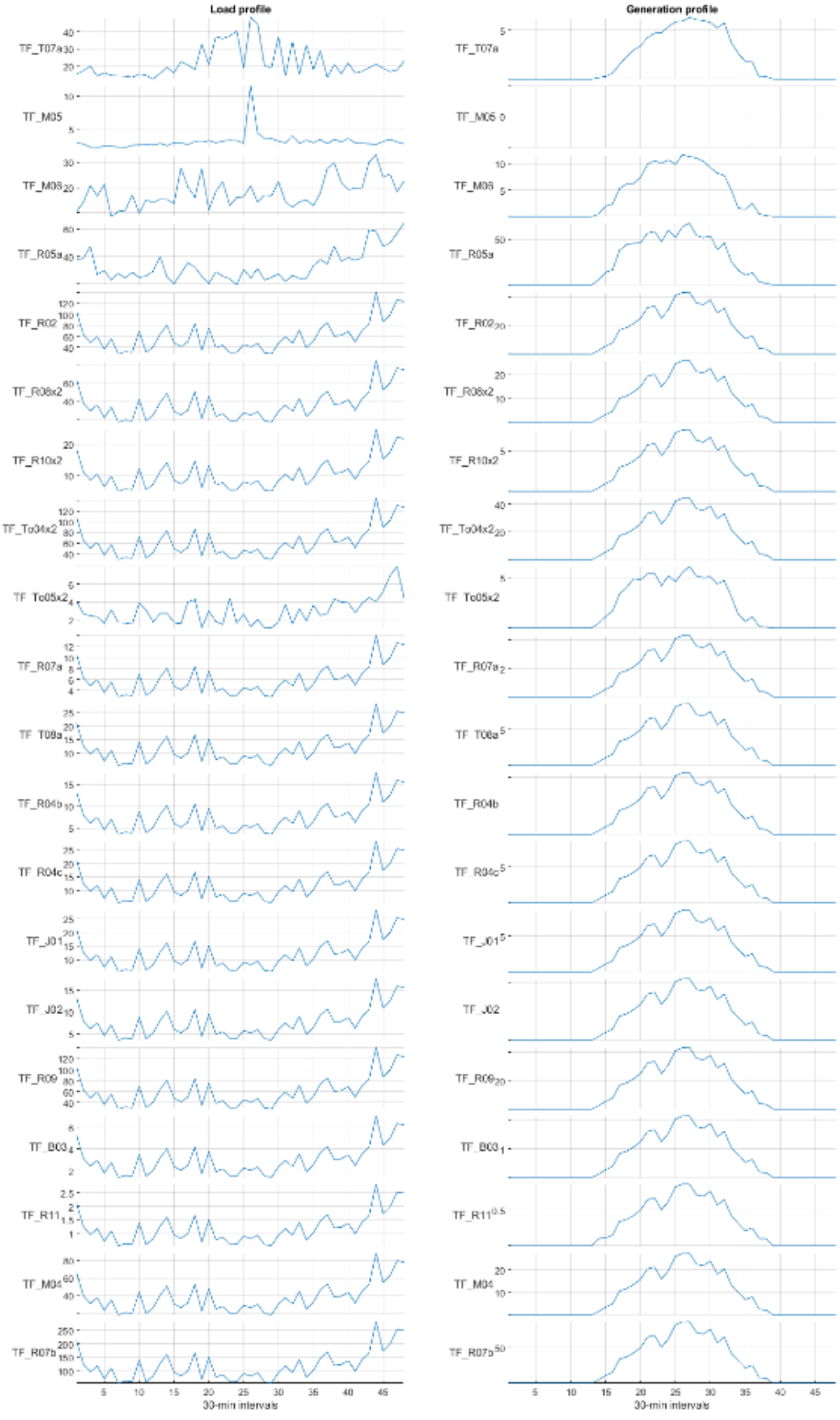

Figure 74: Donald Load & Generation profiles p5 (2)

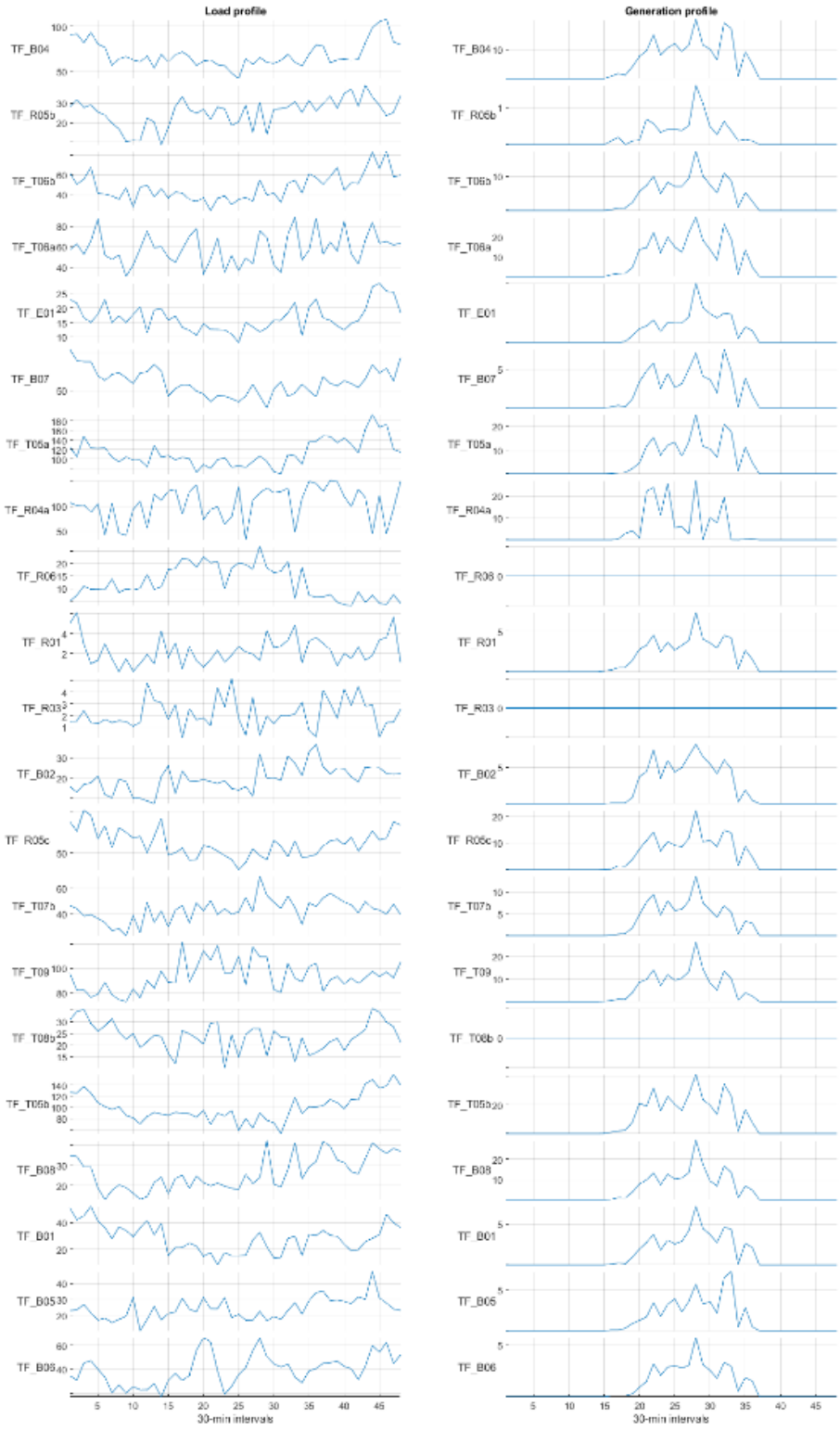

Figure 75: Donald Load & Generation profiles p95 (1)

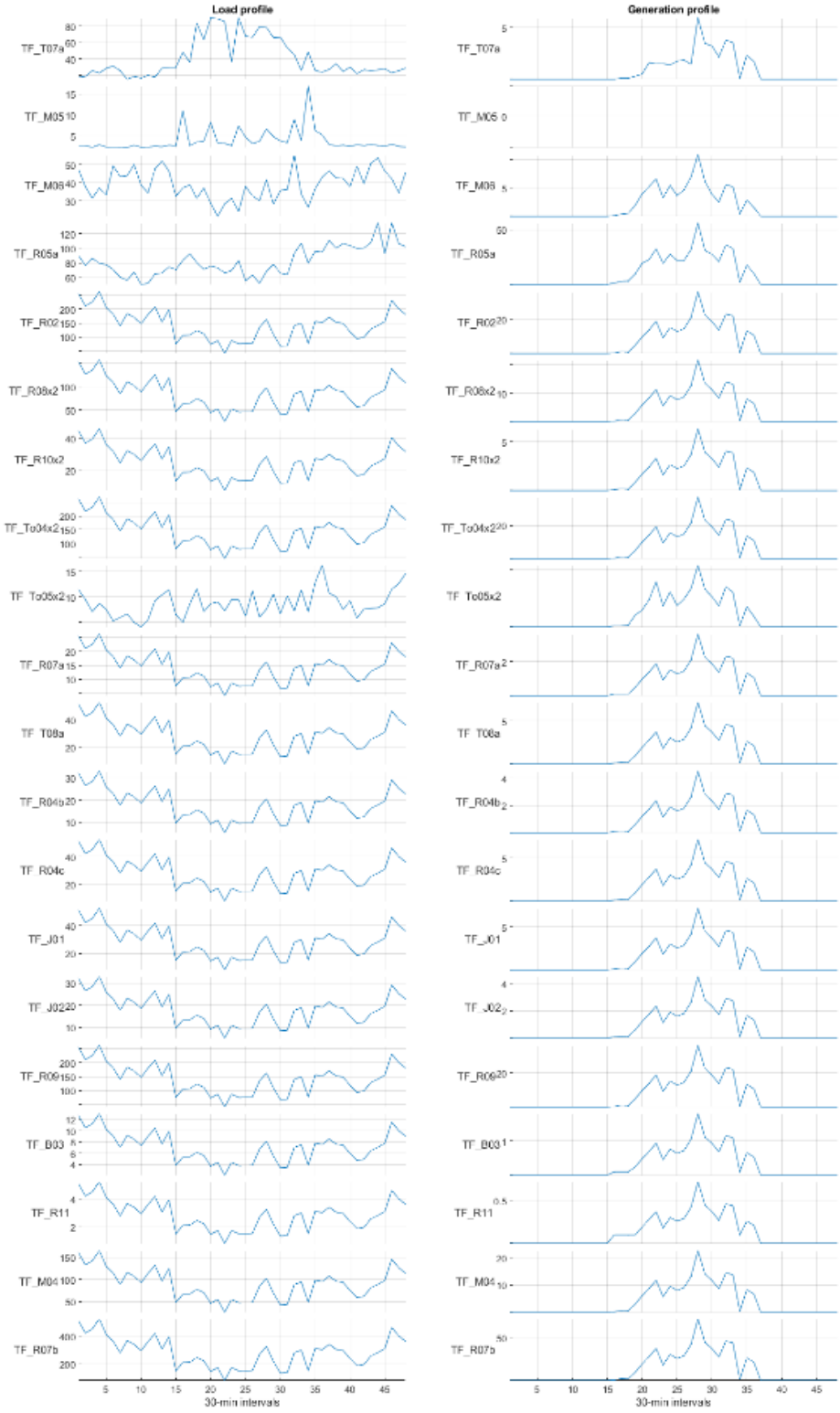

Figure 76: Donald Load & Generation profiles p95 (2)

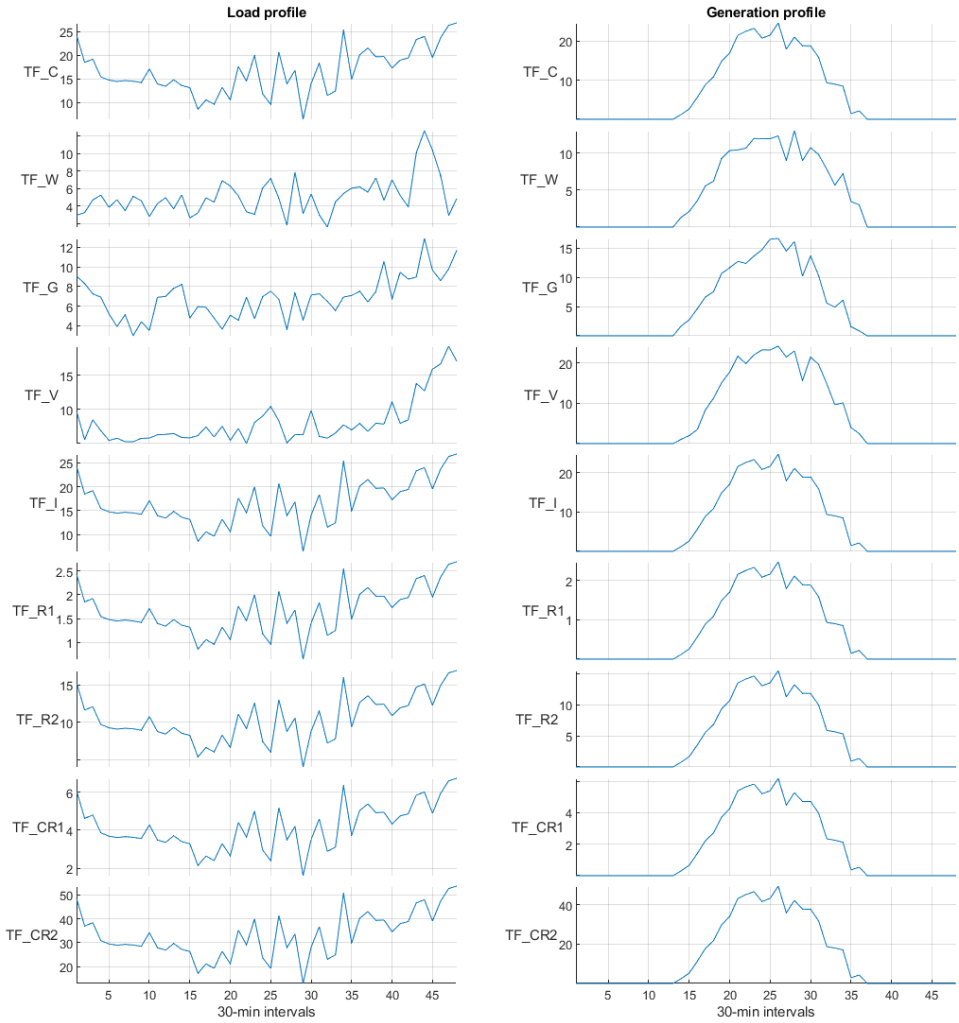

Figure 77: Tarnagulla Load & Generation profiles p5

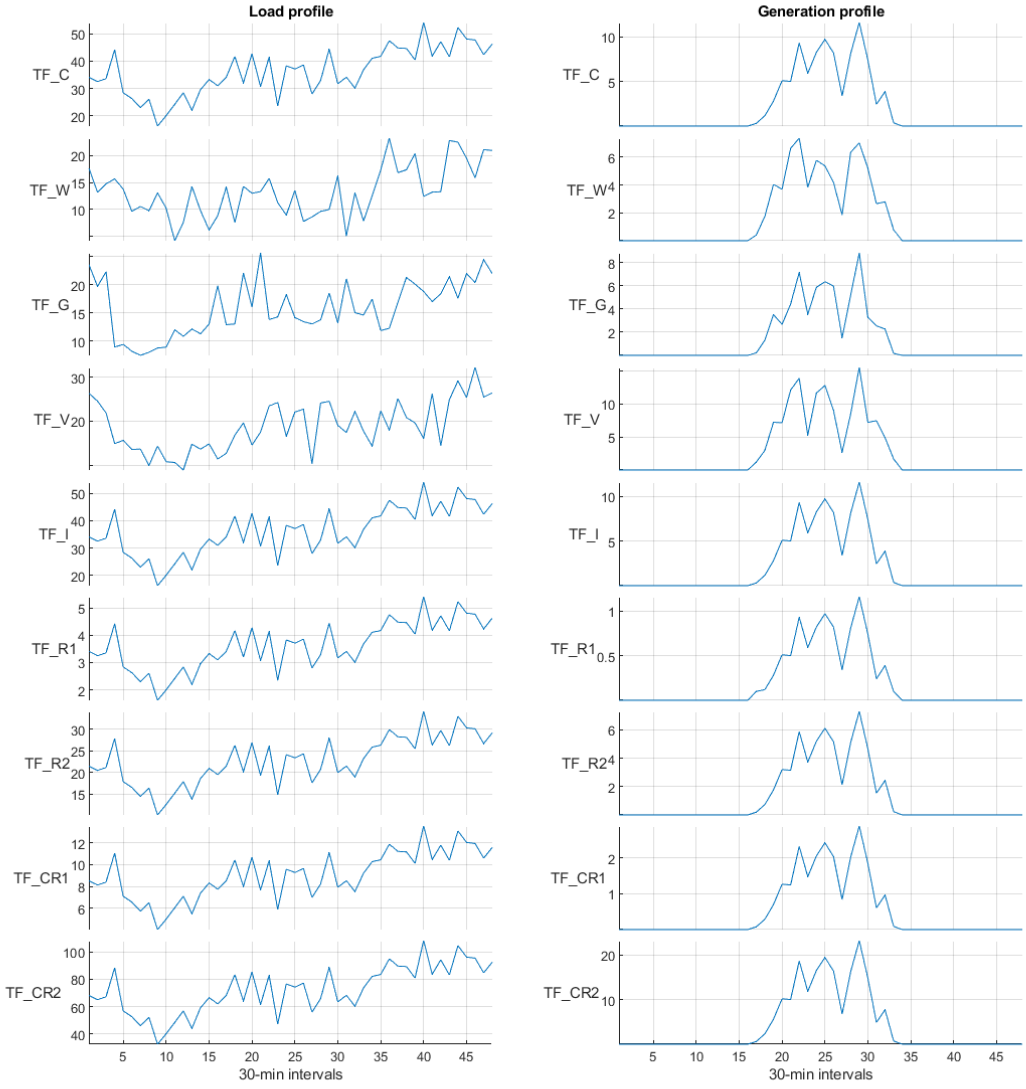

Figure 78: Tarnagulla Load & Generation profiles p95

DER Penetration

To determine the impact of different PV and BESS capacities in the network, the following values have been used:

PV nominal capacity (kW)	BESS nominal capacity (kW)	BESS dispatch mode
- Base case PV - Base case PV + 50% - Base case PV + 100%	- Base case BESS - Base case BESS + 50%	- Charging at 50% - Discharging at 50%

Table 5-2: DER capacity and dispatch variation

It should be noted that the Base case PV applies to both the nominal capacities and daily generation profiles of the PV systems

The following table summarizes the simulated case studies.

Disturbances:

Disturbances
D1 – Load Ramp up
D2 – Gen Ramp down
D3 – Islanding
D4 – Tx loss
D5 – 1Ph fault
D6 – 3Ph fault
D7 – Tx loss (off-grid)

Operating conditions:

Cases	Daily Net Demand	BESS Dispatch	BESS Nominal kW	PV Nominal kW & Dispatch
1	Low net demand (p5)	Charging 50%	Base case BESS	Base case PV
2	Low net demand (p5)	Charging 50%	Base case BESS	Base case PV + 50%
3	Low net demand (p5)	Charging 50%	Base case BESS	Base case PV + 100%
4	Low net demand (p5)	Charging 50%	Base case BESS + 50%	Base case PV
5	Low net demand (p5)	Charging 50%	Base case BESS + 50%	Base case PV + 50%
6	Low net demand (p5)	Charging 50%	Base case BESS + 50%	Base case PV + 100%
7	Low net demand (p5)	Discharging 50%	Base case BESS	Base case PV
8	Low net demand (p5)	Discharging 50%	Base case BESS	Base case PV + 50%
9	Low net demand (p5)	Discharging 50%	Base case BESS	Base case PV + 100%
10	Low net demand (p5)	Discharging 50%	Base case BESS + 50%	Base case PV
11	Low net demand (p5)	Discharging 50%	Base case BESS + 50%	Base case PV + 50%
12	Low net demand (p5)	Discharging 50%	Base case BESS + 50%	Base case PV + 100%

Cases	Daily Net Demand	BESS Dispatch	BESS Nominal kW	PV Nominal kW & Dispatch
1	High net demand (p95)	Charging 50%	Base case BESS	Base case PV
2	High net demand (p95)	Charging 50%	Base case BESS	Base case PV + 50%
3	High net demand (p95)	Charging 50%	Base case BESS	Base case PV + 100%
4	High net demand (p95)	Charging 50%	Base case BESS + 50%	Base case PV
5	High net demand (p95)	Charging 50%	Base case BESS + 50%	Base case PV + 50%
6	High net demand (p95)	Charging 50%	Base case BESS + 50%	Base case PV + 100%
7	High net demand (p95)	Discharging 50%	Base case BESS	Base case PV
8	High net demand (p95)	Discharging 50%	Base case BESS	Base case PV + 50%
9	High net demand (p95)	Discharging 50%	Base case BESS	Base case PV + 100%
10	High net demand (p95)	Discharging 50%	Base case BESS + 50%	Base case PV
11	High net demand (p95)	Discharging 50%	Base case BESS + 50%	Base case PV + 50%
12	High net demand (p95)	Discharging 50%	Base case BESS + 50%	Base case PV + 100%

Table 5-3: Case Studies

In total, 8064 combinations have been simulated for each town, consisting of:

- 3x levels of PV penetration
- 2x levels of BESS penetration
- 2x modes of BESS dispatch
- 7x disturbances
- 2x profiles of net demand
- 48x smart meter data intervals

The following network variables have been measured before and after the applied disturbance.

	Donald	**Tarnagulla**
Bus Voltages	41x LV town buses 1x MV PCC bus 5x MV feeder terminals*	9x LV town buses 1x MV PCC bus 6x MV feeder terminals*
Transformer Loading	41x Distribution Transformers	9x Distribution Transformers
PCC Power Flows	Active power Reactive power	Active power Reactive power

Table 5-4: Measured network variables

Simulation Notes:

- For each variable, two measurements have been extracted: these are referred to as *pre-and post-disturbance* values.
- The operation of tap changing transformers have been disabled to be able to evaluate the net response of the dynamic models and the impact of disturbances
- "D2 - Generation Ramp Down" measurements have been obtained for daytime only when solar generation is available.
- "D5 - 1Ph-G Fault" measurements have been obtained for the steady-state phase-to-ground voltage values of the faulted phase, while all other voltage measurements are line-to-line.
- In off-grid mode, back-up diesel generators (DG) are set to 50% load following (active power only), and a central grid-forming inverter-based battery is used to provide the voltage and frequency reference.
- In Donald simulations, the BESS dispatch mode is set to be purely active power, whereas in Tarnagulla, approx. 15% of the BESS output is set to be reactive power. This is to compare the differences between the two dispatch strategies.

*The MV feeder terminal voltages have been measured at the below marked locations.

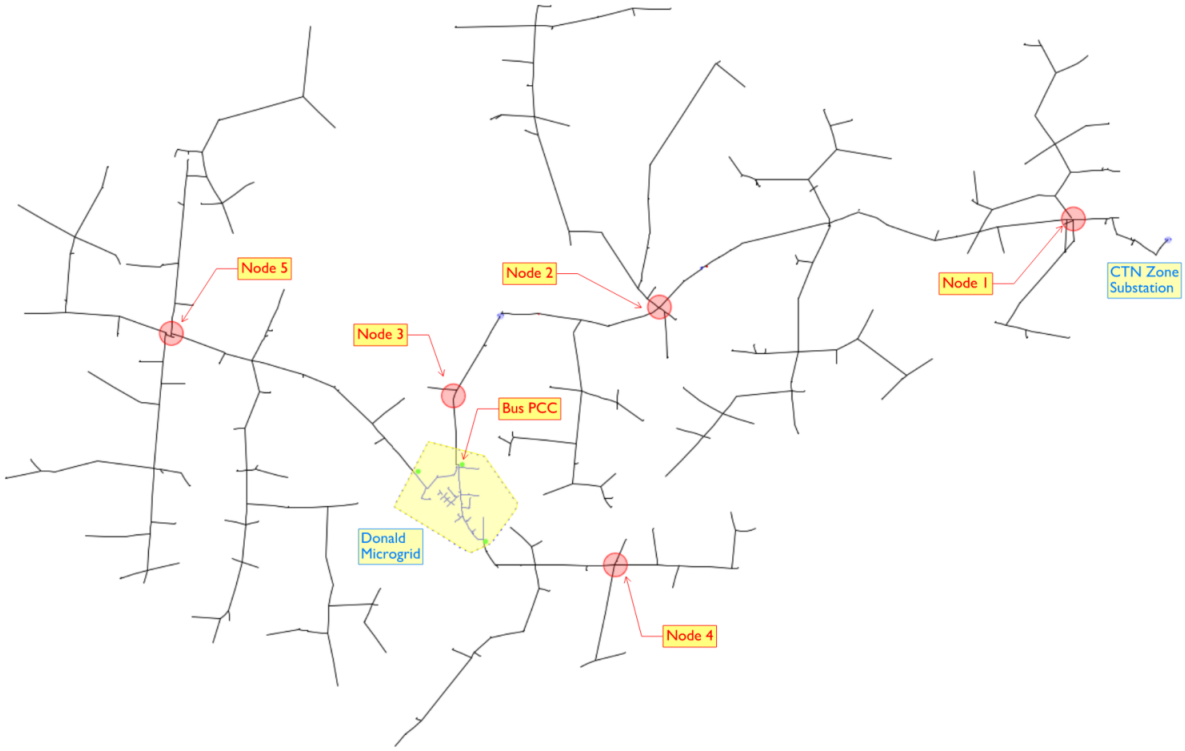

Figure 79: Donald Feeder (CTN6)

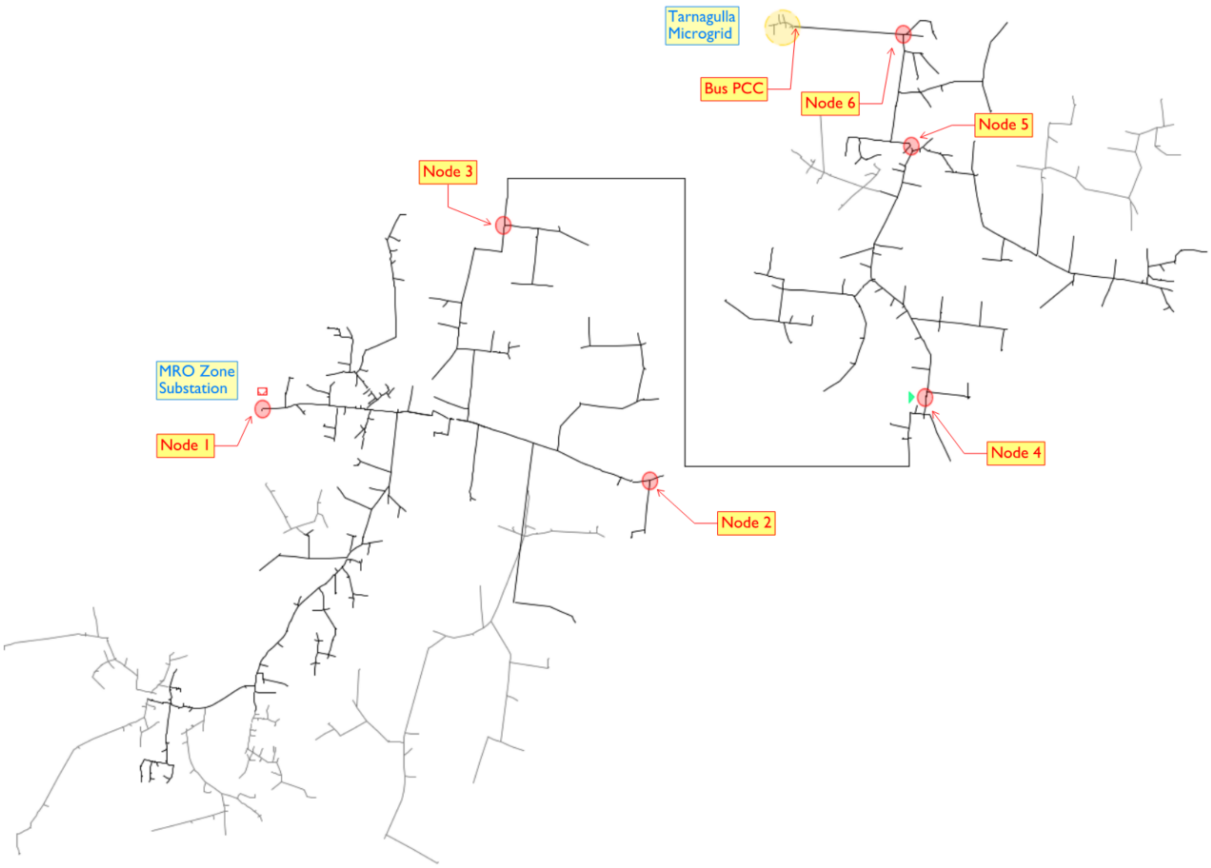

Figure 80: Tarnagulla Feeder (MRO7)

5.2 Disturbance impact analysis

5.2.1 Donald feeder

The following plots illustrate the pre- and post- disturbance voltage profiles across the MV feeder for different PV penetration levels.

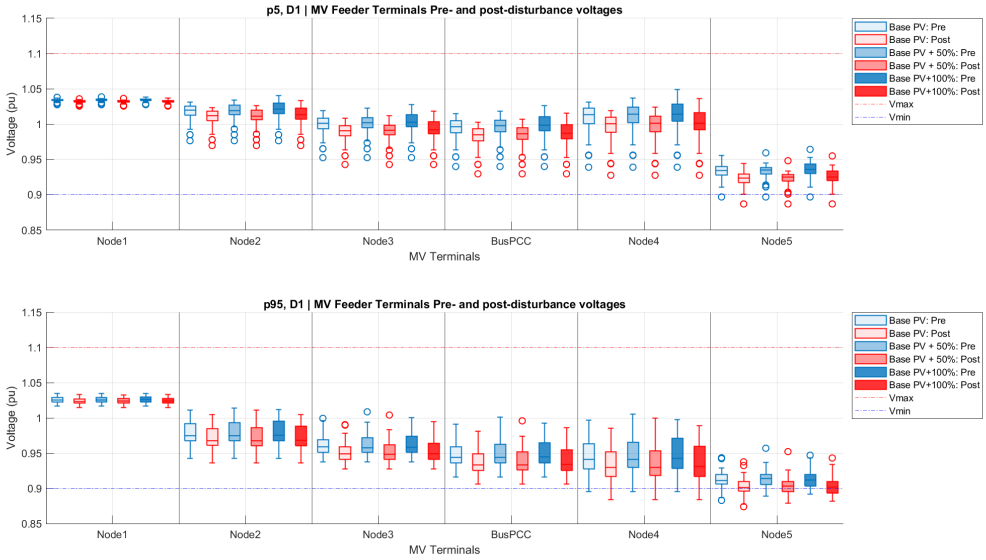

Figure 81: MV feeder terminal voltage profiles – D1

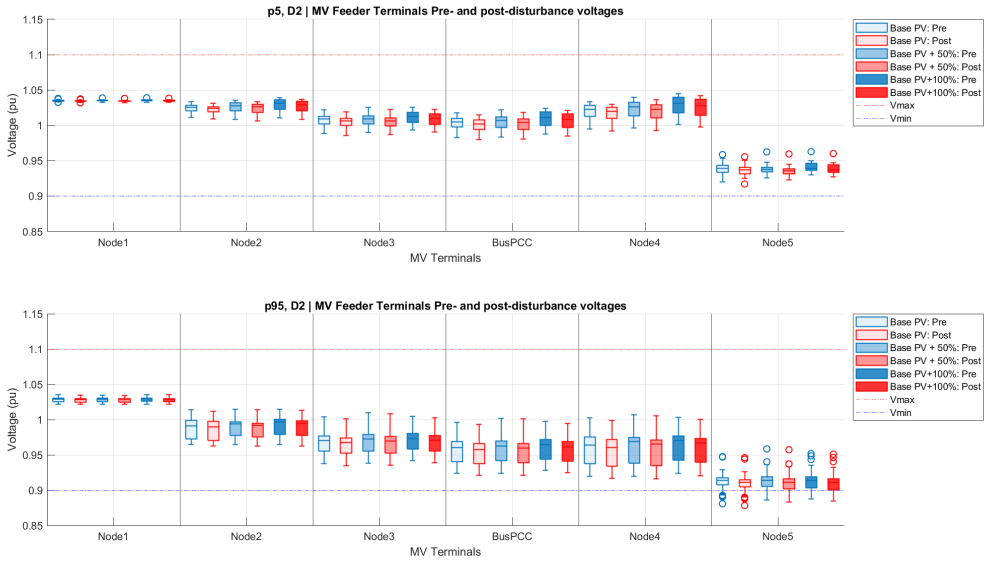

Figure 82: MV feeder terminal voltage profiles – D2

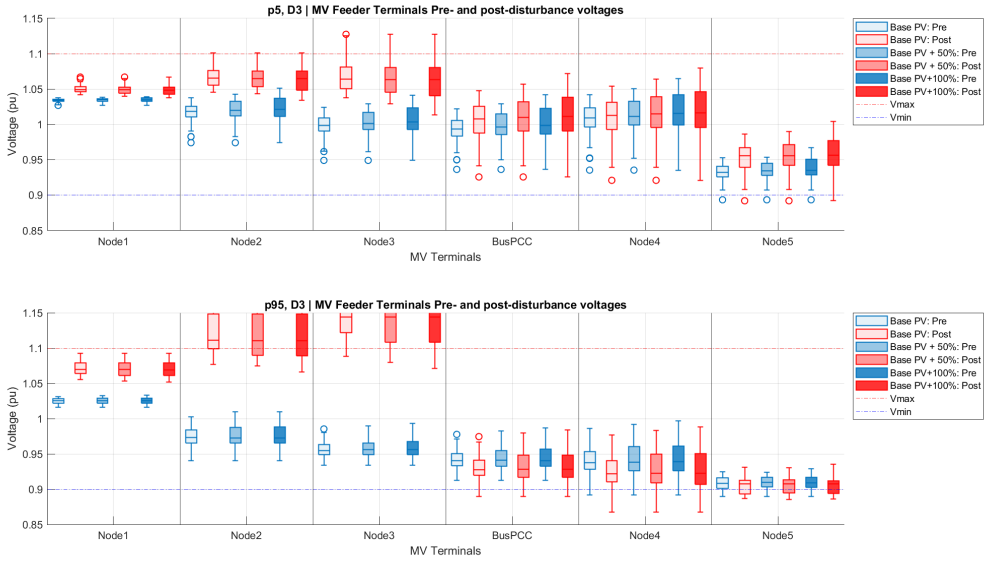

Figure 83: MV feeder terminal voltage profiles – D3

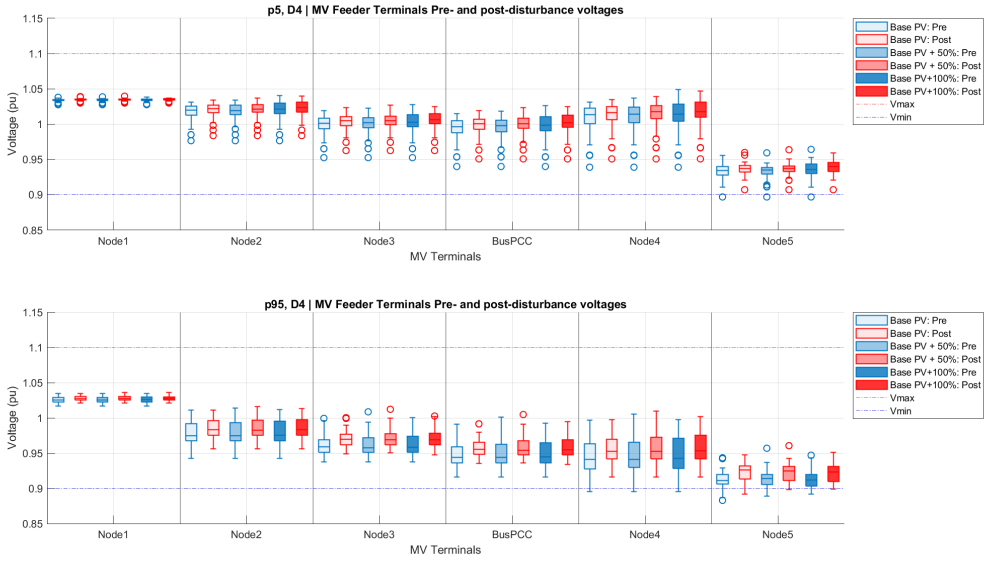

Figure 84: MV feeder terminal voltage profiles – D4

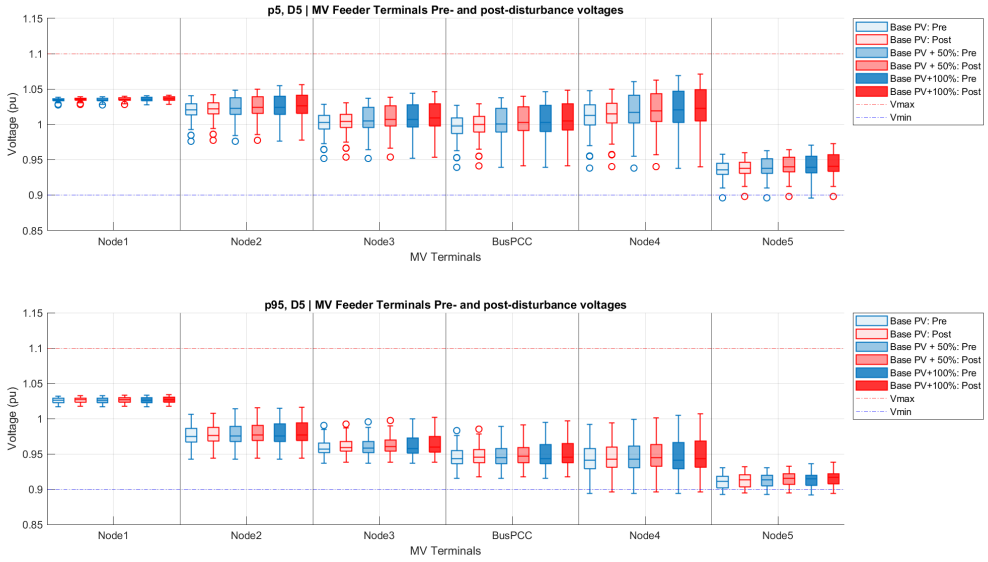

Figure 85: MV feeder terminal voltage profiles – D5

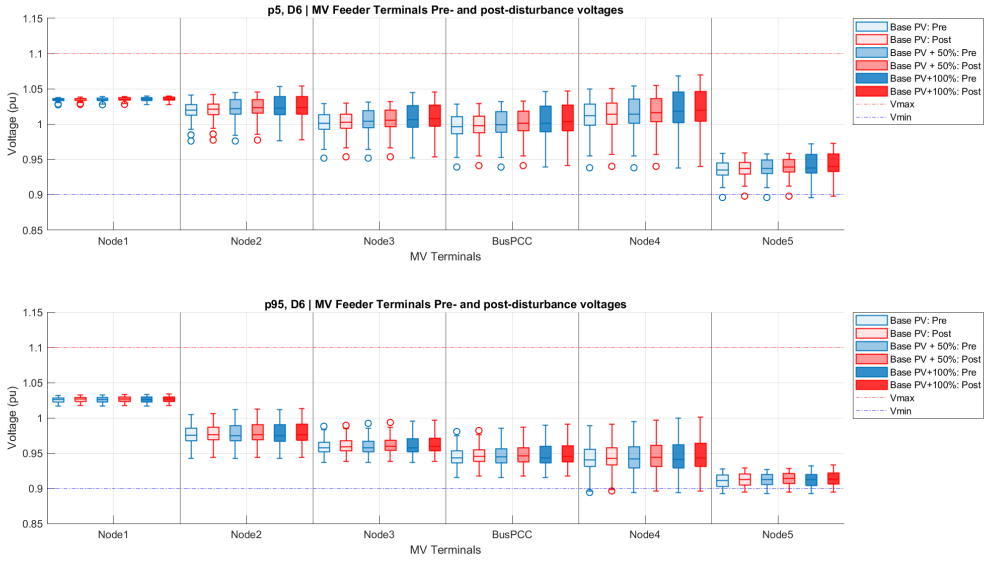

Figure 86: MV feeder terminal voltage profiles – D6

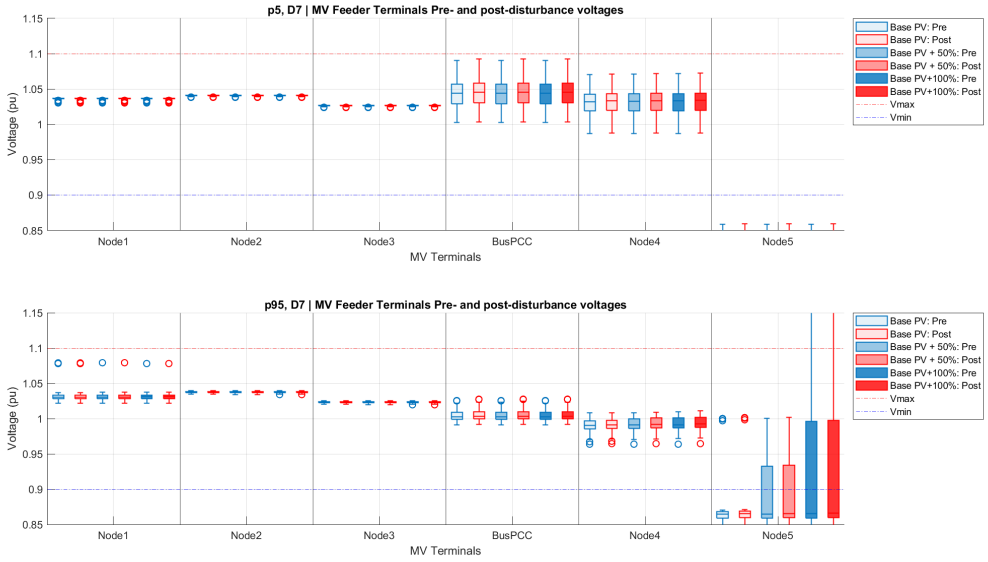

Figure 87: MV feeder terminal voltage profiles – D7

Further plots can be found in the Appendix for different BESS penetration levels and dispatch modes.

In the following table, the impact of different PV and BESS penetration on the microgrid, feeder and distribution transformers is discussed. Detailed simulation plots corresponding to the discussed results can be found in the Appendix.

	Impact on PCC and LV bus voltages	**Impact on MV feeder terminal voltages**	**Impact on Transformer loading**
Increasing PV penetration (%)	Increasing the PV penetration has increased maximum voltage values (typically during midday) across all LV buses and PCC bus.	All feeder terminals had an overall voltage rise with increasing PV penetration. The terminals closer to the microgrid experienced this effect more strongly.	As the PV penetration was increased, the loading of some transformers was observed to increase due to increased export, while in others the loading decreased due to reduced import. However, all transformers remained within their thermal limits both in p5 and p95 profiles.
Increasing BESS penetration (%) at charging vs discharging modes	In both charging and discharging modes, larger BESS penetration slightly improved the post-disturbance voltage profiles, however, this effect was very small compared to increased PV penetration.	Increasing the BESS penetration at either dispatch mode did not yield in noticeable differences in feeder terminal voltages. This is attributed to the small amount of BESS capacity with respect to the feeder loads and the unity power factor in BESS.	Depending on the net load at the transformer level, increasing the BESS penetration while charging either reduced transformer loading due to less export, or increased transformer loading due to increased import. Increasing the BESS penetration while discharging had a similar impact to increasing PV penetration.
Conclusion	In p5 profile, all of PCC and LV bus voltages remained within the operational limits throughout all cases. In p95, consistent undervoltage conditions were observed in most post-disturbance voltages, mainly during the evening and night time when there is no solar generation.	The pre-disturbance voltages remained within the limits in the upstream feeder terminals, however, islanding event resulted in violation of upper voltage limit in Node 2 and 3. The downstream nodes, Node 4 and 5, consistently experienced pre- and post-disturbance undervoltage conditions. Node 4 was impacted under p95 only, while Node 5 was impacted under both demand profiles.	All transformers remained within their thermal limits across all cases and after all disturbances.
Recommendations	- Additional reactive power support can be provided for operation under heavy demand. - Tap changing transformers can be utilized to eliminate the consistent undervoltage conditions during p95	- The upstream feeder voltage rise issues can be mitigated by operation of tap changing transformers. - Additional reactive power support can be provided separately for each downstream town (Litchfield and Donald South) to improve and strengthen their voltage profiles, particularly to Litchfield.	No mitigation is required for the distribution transformers.

Table 5-5: Donald – DER Penetration Impact Assessment

In the following table, the impact of different disturbances on the microgrid PCC voltage and power flow as well as transformer loading is discussed. Detailed simulation plots corresponding to the discussed results can be found in the Appendix.

Disturbance	Changes in PCC voltage	Changes in PCC power flow	Changes in transformer loading (where the disturbance is applied)
D1 – Load Ramp up	A slight voltage drop was observed at the PCC following a load ramp up event. The changes in voltage levels remained approximately the same (0.01 pu) throughout the day across all cases both for p5 and p95 demand profiles.	Following load ramp-up, reduction in reactive power flow was observed during daytime when solar power generation was available. This reduction slightly increased in magnitude as more power was injected by PV and BESS (with increased penetration). During night-time, post-disturbance reactive power flow was observed to increase. The active power flow increased due to the predominantly resistive nature of the load. The increase in the active power flow was approximately the same for both BESS modes.	Both in p5 and p95 profiles, the transformer loading increased. However, during midday period under p5, the change in loading was lower in magnitude as the PV penetration increased.
D2 – Generation Ramp down	A small voltage drop was observed following generation ramp-down event. The changes in voltage values remained approximately in the same range throughout all cases, but smaller net changes were observed around midday with the increased solar penetration.	Reactive power flow decreased following the PV generation ramp-down. Larger reductions were observed with more PV and BESS penetration. The active power flow increased following the reduced generation, and followed a similar pattern to the reactive power changes with respect to the PV and BESS penetration.	Transformer loading increased under p95 profile. However, during midday period under p5, the transformer loading decreased (due to reduced export)
D3 – Islanding	The islanding event resulted in an overall voltage rise at the PCC under light demand, and a voltage drop under heavy demand. The voltage drop was observed mainly in night time when solar generation was zero.	Following the islanding event, the PCC reconnected to a central grid-forming battery, which adjusted the power flow. A reduction in reactive power flow proportionate to the voltage changes was observed. Similarly, a decrease in active power flow was also observed. The changes in active and reactive power flows were smaller at p5 and larger at p95.	The islanding event caused negligible change in transformer loading since the connected load and generation remained unchanged.
D4 – Tx loss	In p5, voltage drops and rises were observed at the PCC throughout the day depending on whether there was net export or import at the disconnected transformer. In p95, a consistent voltage rise can be observed with larger magnitudes than those observed in p5.	A change in active power flow was observed in proportion to the net active power load at the disconnected transformer. A reduction in reactive power flow was observed in proportion to the net reactive power load at the disconnected transformer as well as the reactive power response of inverters.	Transformer load and generation disconnected, therefore, transformer loading dropped to zero.
D5 – 1Ph fault	Minimal changes were observed in the steady state voltage of the phase that was exposed to the fault. The slight voltage rise is attributed to the response of the inverters, which may necessitate a dispatch value reset following the fault clearance.	The PCC reactive power decreased as a result of PV and BESS reactive power response to the fault event. Due to the post-disturbance voltage rise and changes in inverter power outputs, slight reductions and increases were observed in the PCC active power flow, which grew larger in magnitude as the BESS penetration increased.	The transformer loading remained approximately the same as the pre-disturbance levels.
D6 – 3Ph fault	Similar to D5, minimal changes were observed in the steady state voltage values following fault clearance. The changes were observed to be approximately the same in both BESS charging and discharging modes.	The changes in active and reactive power flow are similar to those observed in single-phase-to-ground fault, yet with a larger magnitude due to the response of all three phases and closer proximity of the fault.	The transformer loading remained approximately the same as the pre-disturbance levels.

D7 – **Tx loss (off-grid)**	The loss of a transformer during off-grid mode resulted in minimal change in voltage levels both in light and heavy demand conditions.	A change in active power flow was observed in proportion to the net active power load at the disconnected transformer. A reduction in reactive power flow was observed in proportion to the net reactive power load at the disconnected transformer as well as the reactive power response of inverters.	Transformer load and generation disconnected, therefore, transformer loading dropped to zero

Table 5-6: Donald – Disturbance Impact Assessment

5.2.2 Tarnagulla feeder

The following plots illustrate the pre- and post- disturbance voltage profiles across the MV feeder for different PV penetration levels.

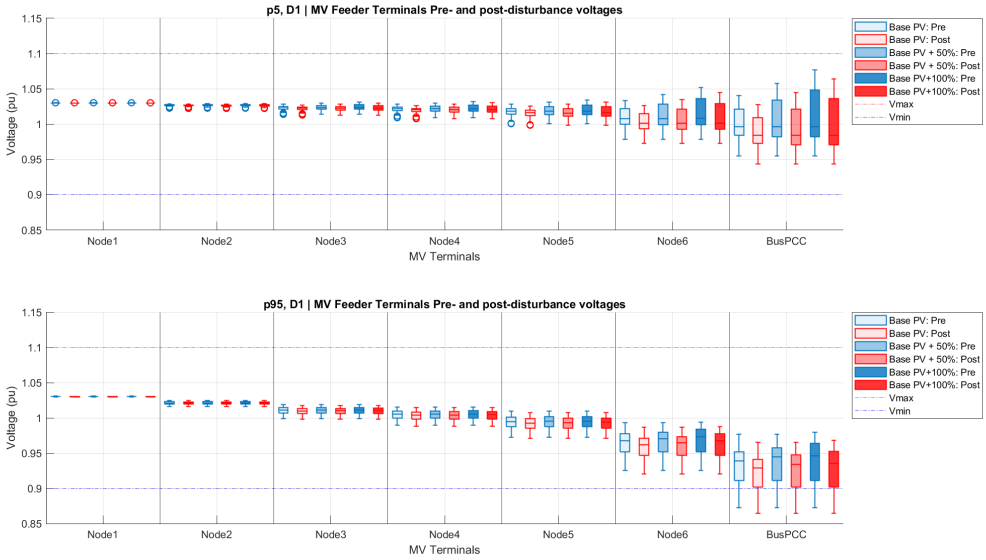

Figure 88: MV feeder terminal voltage profiles – D1

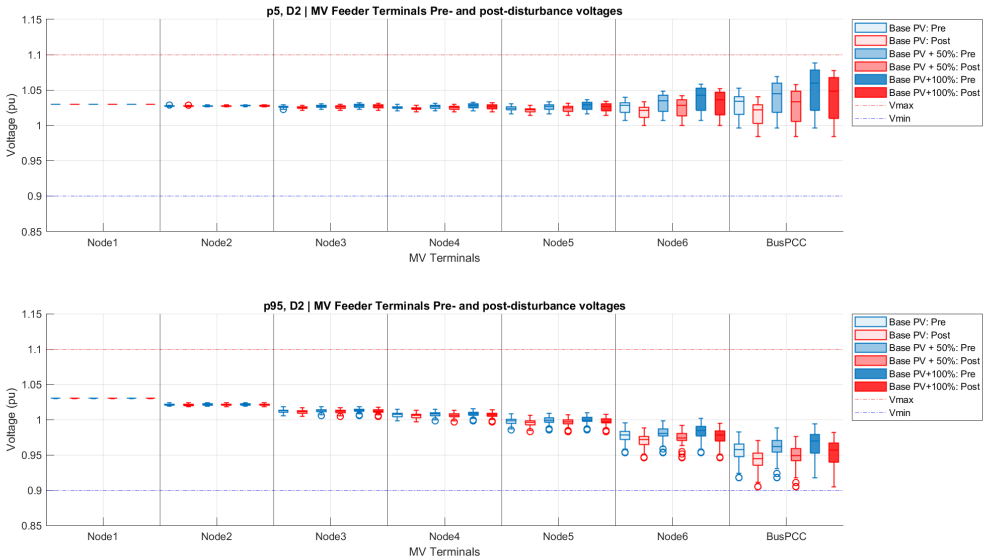

Figure 89: MV feeder terminal voltage profiles – D2

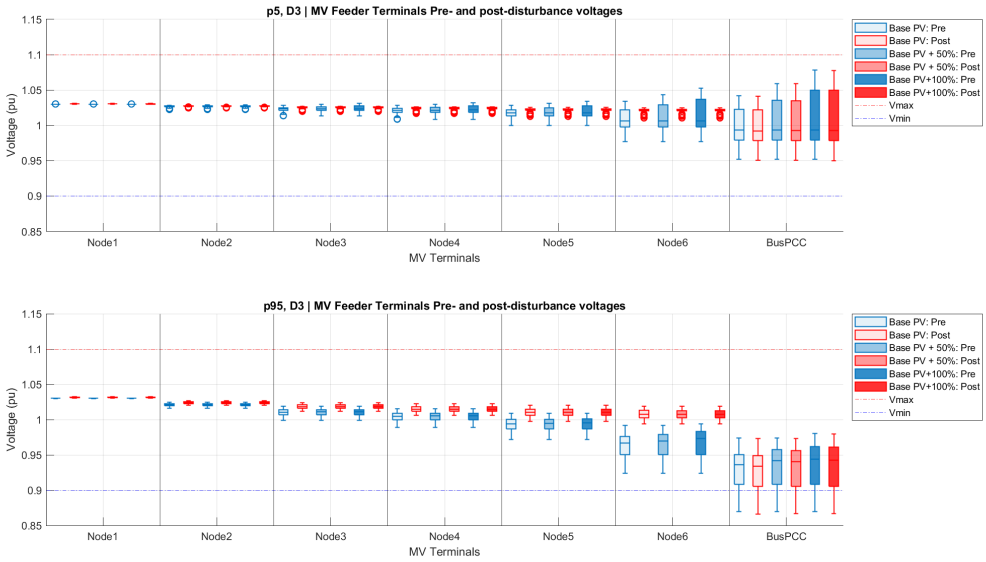

Figure 90: MV feeder terminal voltage profiles – D3

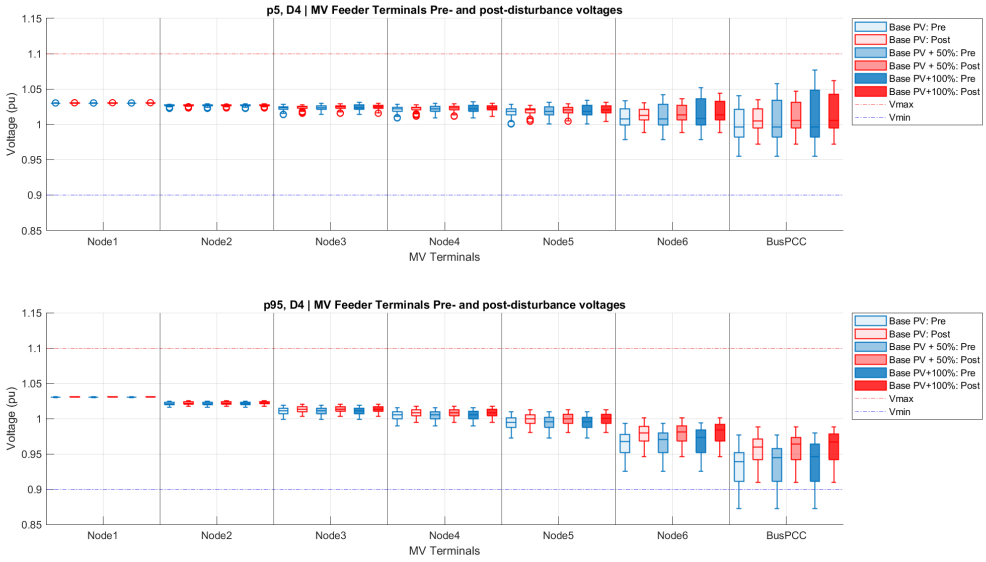

Figure 91: MV feeder terminal voltage profiles – D4

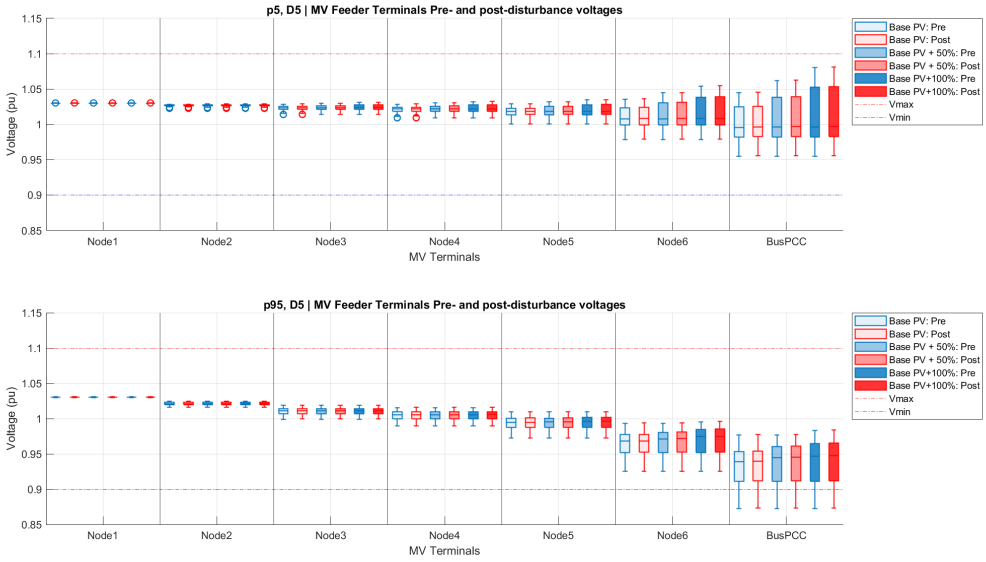

Figure 92: MV feeder terminal voltage profiles – D5

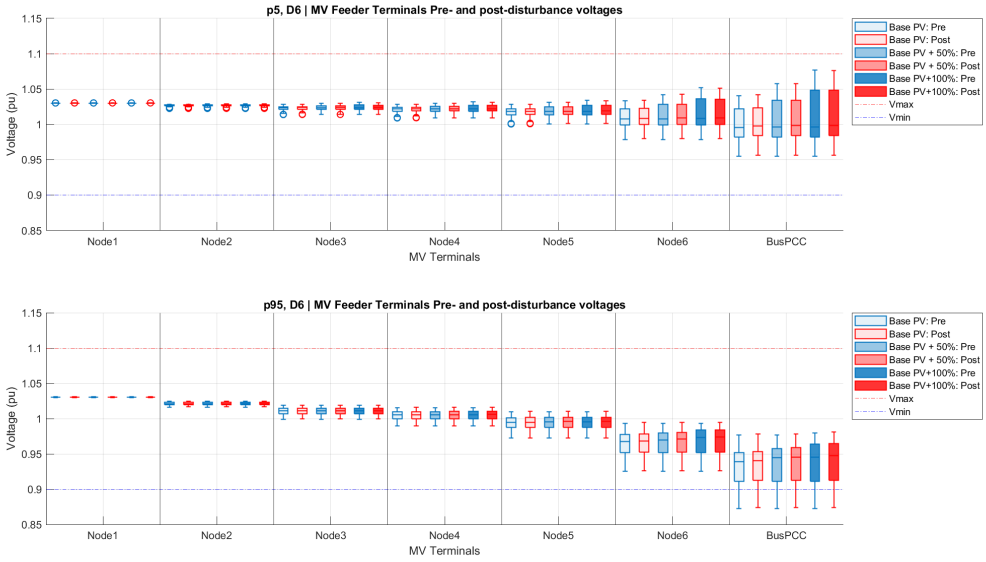

Figure 93: MV feeder terminal voltage profiles – D6

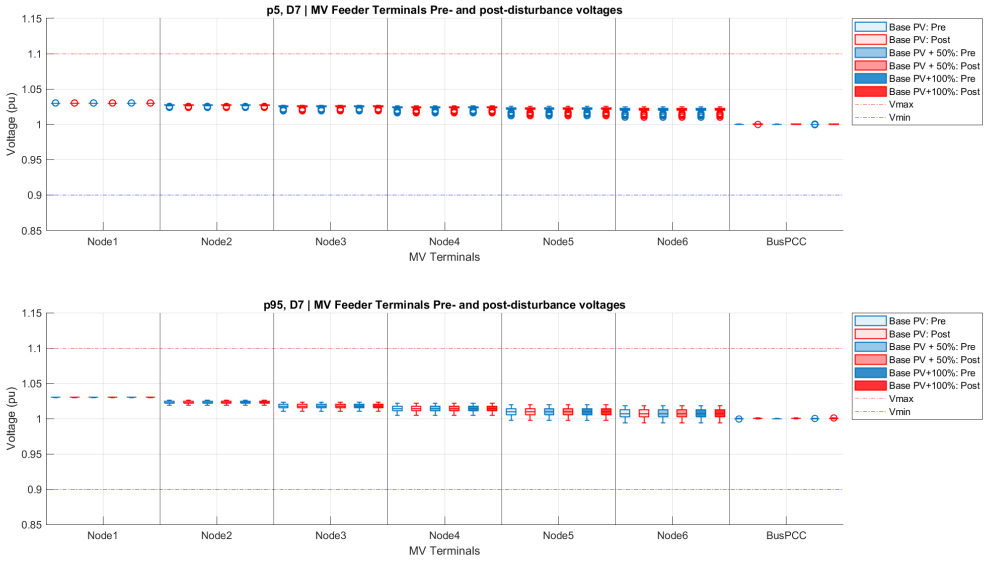

Figure 94: MV feeder terminal voltage profiles – D7

In the following table, the impact of different PV and BESS penetration on the microgrid, feeder and distribution transformers is discussed. Detailed simulation plots corresponding to the discussed results can be found in the Appendix files.

	Impact on PCC and LV bus voltages	**Impact on MV feeder terminal voltages**	**Impact on Transformer loading**
Increasing PV penetration (%)	Increasing the PV penetration has increased maximum voltage values (typically during midday) across all LV buses and PCC bus. At p5 profile, some bus voltages violated the upper voltage limit at double the PV penetration and discharging BESS. This is partly attributed to the reactive power output of the BESS.	Remote terminal voltage values (Nodes 1-5) had negligible effect with increasing PV penetration, and the daily voltage profiles remained highly stiff across the daily load and generation changes. Node 6 had the most noticeable change due to its close proximity to the microgrid. Maximum voltage values have increased as the PV penetration increased. However, it did not result in any voltage violation in either p5 or p95 profiles.	As the PV penetration was increased, the loading of some transformers was observed to increase due to increased export, while in others the loading decreased due to reduced import. However, all transformers remained within their thermal limits both in p5 and p95 profiles.
Increasing BESS penetration (%) at charging vs discharging modes	In charging mode, larger BESS penetration has reduced the bus voltages since the batteries acted as larger loads. On the other hand, while discharging, larger BESS penetration has increased bus voltage values due to larger reactive power injection to the grid. The discharge mode resulted in a slight increase in overall voltage profiles in comparison to the charge mode when compared at the same penetration level.	Increasing the BESS penetration did not yield in noticeable differences in feeder terminal voltages within the same BESS dispatch mode. This is attributed to the small amount of BESS capacity with respect to the feeder loads. However, discharging the batteries have resulted in a very slight increase in Node 6 voltage profile (similar to the observation in LV buses) in comparison to charging mode. However, the difference was negligible. Remote terminal voltages were not affected by the dispatch mode.	Depending on the net load at the transformer level, increasing the BESS penetration while charging either reduced transformer loading due to less export, or increased transformer loading due to increased import. Increasing the BESS penetration while discharging had a similar impact to increasing PV penetration.
Conclusion	In p5 profile, the majority of PCC and LV bus voltages remained within the operational limits throughout all cases. In addition to the p5 overvoltages, at p95 profile, consistent undervoltage values were observed before and after the disturbances, mainly during the evening and night time when there is no solar generation.	All feeder terminal voltages remained stiff and within the operational limits across all cases and after all disturbances.	All transformers remained within their thermal limits across all cases and after all disturbances.
Recommendations	- Tap changing transformers can be used to eliminate the consistent undervoltage conditions during p95. - Overvoltage conditions that are observed with increased PV penetration can be avoided by reducing BESS discharge rate, avoiding reactive power discharge or avoiding discharge mode completely during high solar generation.	No mitigation is required for the feeder terminal voltages.	No mitigation is required for the distribution transformers.

Table 5-7: Tarnagulla – DER Penetration Impact Assessment

In the following table, the impact of different disturbances on the microgrid PCC voltage and power flow as well as transformer loading is discussed. Detailed simulation plots corresponding to the discussed results can be found in the Appendix files.

Disturbance	Changes in PCC voltage	Changes in PCC power flow	Changes in transformer loading (where the disturbance is applied)
D1 – Load Ramp up	A slight voltage drop was observed at the PCC following a load ramp up event. The changes in voltage levels remained approximately the same (0.01 pu) throughout the day across all cases both for p5 and p95 demand profiles.	Following load ramp-up, reduction in reactive power flow was observed during daytime when solar power generation was available. This reduction increased in magnitude as more power was injected by PV and BESS (with increased penetration). During night-time, post-disturbance reactive power flow was observed to increase. The active power flow increased due to the predominantly resistive nature of the load. The increase in the active power flow was slightly larger when the BESS was used in discharge mode.	Transformer loading increased under p95 profile. However, during midday period under p5, the transformer loading decreased (due to reduced export)
D2 – Generation Ramp down	A similar voltage drop was observed following generation ramp-down event. The changes in voltage values remained approximately in the same range throughout all cases, but smaller net changes were observed around midday with the increased solar penetration.	Reactive power flow decreased following the PV generation ramp-down. Larger reductions were observed with more PV and BESS penetration. The active power flow increased following the reduced generation. The increase in power flow was slightly larger when the BESS was in discharge mode.	Transformer loading increased under p95 profile. However, during midday period under p5, the transformer loading decreased (due to reduced export)
D3 – Islanding	The islanding event caused minimal change in voltage levels both in light and heavy demand conditions.	Following the islanding event, the PCC reconnected to a central grid-forming battery, which adjusted the power flow. A slight reduction in reactive power flow proportionate to the voltage changes was observed. Similarly, a slight readjustment in active power flow in the range of several kWs was also observed.	The islanding event caused negligible change in transformer loading since the connected load and generation remained unchanged.
D4 – Tx loss	In p5, voltage drops and rises were observed at the PCC throughout the day depending on whether there was net export or import at the disconnected transformer. In p95, a consistent voltage rise can be observed.	A change in active power flow was observed in proportion to the net active power load at the disconnected transformer. A reduction in reactive power flow was observed in proportion to the net reactive power load at the disconnected transformer as well as the reactive power response of inverters.	Transformer load and generation disconnected, therefore, transformer loading dropped to zero.
D5 – 1Ph fault	Minimal changes were observed in the steady state voltage of the phase that was exposed to the fault. The slight voltage rise is attributed to the response of the inverters, which may necessitate a dispatch value reset following the fault clearance.	During BESS charging mode, the PCC active power flow decreased as a result of batteries switching to discharge mode and prioritising reactive power output to respond to the fault event. On the other hand, during discharge mode, the prioritisation of reactive power response resulted in a gap in active power which increased the PCC active power flow. The reduction in reactive power flow changed in line with BESS and PV penetration	The transformer loading remained approximately the same as the pre-disturbance levels.

D6 – **3Ph fault**	Similar to D5, minimal changes were observed in the steady state voltage values following fault clearance. The changes were observed to be larger when BESS operated in charging mode	The changes in active and reactive power flow are similar to those observed in single-phase-to-ground fault, yet with a larger magnitude due to the response of all three phases and closer proximity of the fault.	The transformer loading remained approximately the same as the pre-disturbance levels.
D7 – **Tx loss (off-grid)**	The loss of a transformer during off-grid mode resulted in minimal change in voltage levels both in light and heavy demand conditions.	A change in active power flow was observed in proportion to the net active power load at the disconnected transformer. A reduction in reactive power flow was observed in proportion to the net reactive power load at the disconnected transformer as well as the reactive power response of inverters.	Transformer load and generation disconnected, therefore, transformer loading dropped to zero

Table 5-8: Tarnagulla – Disturbance Impact Assessment

It should be noted that the Donald feeder (part of CTN6) was more impacted by the town disturbances compared to Tarnagulla feeder MRO7. That may be expected due to the two following factors. First, the generation and load in Donald town is approximately 10 times larger than that of Tarnagulla's town, and the disturbances have been sized in proportion to the load and generation of each town. Second, the Donald feeder has two downstream towns with weaker voltage profiles which deteriorate further the impact of the disturbances. On the other hand, due to the fact that Tarnagulla town is located at the end of a very long and highly loaded feeder, the impact of the disturbances is less pronounced across the upsteam nodes.

5.2.3 Appendix files

For completeness, the following list of simulation results are provided in the Appendix files for both towns:

1. "LV, Tx – all" : Post-disturbance voltages of all LV buses and post-disturbance loading of all transformers across all cases and disturbances
2. "MV feeder – pre, post" : Pre- and post-disturbance voltages of all MV buses and PCC across all cases and disturbances
3. "MV feeder – Trend" : Trend of pre- and post-disturbance voltages of all MV buses and PCC across all cases and disturbances
4. "Tx, PCC – changes" : Changes between pre- and post-disturbance PCC voltage, PCC power flow, largest transformer loading across all cases and disturbances

6 Conclusions

This project developed steady-state and dynamic power system operation models and statistical models for disturbances aiming in evaluating the disturbance impact on the system security and in providing an assessment of the options, risks and benefits of specific control strategies for microgrid operation.

The impact analysis was divided into two investigations. First, the Capacity Adequacy Analysis (Section 4) considered steady-steady operation on a simplified network representation where the capacity adequacy level is measured by the expected energy not supplied. The latter was investigated given probabilistic consideration of outages (including bushfire-induced outages and disruptions) and under different mitigation control strategies. Second, the Dynamic Impact Analysis (Section 5) considered dynamic operation on a detailed network modelled and the dynamic performance of the system under a variety of disturbances was evaluated. In both investigations the base case of hosting capacity was informed by the outcome of Project 5 while increasing capacity cases were also examined.

The key points driven from those investigations are summarized below:

Capacity Adequacy Analysis

- The proposed control strategies, involving emergency response of batteries and import power, improved the capacity adequacy level for both the Donald and Tarnagulla areas. Enabling emergency discharge of batteries has the most significant improvement on capacity adequacy. Moreover, control decisions looking ahead 2 days improved the capacity adequacy level.
- In grid-connected operation, the capacity adequacy level of can be significantly compromised by the increased probability of line outage due to bushfires along the transmission path, while the impact of bushfire-induced fuel supply disruption has minor negative impact. The network operators could adopt preventive strategies on monitoring bushfire risks along the transmission path. Moreover, regular inspection on sub-transmission line health condition may reduce forced outages due to flashover during high bushfire risk periods.
- In off-grid operation, the capacity adequacy level for both towns at the base case hosting capacity is lower than that when they are grid-connected. Thus, additional generation is required to comply with the SAPS regulation rules.
- In off-grid operation, more local diesel storage capacity is required in both towns when considering the trade-off between bushfire-induced fuel supply disruption impact and the overall NPC including both investment costs and loss of load costs.

Dynamic Impact Analysis

- The installation of a grid-forming converter in both towns assisted in reducing the post-disturbance voltage violations in the case of an islanding event.
- In the Tarnagulla feeder, the voltages of all upstream nodes remained stiff and within the operational limits across all cases and after all disturbances. In the Donald feeder, the islanding event resulted in over-voltage violations at the upstream nodes to the town. In addition, the downstream nodes (Donald South and Litchfield) consistently experienced pre- and post-disturbance undervoltage conditions.
- The long and highly loaded feeder of Tarnagulla contributed to a less pronounced impact of the disturbances on the upstream nodes. In contrast, the Donald feeder has two downstream towns to Donald town, with already weaker voltage profiles which further deteriorate the impact of the town disturbances. The Donald feeder seems more sensitive to disturbances also because the

generation and load in Donald is approximately 10 times larger than that of Tarnagulla, and the disturbances are sized in proportion to the load and generation of each town.

- All distribution transformers in both towns remained within their thermal limits across all cases and after all disturbances.
- Inverters equipped with Volt-Var control increased system flexibility and reduced over/under-voltage events in transient analysis compared to static inverters.
- Heavy net demand resulted in more under-voltage violations in both towns for both pre- and post-disturbance operating points.
- To mitigate the under/over-voltage problems, coordinated scheduling and real-time control algorithms for the inverters and LTC transformers need to be further designed.

Additional key points were driven during the process of disturbance modelling (Section 3). Specifically, the statistical models prepared to forecast PV generation and demand in the two towns revealed the following points.

Forecasting PV generation and demand

- The random forest regression proved to be more accurate for the PV generation and demand signals compared several state-of-the-art methods.
- The probabilistic forecast error interval models assisted in evaluating the disturbance volume with regards to generation and load uncertainty.
- The forecast error was reduced when the proposed (estimated) individual PV generation and demand signals were used as input, instead of the import/export signals from smart meter data.

References

[1] CIGRE WG C6.24 - Capacity of Distribution Feeders for Hosting DER, June 2014
[2] Dr Andreas T. Procopiou, “Increasing PV Hosting Capacity in Distribution Network: Challenges and Opportunities”, The University of Melbourne, MEI Symposium, Dec 2018
[3] ASNZS 4777.2:2020, “Grid Connection of Energy Systems via Inverters - Part 2: Inverter Requirements”
[4] VDE FNN, “Power Generating Plants in the Low Voltage Network (VDE-AR-N 4105), 2018 [Online], Available: https://www.vde.com/en/fnn/topics/technical-connection-rules/power-generating-plants
[5] EUR-Lex, “Network Code Requirements for Generators (RfG)”, 2016, [Online], Available: https://eur-lex.europa.eu/legal-content/EN/TXT/?uri=OJ:JOL_2016_112_R_0001
[6] T. Gush et al, "Optimal Smart Inverter Control for PV and BESS to Improve PV Hosting Capacity of Distribution Networks Using Slime Mould Algorithm," in IEEE Access, vol. 9, pp. 52164-52176, 2021, doi: 10.1109/ACCESS.2021.3070155.
[7] Mohamed M. Aly, et al, “Assessment of reactive power contribution of photovoltaic energy systems on voltage profile and stability of distribution systems”, International Journal of Electrical Power & Energy Systems, vol. 61, pp. 665-672, 2014, https://doi.org/10.1016/j.ijepes.2014.02.040
[8] R. Allan and R. Billinton, “Reliability evaluation of power systems”, Plenum Press, 1984
[9] Powercor, Operation Diagram CTN SOUTH 22kV
[10] Powercor, “2016-2020 Price Reset Appendix E: Capital Expenditure”, April 2015
[11] Climate Change in Australia, “Electricity Sector Climate Information: Climate Data”, https://www.climatechangeinaustralia.gov.au/en/projects/esci/
[12] Powercor, Operation Diagram MRO EAST 22kV
[13] Powercor Australia, “Distribution Annual Planning Report”, Dec 2019. Available: https://media.powercor.com.au/wp-content/uploads/2020/01/22153352/Final-Powercor-Distribution-Annual-Planning-Report-2019.pdf
[14] https://www.climatechangeinaustralia.gov.au/en/projects/esci/esci-case-studies/case-study-fire-transmission/
[15] J.M. Cainey, "Resilience and reliability for electricity networks." *Proceedings of the Royal Society of Victoria*, vol.131, pp: 44-52, 2019. doi: 10.1071/RS19005
[16] S.Islam, et.al.,“Islanding Design and Cost Analysis for Donald and Tarnagulla Microgrid Feasibility Study”, RMIT and Federation University
[17] National Electricity Amendment (Regulated stand-alone power systems) Rule 2022, Clause 5.10.2. Available: https://www.aemc.gov.au/sites/default/files/2022-02/SAPS%20NER%20amending%20rule%20final%202022.pdf
[18] NREL, “Valuing Energy Security: Customer Damage Function Methodology and Case Studies at DoD Installations, Technical report”, NREL/ TP-7A30-55913, Oct 2013
[19] Australian Government Productivity Commission, “Electricity Network Regulatory Frameworks, Productivity Commission Inquiry Report”, Vol. 2 No.62, pp.539, April 2013
[20] PJM, “2017 PJM RTEP Process Scope and Input Assumptions,” 2017.